Centrally Active Multitarget Anti-Alzheimer Agents Derived from the Antioxidant Lead CR-6

Centrally Active Multitarget Anti-Alzheimer Agents Derived from the Antioxidant Lead CR-6

F. Javier Pérez-Areales,[†] María Garrido,[‡] Ester Aso,[§] Manuela Bartolini,[Δ] Angela De Simone,[¶] Alba Espargaró,[#] Tiziana Ginex,[⊥] Raimon Sabate,[#] Belén Pérez,[//] Vincenza Andrisano,[▽] Dolors Puigoriol-Illamola,[»] Mercè Pallàs,[»] F. Javier Luque,[⊥] María Isabel Loza,[⌂] José Brea,[⌂] Isidro Ferrer,[§,◊] Francisco Ciruela,[§] Angel Messeguer,[‡] Diego Muñoz-Torrero[,†]*

[†]Laboratory of Medicinal Chemistry (CSIC Associated Unit), Faculty of Pharmacy and Food Sciences, and Institute of Biomedicine (IBUB), University of Barcelona (UB), E-08028 Barcelona, Spain

[‡]Department of Biological Chemistry, Institute of Advanced Chemistry of Catalonia (IQAC-CSIC), E-08034 Barcelona, Spain

[§] Department of Pathology and Experimental Therapeutics, Neurosciences Institute, UB, and Bellvitge University Hospital - IDIBELL, E-08908 L'Hospitalet de Llobregat, Spain

[Δ]Department of Pharmacy and Biotechnology, University of Bologna, I-40126 Bologna, Italy

[¶]Department of Drug Science and Technology, University of Turin, I-10125 Torino, Italy

[#]Department of Pharmacy, Pharmaceutical Technology and Physical-Chemistry, Faculty of Pharmacy and Food Sciences, and Institute of Nanoscience and Nanotechnology (IN2UB), UB, E-08028 Barcelona, Spain

[⊥]Department of Nutrition, Food Science and Gastronomy, Faculty of Pharmacy and Food Sciences, IBUB, and Institute of Theoretical and Computational Chemistry (IQTC), UB, E-08921 Santa Coloma de Gramenet, Spain

[||]Department of Pharmacology, Therapeutics, and Toxicology, Autonomous University of Barcelona, E-08193 Bellaterra, Spain

[▽]Department for Life Quality Studies, University of Bologna, I-47921 Rimini, Italy

[»] Pharmacology Section, Department of Pharmacology, Toxicology and Therapeutic Chemistry, Faculty of Pharmacy and Food Sciences, and Institute of Neuroscience (NeuroUB), UB, E-08028 Barcelona, Spain

[⌂]BioFarma Research Group, Centro Singular de Investigación en Medicina Molecular y Enfermedades Crónicas (CIMUS), Universidade de Santiago de Compostela, Av. de Barcelona s/n, E-15782, Santiago de Compostela, Spain

[◊]CIBERNED, E-28031 Madrid, Spain

ABSTRACT: Oxidative stress is a major pathogenic factor in Alzheimer's disease, but it should not be tackled alone but together with other key targets to derive effective treatments. Combination of the scaffold of the polar antioxidant lead CR-6 (7-methoxy-2,2-dimethylchroman-6-ol) with that of the lipophilic cholinesterase inhibitor 6-chlorotacrine results in compounds with favorable brain permeability and multiple activities in vitro (acetylcholinesterase, butyrylcholinesterase, BACE-1, and Aβ42 and tau aggregation inhibition). In in vivo studies in wild-type and APP/PS1 mice, two selected compounds were well tolerated and led to positive trends, albeit statistically non-significant in some cases, on memory performance, amyloid pathology (reduced amyloid burden and potentiated non-amyloidogenic APP processing), and oxidative stress (reduced cortical oxidized proteins and increased antioxidant enzymes SOD2, catalase, GPX1, and Hmox1, and transcription factor Nrf2). These compounds emerge as interesting brain permeable multitarget compounds, with a potential as anti-Alzheimer agents beyond that of the original lead CR-6.

INTRODUCTION

Alzheimer's disease (AD) remains one of our most urgent unmet medical needs. Indeed, the figures associated with AD are really worrying. It is the most prevalent chronic neurodegenerative disorder and the main cause of dementia. Currently, some 50 million people worldwide suffer from dementia, with around 35 million having AD.[1] This number is estimated to triple to more than 150 million by 2050. The incidence is also reaching alarming proportions, with more than 10 million new cases per year. The huge incidence and prevalence of AD together with the fact that it is a fatal disease make it the 7th leading cause of death worldwide. However, unlike other major causes of death, AD cannot be cured, prevented, or even slowed down. Beyond its devastating effects on AD patients health, this pathology also strongly affects the quality of life of caregivers, who by more than 50% see how their social life, work, and even health are negatively affected as a consequence of their caring responsibilities.[2] To further aggravate the situation, the economic burden of AD is really a major issue for health systems worldwide, with a total estimated cost of around 1 trillion US dollar, which is expected to double in just ten years.

Indeed, the devastating consequences of AD are due to the lack of effective drugs that can positively impact disease progression. Currently, only four drugs are available for AD management, namely the acetylcholinesterase (AChE) inhibitors donepezil, rivastigmine, and galantamine, and the glutamate NMDA receptor antagonist memantine, which are used to temporarily alleviate the cognitive and functional symptoms. Very intensive research efforts have been devoted in the past two decades to discovering disease-modifying drugs that could halt disease progression, mainly focused on interfering the biology of β-amyloid peptide (Aβ), widely regarded as a key culprit of AD. Despite high expectations, all putative disease-modifying drug

candidates have disappointingly failed to demonstrate efficacy in advanced clinical trials, which has made AD drug discovery one of the areas with highest attrition rate, with a failure rate of 99.6% since the launching of memantine, so far the last approved drug.[1] In this scenario, it becomes evident that AD is a matter of tremendous social concern worldwide, with up to 95% of people thinking they will develop dementia in their lifetime, and 25% that there is nothing that can be done about it.[2]

To meet the desperate need for effective therapies, alternative ways to approach AD should be tested. There is a growing awareness that AD is a complex disorder in which multiple factors concur to the onset of the pathological scenario and that cannot be efficiently cured by modulating a single biological target or pathological event, but with combinations of drugs[1] or with multitarget drugs, i.e. single molecules that are able to hit more than one target with a key role in the pathological network of AD.[3] Indeed, simultaneous modulation of several crucial biological targets of AD is being increasingly accepted as a realistic option to inflict a serious damage to AD network and derive effective treatments.[4] As a result, together with cancer, AD is the area in which the development of multitarget agents seems to have experienced a greater growth in the last fifteen years.[5]

Thus far, a large number of multitarget agents, usually designed by combination of different pharmacophores, has been developed to hit several key biological targets or pathological events of AD.[6] Apart from modulating Aβ biology (inhibition of Aβ formation by proteolytic cleavage of the amyloid precursor protein (APP) by the β-site APP cleaving enzyme (BACE-1 or β-secretase) and γ-secretase or inhibition of Aβ aggregation), inhibition of cholinesterases (AChE and butyrylcholinesterase (BChE)) is also commonly considered for the design of multitarget anti-AD agents.[7]

Another crucial pathological event of AD is oxidative stress. Because of its high demand for oxygen, high levels of peroxidizable lipids (polyunsaturated fatty acids), and deficiency of antioxidant defense systems, brain is highly vulnerable to oxidative stress.[8] Thus, increased levels of markers of cell component oxidation and altered levels of antioxidant enzymes are found in brains of AD patients. Indeed, increased levels of protein oxidation markers, such as carbonylated proteins, are found not only in AD brains but also in patients suffering from amnestic mild cognitive impairment (MCI). The latter finding supports the idea that oxidative stress is involved in the early stages of AD. Additionally, oxidative stress could be necessary for the deployment of other pathological mechanisms of AD, such as Aβ- and tau-induced neurotoxicity, which makes it a key pathogenic element in AD.[9] Removal or prevention of the formation of reactive oxygen species (ROS) may, hence, be helpful to halt AD progression. In this light, antioxidants have been evaluated as a potential treatment of AD or even MCI. However, results from clinical trials have been disappointing,[10] with poor brain permeation likely accounting, at least in part, for the lack of clinical efficacy of antioxidants.[11]

This was a major drawback of the so-called CR-6 (**1**, Figure 1), the most potent antioxidant within a series of chroman derivatives developed by some of us. This compound showed a very interesting in vitro antioxidant profile, including inhibitory effect on lipid peroxidation,[12] NO scavenging activity and protective effect against glutamate-induced neurotoxicity in cultured cerebellar neurons,[13] and against hydrogen peroxide-induced apoptosis in human neuroblastoma SH-SY5Y cells.[14] The neuroprotective effect of CR-6 has been also demonstrated in an in vivo study, which revealed a reduction of oxidative damage after a cerebral ischemia/reperfusion process in rats.[15] However, despite the fact that CR-6 was detected in the brain, its concentration was not high enough to elicit the desired neuroprotective effects at the desired level. Indeed, the

permeability (P_e) of CR-6 measured in the parallel artificial membrane permeation assay (PAMPA) for blood–brain barrier (BBB) had been found to be negligible (Figure 1). As a first attempt to overcome this limitation, the CR-6 scaffold has been recently conjugated with essential brain nutrients such as amino acids or glucose that are recognized by active transport systems (for example, compound **2**, Figure 1).[16]

Apart from the limitation of poor brain permeation of most antioxidants, targeting oxidative stress alone does not seem a realistic option to derive a clinically efficacious treatment.[9a] The use of antioxidant cocktails or combination of antioxidants with drugs targeting other underlying causes of AD has been proposed as a more realistic option to cope with the multifactorial nature of AD.[8] However, the use of antioxidants in drug combinations would not avoid the brain permeation issues that is inherent to many antioxidants. A very convenient way to conciliate both needs is the design of hybrid compounds in which the antioxidant moiety is attached to a second, more lipophilic pharmacophore, i.e. the design of lipophilic multitarget compounds featuring an antioxidant moiety, such as melatonin or trolox, among others.[17]

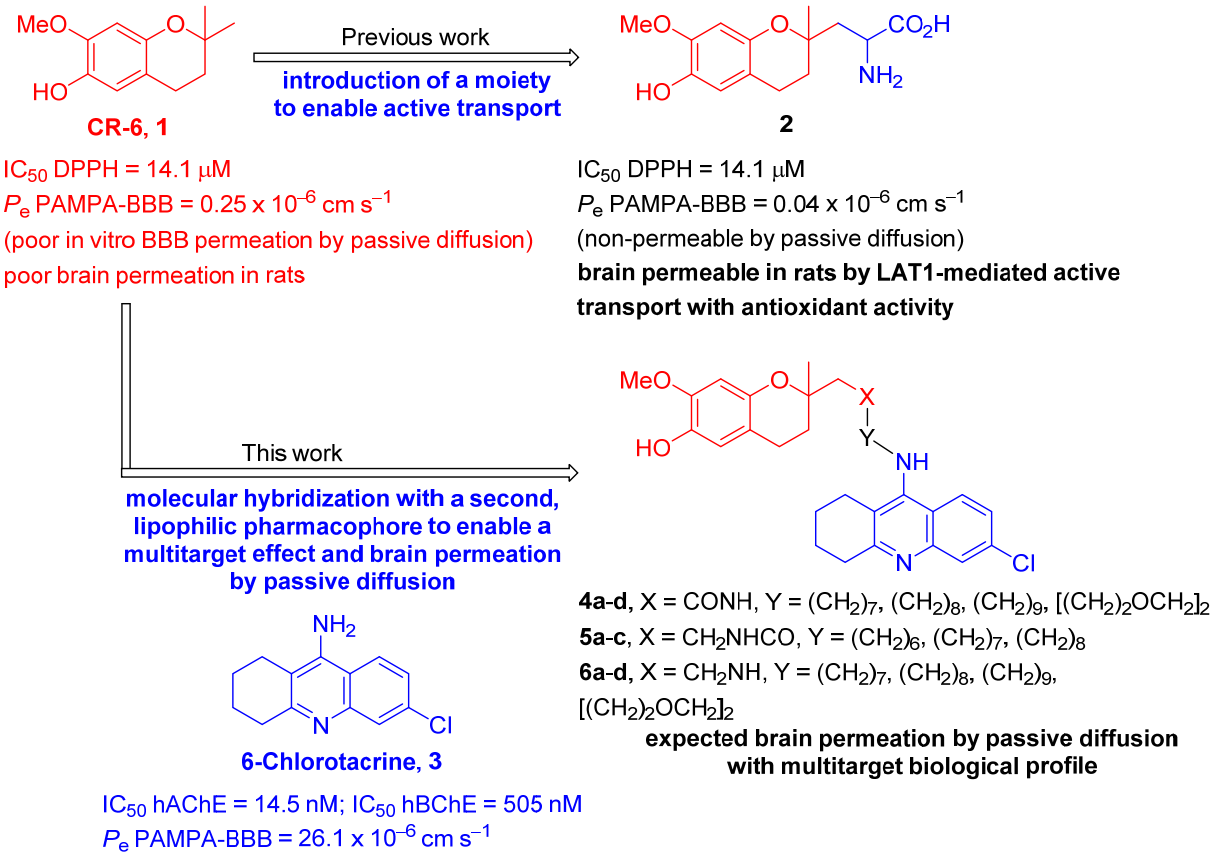

Figure 1. Design strategy of the CR-6–chlorotacrine hybrids.

Herein, we describe the synthesis and in vitro and in vivo biological evaluation of a new class of multitarget hybrids that combine the scaffold of the polar non-brain permeable antioxidant lead CR-6 with 6-chlorotacrine (**3**, Figure 1), a very potent lipophilic AChE inhibitor, through linkers with different lengths and functionalities. We inferred that the 6-chlorotacrine moiety (P_e PAMPA-BBB = 26.1 × 10^{-6} cm s^{-1}) should impart brain permeability to the resulting CR-6-based hybrids, as well as a second biological activity (AChE inhibition) of interest for AD treatment.[18] Apart from the biological activities resulting from the modulation of the primary targets (antioxidant and anticholinesterase activity), we have quite consistently observed that hybrid compounds bearing two aromatic systems separated by linkers of suitable length are able

to inhibit the aggregation of Aβ42 and tau,[19] two key pathogenic actors in AD, as well as other non-related amyloidogenic proteins,[20] thereby expanding their multitarget profile. Additionally, some of these hybrids, featuring a protonatable tacrine (**3**, Figure 1), 6-chlorotacrine or a structurally related huprine moiety have been found to inhibit BACE-1, the enzyme that catalyzes the first rate-limiting step of Aβ formation.[19a,b,21] Thus, the novel CR-6–chlorotacrine hybrids herein reported were tested in vitro for their antioxidant effect, their inhibitory activities against human cholinesterases (hAChE and hBChE), Aβ42 and tau aggregation, and human BACE-1, and their brain permeabilities. The in vivo efficacy of two selected compounds was evaluated in APP/PS1 mice, a well-established mouse model of AD, in terms of their effect on cognition and markers of oxidative stress and amyloid pathology.

RESULTS AND DISCUSSION

Design. The presence of a hydroxyl group at position 6 of the chroman scaffold of CR-6 is the most important structural feature for its antioxidant effects, and, hence, it had to be preserved in the hybrids. In contrast, derivatization of CR-6 by functionalization at position 2 does not affect the antioxidant activity.[16] Indeed, the previously mentioned CR-6 derivative **2**, functionalized at this position with an amino acid side chain is equipotent to the lead CR-6 (Figure 1). Likewise, the CR-6 derivative **7** (Scheme 1), substituted at position 2 of the chroman scaffold with an acetic acid chain displays an even slightly higher antioxidant effect (IC_{50} DPPH = 8.4 μM).[16] The carboxylic acid of compound **7** was ideal for the introduction of the linker attached to the 6-chlorotacrine moiety through an amide bond. Thus, compound **7** was selected as the starting material for the synthesis of a first series of CR-6–chlorotacrine hybrids featuring an amide functionality within the linker (hybrids **4a-d**, Figure 1, Scheme 1). The synthesis of two other series of hybrids that featured a reverse amide (hybrids **5a-c**, Figure 1, Scheme 2) or an amine

(hybrids **6a-d**, Figure 1, Scheme 3) within the linker was also envisaged, starting from the CR-6 derivatives **14** and **16**, respectively,[16] to further assess the effect of the linker amide or a protonatable amino group on the interaction with the putative biological targets. We have developed other families of multitarget compounds featuring a chlorotacrine or huprine moiety linked to a second polycyclic pharmacophore through an amide-containing tether chain. Those hybrids with a total linker length of 10−12 atoms, from the amino group of chlorotacrine or huprine to the other polycyclic system (counting the atoms of the amide group), were found to display a better overall biological profile including AChE, BACE-1, and/or Aβ42 and tau aggregation inhibition.[19a,c,d] On the basis of these premises, our main interest was the synthesis of parallel series of CR-6–chlorotacrine hybrids with total linker lengths of 10 atoms (**4-6a**, **11a**, **12a**), 11 atoms (**4-6b**, **11b**, **12b**), and 12 atoms (**4-6c**, **11c**, **12c**). Additionally, shorter homologs with total linker length of 9 atoms (**11e**, **12e**) and analogs containing an ethylene glycol group within the linker (**4d**, **6d**), aiming to increase aqueous solubility, were synthesized for some, but not all, of the series in light of their less favorable biological activities (see below).

Synthesis. Hybrids **4a-d** were synthesized in racemic form in good yield (67–91%) in just one step, by *N*-(3-dimethylaminopropyl)-*N′*-ethylcarbodiimide hydrochloride (EDC·HCl) / 1-hydroxy-1*H*-benzotriazole (HOBt)-mediated amide coupling of racemic carboxylic acid **7**[16] with the known aminoalkyltacrines **10a-c**[22] and **10d**,[23] which were readily prepared by aromatic nucleophilic substitution of dichloroacridine **9**[24] with commercially available diamines (Scheme 1).

The yield of the latter amide coupling reactions could be still improved when protecting the hydroxyl group at position 6 of the chroman carboxylic acid. Thus, reaction of racemic *O*-benzylated carboxylic acid **8**[16] with amines **10a-c**,**e**[22] in the presence of EDC·HCl and HOBt led

to *O*-benzylated amides **11a-c**,**e** in 83% to quantitative yield. With these amides in hand, we performed a double *O*-debenzylation/dechlorination reaction by hydrogenolysis under Pd/C catalysis, which afforded in excellent yields a parallel series of hybrids featuring the amide group at the linker and an unsubstituted tacrine unit (hybrids **12a-c**,**e**, Scheme 1).

Scheme 1. Synthesis of the CR-6–(Chloro)Tacrine Hybrids 4a-d, 11a-c,e, and 12a-c,e[a]

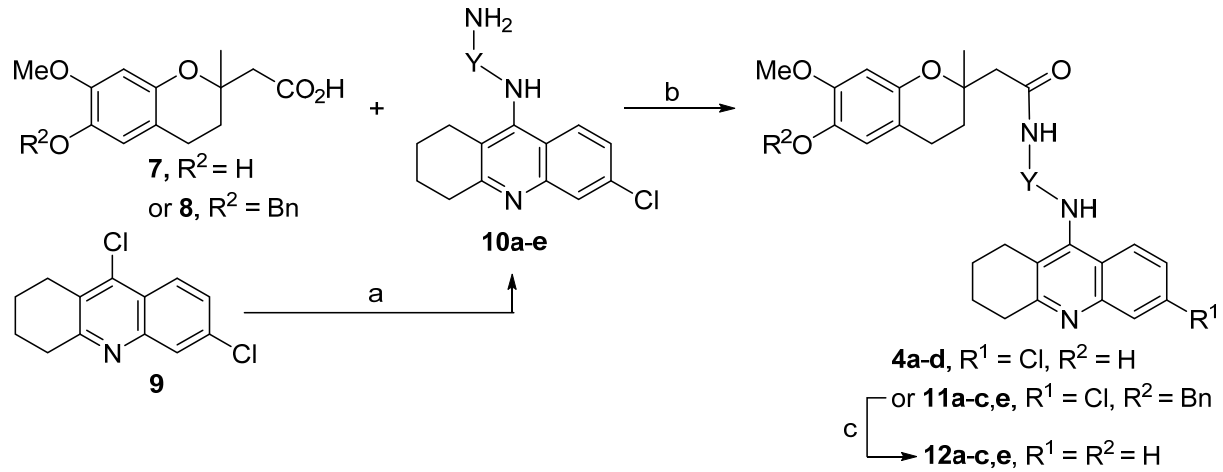

a: Y = $(CH_2)_7$; **b**: Y = $(CH_2)_8$; **c**: Y = $(CH_2)_9$; **d**: $[(CH_2)_2OCH_2]_2$; **e**: Y = $(CH_2)_6$

[a]Reagents and conditions: (a) diamine, 1-pentanol, reflux or closed vessel, 18-24 h, 59% (**10a**), 69% (**10b**), 59% (**10c**), 77% (**10d**), 32% (**10e**); (b) **7** or **8**, EDC·HCl, HOBt, Et_3N, EtOAc / DMF, rt, 15 min; then, **10a-e**, EtOAc / DMF, rt, 24 h, 67% (**4a**), 67% (**4b**), 86% (**4c**), 91% (**4d**), 83% (**11a**), 92% (**11b**), 90% (**11c**), 100% (**11e**); (c) H_2 (1 atm), 10% w/w Pd/C, EtOH, rt, overnight, 72% (**12a**), 99% (**12b**), 99% (**12c**), 99% (**12e**).

The synthesis of the reverse amide hybrids **5a-c** was accomplished in two steps from the known cyanoalkyltacrines **13a-c**.[25] Alkaline hydrolysis of nitriles **13a-c**, followed by acidification with a dioxane or Et_2O solution of HCl led to the corresponding carboxylic acids, which were isolated in the form of quinoline hydrochloride salts. EDC/HOBt-mediated amide coupling of these crude carboxylic acids with racemic CR-6-derived primary amine **14**[16] afforded the target reverse amide

hybrids **5a-c** in racemic form in moderate to good overall yields (52–87% overall from nitriles **13a-c**, Scheme 2).

Finally, racemic hybrids **6a-d** bearing a protonatable aliphatic secondary amine within the linker were synthesized in low to moderate yields (24–59%) by alkylation of the primary amines **10a-d**[22] with the new CR-6-derived tosylate **15**, which, in turn, was readily prepared by hydrogenolysis of its racemic *O*-benzylated precursor **16**[16] (Scheme 3).

The CR-6–chlorotacrine hybrids are chiral due to the presence of a stereocenter at position 2 of the chroman moiety. They were prepared and tested in racemic form. We envisaged the resolution of the CR-6-based racemic carboxylic acid **8**. However, different resolution attempts via formation of diastereomeric esters with the enantiopure alcohols (*S*)-3-hydroxy-4,4-dimethyl-1-phenylpyrrolidin-2-one ((*S*)-*N*-phenylpantolactam),[26] and (1*R*,2*S*,5*R*)-2-isopropyl-5-methylcyclohexanol ((–)-menthol), followed by silica gel column chromatography separation, or via diastereomeric salts with (*S*)-(–)-1-phenyethylamine, followed by recrystallization were fruitless. Taking into account these results and the fact that no big difference was expected for the enantiomers of the CR-6–chlorotacrine hybrids neither in their antioxidant effects nor in their AChE and BChE inhibitory activities, as predicted by molecular dynamics simulations (see below), we did not undertake further resolution attempts.

Scheme 2. Synthesis of the CR-6–Chlorotacrine Hybrids 5a-c[a]

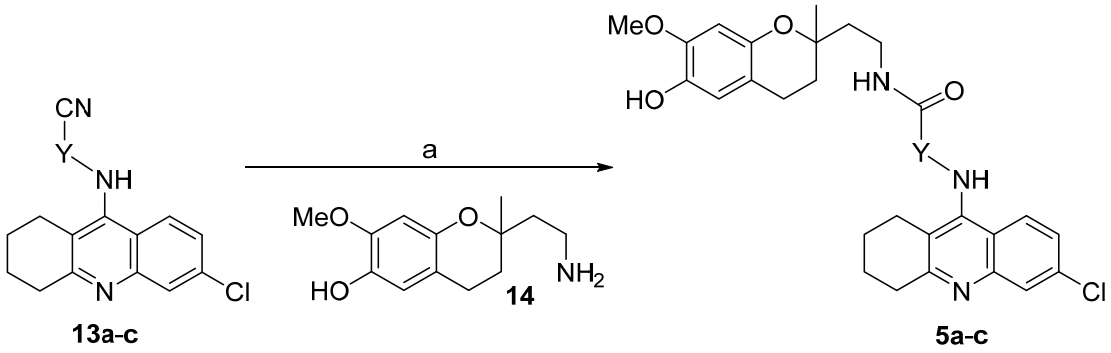

a: Y = $(CH_2)_6$; **b**: Y = $(CH_2)_7$; **c**: Y = $(CH_2)_8$

[a]Reagents and conditions: (a) **13a-c**, 40% methanolic KOH, reflux, 3 h; H_2O, reflux, overnight; HCl in dioxane or Et_2O; resulting carboxylic acid, EDC·HCl, HOBt, Et_3N, EtOAc / DMF, rt, 15 min; then, **14**, EtOAc / DMF, rt, 24 h, 87% (**5a**), 55% (**5b**), 52% (**5c**).

Scheme 3. Synthesis of the CR-6–Chlorotacrine Hybrids 6a-d[a]

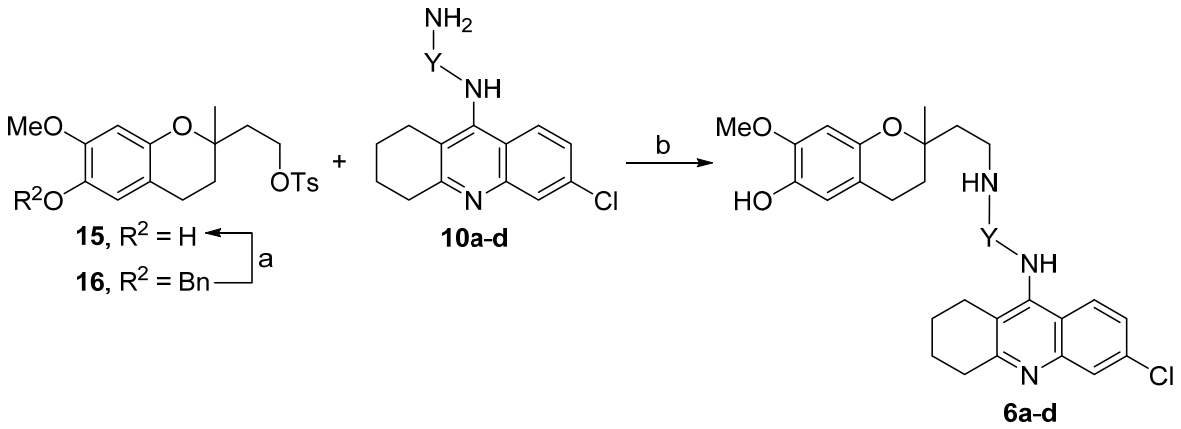

a: Y = $(CH_2)_7$; **b**: Y = $(CH_2)_8$; **c**: Y = $(CH_2)_9$; **d**: $[(CH_2)_2OCH_2]_2$

[a]Reagents and conditions: (a) H_2 (1 atm), 10% w/w Pd/C, THF, rt, overnight, 90%; (b) Et_3N, CH_3CN, 80 ºC, 48 h, 24% (**6a**), 57% (**6b**), 59% (**6c**), 30% (**6d**).

Purity of the Compounds. Apart from the target CR-6–chlorotacrine hybrids (**4a-d**, **5a-c**, and **6a-d**) and the CR-6–tacrine hybrids **12a-c**,**e**, we also subjected the *O*-benzylated CR-6–

chlorotacrine hybrids **11a-c**,**e** to biological evaluation. Even though the latter compounds should be devoid of antioxidant effect, due to the substitution at the key hydroxyl group of the chroman scaffold, we wanted to assess the effect of this substitution on the rest of biological activities under evaluation. All these hybrids were transformed into the corresponding hydrochloride or dihydrochloride salts for their chemical characterization and biological profiling. The analytical samples of all the tested hybrids possessed a purity > 95%, according to NMR spectra with full assignments and HPLC-UV / HRMS measurements (for more details see the Experimental Section and Supporting Information).

In Vitro hAChE and hBChE Inhibition. The anti-cholinesterase activity of the new hybrids was evaluated in vitro by the method of Ellman,[27] using human recombinant AChE (hAChE) and BChE from human serum (hBChE). The parent 6-chlorotacrine (Cl-THA), tacrine (THA), and CR-6-derived carboxylic acid **7** and amine **14** were also tested as reference compounds.

All CR-6–chlorotacrine hybrids (**4a-d**, **5a-c**, **6a-d**, and **11a-c**,**e**) were more potent hAChE inhibitors than the parent Cl-THA (IC_{50} = 14.5 nM), with IC_{50} values in the single-digit nanomolar or subnanomolar range, with the sole exception of **4d**, featuring an ethylene glycol-containing linker (Table 1). The order of potencies among the different series was: amines (**6a-d**) > amides (**4a-d**) > reverse amides (**5a-c**) > *O*-benzylated amides (**11a-c**,**e**). In the oligomethylene-linked hybrids, all linker lengths were well tolerated, even though, in general, octa- and nona-methylene-linked hybrids were slightly more potent. Conversely, the presence of an ethylene glycol motif within the linker had a clear detrimental effect on hAChE inhibitory activity, with hybrids **4d** and **6d** being 13- and 69-fold less potent than their counterparts **4b** and **6b**, respectively, which have an equivalent linker length. Overall, the most potent CR-6–chlorotacrine hybrids for hAChE

inhibition were the amines **6a** (IC_{50} = 442 pM), **6b** (IC_{50} = 121 pM), and **6c** (IC_{50} = 272 pM), which were 33-, 1200-, and 53-fold more potent than the parent Cl-THA, respectively.

Taking into account that the parent CR-6-based carboxylic acid **7** and amine **14** are essentially inactive or only very weakly active against hAChE, the fact that the vast majority of CR-6–chlorotacrine hybrids are more potent than 6-chlorotacrine indicates that the CR-6 scaffold of the novel hybrids positively contributes to their hAChE inhibitory potency, thereby highlighting the success of the hybridization strategy. It is well-known that 6-chlorotacrine interacts at the so-called catalytic anionic site (CAS) of AChE, placed at the bottom of a 20 Å-deep gorge.[28] We anticipated that the higher potency of the novel CR-6–chlorotacrine hybrids might arise from the simultaneous binding to CAS by the 6-chlorotacrine moiety and to a secondary binding site, the peripheral anionic site (PAS), located at the entrance of the catalytic gorge, by the CR-6 scaffold, as found in other families of tacrine-based hybrids.[29] In the case of hybrids **6a**-**c**, the presence of a basic aliphatic amino group within the linker, which should be protonated at physiological pH (and under the conditions of the assay of AChE inhibition), could enable additional interactions with aromatic or anionic midgorge residues, thereby leading to a triple site binding mode.[19b,30]

In 6-chlorotacrine-based hybrids, the chlorine atom, which is accommodated at a hydrophobic pocket within the CAS, greatly contributes to the inhibitory potency.[31] Thus, quite expectedly, hybrids **12a**-**c**,**e**, which feature an unsubstituted tacrine moiety, were 20–30-fold less potent hAChE inhibitors than the 6-chlorotacrine-based counterparts (**4a**-**c**), but still more potent (up to 5-fold) than tacrine itself (IC_{50} = 320 nM), further indicating a beneficial contribution of the CR-6 moiety and of the linker to the inhibitory activity towards hAChE.

Table 1. In Vitro Biological Profiling of the Novel CR-6–(Chloro)Tacrine Hybrids

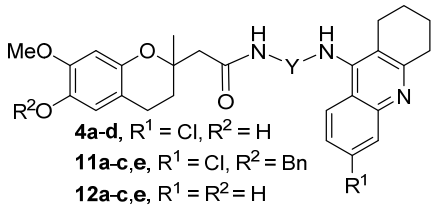

4a-d, R^1 = Cl, R^2 = H
11a-c,**e**, R^1 = Cl, R^2 = Bn
12a-c,**e**, R^1 = R^2 = H
Y: **a**, $(CH_2)_7$; **b**, $(CH_2)_8$; **c**, $(CH_2)_9$; **d**, $[(CH_2)_2OCH_2]_2$; **e**, $(CH_2)_6$

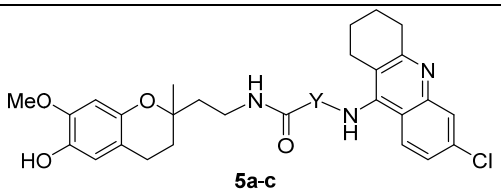

5a-c
Y: **a**, $(CH_2)_6$; **b**, $(CH_2)_7$; **c**, $(CH_2)_8$

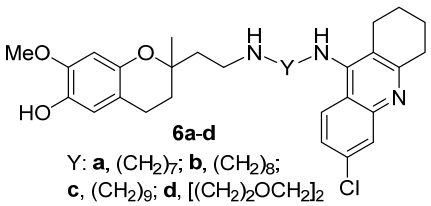

6a-d
Y: **a**, $(CH_2)_7$; **b**, $(CH_2)_8$; **c**, $(CH_2)_9$; **d**, $[(CH_2)_2OCH_2]_2$

Compd	hAChE IC_{50} (nM)[a]	hBChE IC_{50} (nM)[a]	DPPH IC_{50} (μM)[b]	BACE-1 % inhibition @5 μM (IC_{50} μM)[c]	Aβ42 aggregation % inhibition @10 μM[d]	tau aggregation % inhibition @10 μM[d]	PAMPA-BBB Permeability[e]
4a	5.43 ± 0.27	79.1 ± 3.7	15.2 ± 5.6	na[f]	< 10	< 10	9.7 ± 0.7 (CNS+)
4b	3.69 ± 0.19	170 ± 9	19.1 ± 5.6	19.0%	< 10	15.0 ± 2.1	9.6 ± 0.6 (CNS+)
4c	2.05 ± 0.11	168 ± 5	13.4 ± 5.1	na[f]	11.2 ± 3.1	12.6 ± 3.3	8.2 ± 0.5 (CNS+)
4d	47.9 ± 2.5	1840 ± 130	16.8 ± 5.0	na[f]	< 10	10.7 ± 2.0	7.0 ± 0.2 (CNS+)
5a	3.80 ± 0.24	102 ± 8	8.9 ± 1.6	na[f]	< 10	< 10	7.8 ± 0.2 (CNS+)
5b	7.94 ± 0.31	187 ± 7	15.1 ± 2.3	14.0%	< 10	12.5 ± 2.1	8.3 ± 1.3 (CNS+)
5c	6.23 ± 0.36	148 ± 4	13.1 ± 2.9	na[f]	11.0 ± 2.5	18.5 ± 3.1	8.7 ± 0.8 (CNS+)
6a	0.44 ± 0.04	17.4 ± 1.6	16.5 ± 3.7	na[f]	17.9 ± 4.0	29.0 ± 3.2	10.3 ± 0.2 (CNS+)
6b	0.12 ± 0.01	13.4 ± 0.9	6.9 ± 1.6	24.8%	27.9 ± 3.3	35.5 ± 2.8	12.5 ± 0.6 (CNS+)
6c	0.27 ± 0.02	18.3 ± 0.4	18.5 ± 1.7	28.1%	34.0 ± 2.8	48.2 ± 2.9	10.1 ± 1.3 (CNS+)
6d	8.35 ± 0.51	180 ± 9	17.8 ± 5.8	19.9%	< 10	17.6 ± 3.3	9.7 ± 0.6 (CNS+)
11a	6.99 ± 0.35	51.0 ± 1.8	na[f]	12.5 ± 0.4	< 10	20.8 ± 2.5	11.5 ± 0.5 (CNS+)
11b	10.4 ± 0.6	100 ± 5	na[f]	8.31 ± 0.26	24.4 ± 2.9	40.4 ± 2.8	12.3 ± 0.2 (CNS+)
11c	7.89 ± 0.42	30.6 ± 2.2	na[f]	7.19 ± 0.12	41.8 ± 2.5	55.2 ± 2.1	10.4 ± 0.7 (CNS+)
11e	11.0 ± 0.6	201 ± 11	na[f]	18.0 ± 1.9	4.4 ± 3.0	12.9 ± 3.5	10.7 ± 1.0 (CNS+)
12a	111 ± 5	4.28 ± 0.31	13.6 ± 5.6	na[f]	< 10	< 10	6.6 ± 0.8 (CNS+)

12b	69.8 ± 6.4	5.33 ± 0.49	19.4 ± 6.6	na[f]	17.4 ± 3.8	< 10	7.3 ± 0.9 (CNS+)
12c	57.8 ± 4.8	5.36 ± 0.24	14.7 ± 4.9	6.75%	16.4 ± 3.6	12.7 ± 2.1	8.9 ± 0.5 (CNS+)
12e	275 ± 38	4.99 ± 0.36	22.9 ± 6.7	na[f]	< 10	< 10	4.3 ± 0.3 (CNS±)
CR-6	nd[g]	nd[g]	17.4 ± 5.7	nd[g]	nd[g]	nd[g]	0.25[h]
7	na[i]	na[i]	14.9 ± 2.5	nd[g]	< 10	< 10	0.4 ± 0.02 (CNS–)
14	> 100,000[j]	> 23,000[k]	14.0 ± 3.3	nd[g]	< 10	< 10	1.0 ± 0.05 (CNS–)
THA	320 ± 10	35.2 ± 5.1	nd[g]	na	< 10	< 10	22.5 ± 0.3 (CNS+)
Cl-THA	14.5 ± 0.9	505 ± 28	na[f]	nd[g]	< 10	< 10	26.1 ± 0.6 (CNS+)

[a] IC_{50} inhibitory concentration (nM) towards human recombinant AChE and BChE from human serum. IC_{50} values are expressed as mean ± standard error of the mean (SEM) of at least two experiments, each performed in triplicate. [b] IC_{50} inhibitory concentration (μM) for DPPH radical scavenging activity. Values are expressed as mean ± standard deviation of single experiments performed in triplicate. Trolox (IC_{50} = 15.7 ± 0.9 μM) was also used as a reference compound. [c] % Inhibition of human recombinant BACE-1 at 5 μM or IC_{50} inhibitory concentration (μM). Values are expressed as mean ± standard deviation (SD) of two independent experiments, each performed in triplicate. Myricetin (IC_{50} = 3.82 ± 0.87 μM) was used as reference compound. [d] % Inhibition of Aβ42 and tau protein aggregation at 10 μM in intact *E. coli* cells. Values are expressed as mean ± SEM of nine independent experiments, each performed in duplicate. DP128[20] (% inhibition of Aβ42 and tau aggregation of 68.2 ± 2.1 and 72.2 ± 2.1, respectively, at 10 μM) was used as reference compound. [e] Permeability values (*Pe*, 10^{-6} cm s^{-1}) from the PAMPA-BBB assay. Values are expressed as the mean ± SD of three independent experiments, each performed in triplicate. [f] Not active. [g] Not determined. [h] Value taken from ref 16. [i] Not active at 100 μM. [j] IC_{50} = 101 ± 9 μM. [k] IC_{50} = 23.2 ± 1.1 μM.

Because the levels of AChE diminish as AD progresses, hydrolysis of the neurotransmitter acetylcholine is increasingly operated by BChE, which, thereby, is also considered an important target for AD treatment.[32] In contrast to the positive effect of the chlorine atom of 6-chlorotacrine on AChE inhibitory activity, its presence is detrimental for BChE inhibition, due to steric hindrance effects at the enzyme active site.[19b,30,33] Thus, tacrine (IC_{50} = 35.2 nM) is a clearly more potent hBChE inhibitor than 6-chlorotacrine (IC_{50} = 505 nM). Accordingly, the CR-6–chlorotacrine hybrids were found to be less potent inhibitors towards hBChE than hAChE.

Notwithstanding the AChE over BChE selectivity of these compounds, they still displayed potent hBChE inhibitory activity, with IC_{50} values in the two-digit nanomolar range in most cases (Table 1). Indeed, all of them turned out to be more potent hBChE inhibitors (3–40-fold) than the parent 6-chlorotacrine, with the sole exception of hybrid **4d**, bearing an ethylene glycol motif within the linker. Very gratifyingly, some of them (**6a**-**c** and **11c**) were even slightly more potent hBChE inhibitors than tacrine, despite the presence of the chlorine atom at their tacrine moiety. Some trends observed for hAChE inhibition were also found for hBChE inhibition. Thus, the potency within the different series varied in the same order: amines > amides > reverse amides; within a given series, similar potencies were found for the different oligomethylene-linked homologs; and the presence of an ethylene glycol within the linker caused a drop of activity. The only difference was the slightly higher potency of the *O*-benzylated amides **11** relative to the O-deprotected counterparts **4**.

Again, amines **6a** (IC_{50} = 17.4 nM), **6b** (IC_{50} = 13.4 nM), and **6c** (IC_{50} = 18.3 nM) were the most potent CR-6–chlorotacrine hybrids for hBChE inhibition, being 29-, 38-, and 28-fold more potent than the parent 6-chlorotacrine, and 2–3-fold more potent than tacrine.

Obviously, the hBChE inhibitory activity was even higher in the CR-6–tacrine hybrids **12a**-**c**,**e**, bearing a tacrine instead of a 6-chlorotacrine moiety. These hybrids displayed single-digit nanomolar hBChE inhibitory potencies, around 5 nM, i.e. potencies approximately 7-fold higher than that of tacrine.

Like for hAChE inhibition, the CR-6-based carboxylic acid **7** was inactive for hBChE inhibition, whereas the amine **14** displayed only moderate potency (IC_{50} = 23.2 μM).

All together, these results suggest that introduction of an inactive or weakly active CR-6 moiety adequately linked to the structure of the potent hAChE and hBChE inhibitors 6-chlorotacrine and

tacrine, respectively, significantly increases the anti-cholinesterase potencies of the resulting hybrids relative to both parent compounds.

The mechanism of inhibition of hAChE by the most potent compound, **6b**, was investigated by kinetic and propidium displacement studies, and by molecular dynamics simulations. Kinetic studies showed that **6b** acts as a mixed-type inhibitor of hAChE, hence presumably acting as a dual site inhibitor. It displayed an inhibitor dissociation constant (K_i) of 132 ± 36 pM and a dissociation constant for the enzyme–substrate–inhibitor complex (K'_i) equals to 258 ± 2 pM (Figure 2, left). We had inferred that the 6-chlorotacrine moiety of the hybrids should interact at the CAS of AChE, whereas the CR-6 scaffold would be interacting at the PAS. To further confirm interaction with PAS and estimate the inhibitor's affinity for this site, the ability of **6b** to displace the known PAS ligand propidium was assessed (Figure 2, right). Hybrid **6b** showed a dissociation constant K_D = 2.03 ± 0.09 μM, which further confirmed the ability to interact with the PAS of AChE, albeit with a lower affinity than that of the specific PAS ligand propidium (K_D = 0.7 μM).

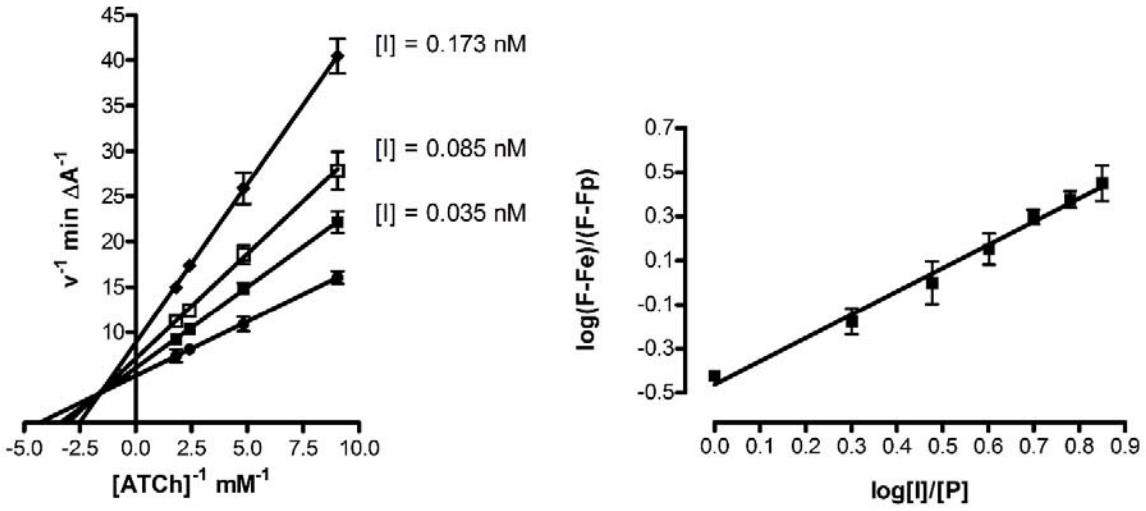

Figure 2. Mechanism of inhibition of hAChE by hybrid **6b**. Left, overlaid Lineweaver-Burk reciprocal plots showing the variation of the initial velocity rate (v) as a function of increasing substrate (acetylthiocholine - ATCh) in the absence and presence of increasing concentrations of **6b**. The mechanism of inhibition was assessed by two independent experiments, each performed in triplicate. Right, propidium displacement studies to determine the affinity for the PAS of AChE: P and I stand for propidium iodide and inhibitor (**6b**), respectively; F_e is the initial fluorescence intensity when enzyme sites are saturated with P; F_P is the fluorescence intensity when propidium is completely displaced from the enzyme; and F denotes the fluorescence intensity after adding a determined amount of displacing agent during the titration experiment. Data are the average of three independent experiments.

Finally, the binding mode and mechanism of inhibition of AChE by **6b** and its AChE over BChE selectivity was further studied by molecular dynamics (MD) simulations. In addition, MD were employed to decipher the molecular features responsible for the high BChE inhibitory activity of the most potent hybrid, **12a**. In these studies, the potential effect of the absolute configuration of the stereocenter at position 2 of the CR-6 moiety was assessed.

The stability of all the simulated enzyme–ligand complexes was confirmed by the RMSD analysis of the residues that define the binding site after the rearrangement of the peripheral site and the concomitant accommodation of the CR-6 moiety along the AChE gorge (Figure S1 of Supporting Information). Representative snapshots for (*R*)-**6b** and (*S*)-**6b** bound to AChE derived from MD simulations are shown in Figure 3. Both enantiomers of **6b** exhibit a very similar pattern of interactions except for the chroman moiety, which seems to take slightly different orientations along the gorge according to its stereochemistry. The 6-chlorotacrine moiety is stably stacked

against Trp86 and Tyr337 in the CAS (average distances of 3.6 and 4.3 Å from the planes of the chlorotacrine ring to the indole and phenol rings, respectively). The chlorine atom is placed into a small hydrophobic cavity formed by Trp439, Pro446, and Tyr449. The protonated quinoline nitrogen atom of the chlorotacrine moiety is engaged in hydrogen-bonding interaction with the carbonyl oxygen of the catalytic residue His447 (average N•••O distance of 2.8 Å). In addition, a salt bridge between the protonated aliphatic secondary amino group within the linker of **6b** and the carboxylate of Asp74 (average N•••O distance of 2.7 Å) confers stability to the aliphatic linker along the gorge in both enantiomers. This might contribute to stabilize the gorge through a network of interactions reinforced by the salt bridge formed between Asp74 with (*R*)-**6b** and (*S*)-**6b** (Figure 3). These interactions closely resemble those observed for the binding of tacrine–donepezil hybrids to hAChE.[34] In contrast with the common pattern of interactions observed for the 6-chlorotacrine ring and the tether in the AChE complexes with (*R*)-**6b** and (*S*)-**6b**, binding of the chroman moiety exhibits slight differences for the two enantiomers. Thus, the CR-6 moiety is located close to Trp286, even though without forming stacking interactions with this latter residue, adopting distinct arrangements in the two complexes. In turn, this suggests that the CR-6 moiety has a weak contribution to the binding affinity, which may be understood from the larger flexibility of the peripheral site (PAS) compared to the tight packing observed at the CAS, and the solvent exposure of the CR-6 moiety bound to the PAS cavity.

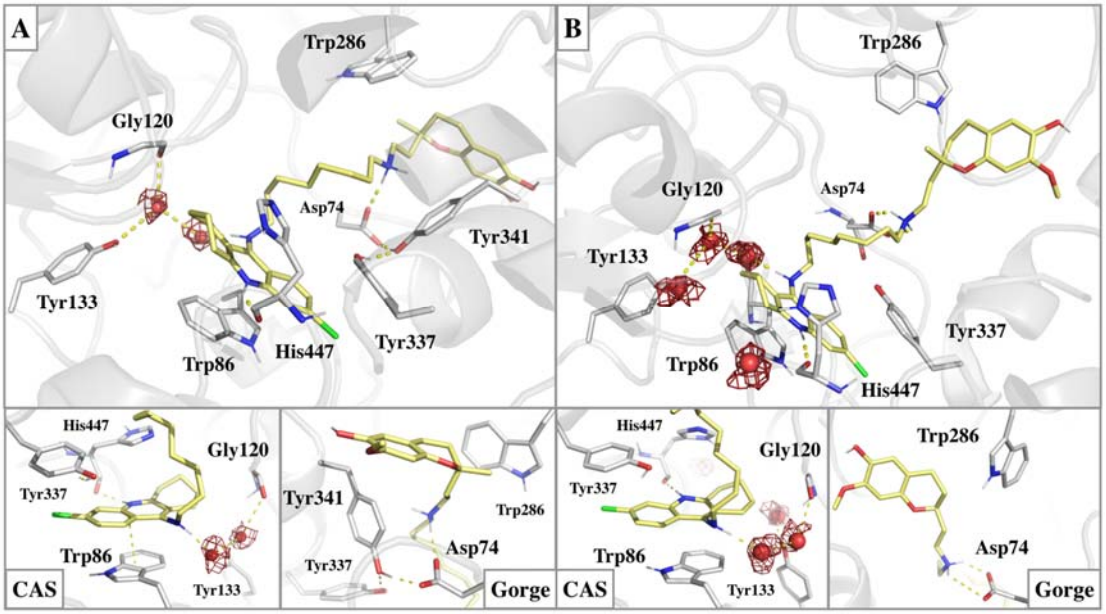

Figure 3. Representative snapshots of the complexes of (A) (*R*)-**6b** and (B) (*S*)-**6b** bound to hAChE taken from Molecular Dynamics simulations (started from PDB structure 1Q83). Bottom panels show details of the interactions at the CAS and along the gorge. Density maps for structural water molecules (shown as red spheres) within the catalytic site are depicted as red isomesh. Selected interactions are shown as yellow dashed lines.

Notwithstanding its higher activity towards hAChE (IC_{50} = 121 pM), hybrid **6b** can be definitively considered a very potent hBChE inhibitor (IC_{50} = 13.4 nM). To shed light on the AChE over BChE selectivity of **6b**, its binding mode within BChE was also studied by MD simulations. Hybrid **6b** adopts an extended conformation along the gorge of BChE, which resembles the arrangement found in the AChE complex (Figures S2 and S3 of Supporting Information). The structural integrity of the binding mode in the three independent MD simulations is supported by the stability of the RMSD profiles (Figure S2 of Supporting Information). However, the lower inhibitory activity against BChE may be attributed to the loss of the hydrophobic subpocket that

accommodates the chlorine atom of chlorotacrine due to replacement of Pro446 (in AChE) with Met437 (in BChE), necessary to stabilize the chlorine atom[35] as well as to the loss of the salt bridge formed between the protonated aliphatic nitrogen and Asp74, thus leading to the AChE over BChE selectivity profile of hybrid **6b**.

Finally, MD simulations were also run for both enantiomers of the tacrine-based hybrid **12a**, which is a selective BChE inhibitor (Figure 4; RMSD profiles are shown in Figure S4 of Supporting Information). A similar pattern of interactions was found for both enantiomers, especially regarding the chlorotacrine and tether moieties. The tacrine moiety of **12a** is stacked against Trp82 (average distance of 3.5 Å), with the protonated quinoline nitrogen atom being hydrogen-bonded to the carbonyl oxygen of His438 (average N•••O distance of 2.9 Å for both enantiomers). The absence of the chlorine atom at the tacrine moiety prevents the steric clash with Met437, thus contributing to the 3-fold enhanced BChE inhibitory activity of **12a** relative to **6b**. An extensive water-assisted hydrogen-bonding network involving Trp82, Tyr128, Glu197 and the aromatic amine nitrogen enables the stabilization of the protein–ligand complex. At the gorge, the linker amide group acts as hydrogen-bond acceptor with Asn68 (average N•••O distances of 3.0 Å for both enantiomers) and as a hydrogen-bond donor with Gln119/Ser287 (average N•••O distances of 2.8 (Gln119) and 3.5 (Ser287) Å) in the (*R*)- and (*S*)-enantiomers, respectively. Finally, the CR-6 moiety of hybrid **12a** is located at the PAS and forms transient hydrogen-bonding interactions with the main chain of Thr284 and Val279 (Figure 4A) and Val280 (Figure 4B).

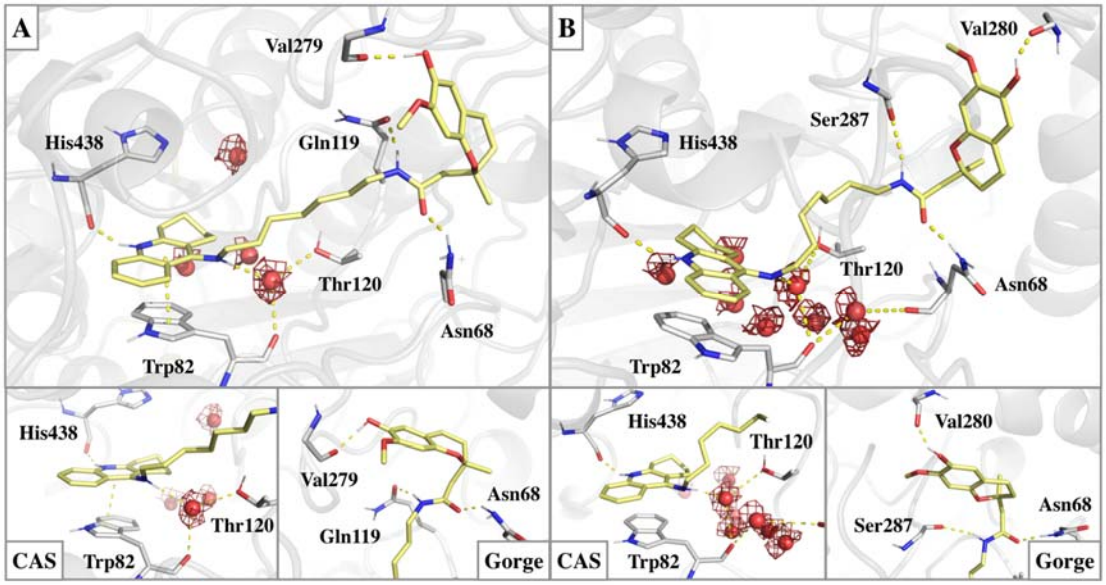

Figure 4. Representative snapshots of the complexes of (A) (*R*)-**12a** and (B) (*S*)-**12a** bound to hBChE taken from Molecular Dynamics simulations (started from PDB structure 5K5E). Bottom panels show details of the interactions at the catalytic site and along the gorge. Density maps for structural water molecules (shown as red spheres) within the catalytic site are depicted as red isomesh. Selected interactions are shown as yellow dashed lines.

Overall, both in vitro studies (kinetic and propidium displacement studies) and MD simulations support a multisite binding mode, with both pharmacophoric moieties and the functional group within the linker (amide or aliphatic amine) contributing to the stabilization of the binding. These multiple interactions account for the high inhibitory potency towards both enzymes.

In Vitro Antioxidant Activity. The in vitro antioxidant activity of the novel hybrids was evaluated by the widely used DPPH assay, which is based on the ability of antioxidant compounds to donate a hydrogen atom to scavenging the 2,2-diphenyl-1-picrylhydrazyl (DPPH) free radical.[36] Derivatization of the antioxidant lead CR-6 (IC_{50} DPPH = 17.4 μM) by introduction of distinct side chains at position 2 is compatible with the retention of the antioxidant activity.[16] Indeed, the CR-6-derived carboxylic acid **7** and amine **14** display the same antioxidant activity of the lead

(IC_{50} = 14.9 μM and 14.0 μM, respectively). Likewise, all the novel CR-6–chlorotacrine and CR-6–tacrine hybrids featuring a free hydroxyl group at position 6 of the CR-6 scaffold (**4a-d**, **5a-c**, **6a-d**, and **12a-c**,**e**) retain the antioxidant activity of the parent CR-6 or are even slightly more potent, with IC_{50} values in the 6.9–22.9 μM range (Table 1). As expected, hybrids **11a-c**,**e**, in which this key hydroxyl group is benzylated, were not active in this assay.

Thus, hybridization of the antioxidant lead CR-6 with 6-chlorotacrine or tacrine, devoid of antioxidant activity, resulted in compounds that displayed similar antioxidant activity as the lead or trolox (IC_{50} = 15.7 μM).[16]

In Vitro BACE-1 Inhibition. BACE-1 is the enzyme involved in the first rate-limiting step of the formation of Aβ by proteolytic cleavage of APP, and, hence, it is also a very important biological target in AD drug discovery.[37] Different classes of (chloro)tacrine-based hybrids have been found to be able to inhibit BACE-1[19b,38] with low micromolar potencies. We have recently found a novel class of hybrids bearing a huprine moiety, structurally related to 6-chlorotacrine, which displayed nanomolar BACE-1 inhibitory activity (IC_{50} = 80 nM).[19a,21] The 4-aminoquinoline system of the huprine moiety of these hybrids must be mostly protonated at physiological pH and in the acidic endosomal compartments (pH 4.5 to 6.5) where BACE-1 localizes. Molecular dynamics simulations have suggested that the protonated huprine moiety may establish a salt bridge with the aspartate residues of the catalytic dyad of BACE-1, whereas the second pharmacophore of these hybrids (the hydroxianthraquinone moiety of rhein) interacts with a transient secondary binding site, located at the edge of the catalytic site, mainly establishing a hydrogen bond between a carbonyl group of the hydroxianthraquinone moiety of the hybrid and the guanidinium group of Arg307.[21]

In this light, we screened the novel CR-6–(chloro)tacrine hybrids in vitro against human recombinant BACE-1, using the Panvera substrate. Most of the novel hybrids were found to be inactive or weak BACE-1 inhibitors, with percentages of inhibition below 30% at an inhibitor concentration of 5 μM. Only the *O*-benzylated hybrids **11a-c**,**e** displayed moderate inhibitory potency, with IC_{50} values from 7 μM to 18 μM (Table 1), i.e. in the same range of potency of other (chloro)tacrine-based hybrids but seemingly less potent that the rhein–huprine hybrid. However, it must be mentioned that the assay conditions used to assess the BACE-1 inhibitory activity of these novel hybrids and other previously developed in our group, including the rhein–huprine hybrids, were different.[19a-c] Previously, we had used the fluorogenic methoxycoumarin-Ser-Glu-Val-Asn-Leu~Asp-Ala-Glu-Phe-Lys-dinitrophenyl (M-2420), which mimics the APP sequence comprising the Swedish mutation, as the substrate. The M-2420 substrate is widely used due to its high specificity, predictivity, and quenching efficacy. However, M-2420 is not suitable for the characterization of all types of BACE-1 inhibitors due to its poor selective wavelengths for fluorescence measure ($\lambda_{ex}/\lambda_{em}$ 320/420). Indeed, due to fluorescence interferences of the novel CR-6–chlorotacrine hybrids under those assay conditions, we performed a FRET assay using Panvera substrate, instead of M-2420. The Panvera substrate is an octapeptide (Glu-Val-Asn-Leu~Asp-Ala-Glu-Phe) bearing the Swedish APP mutation. The k_{cat}/K_M value established for this sequence is 9.5-fold higher than that calculated for M-2420 decapeptide. On the contrary, the entire Panvera substrate is characterized by a reduced rate of substrate cleavage, which implies a longer incubation time than that required for M-2420 substrate. This can be likely ascribed to some steric hindrance due to the presence of the bulky rhodamine fluorophore and quenching group of the Panvera substrate. Despite the lower predictivity of the assay with Panvera substrate relative to that of the assay with M-2420, its

highly selective wavelengths for fluorescence measures enable the evaluation of the BACE-1 inhibitory activity for the majority of compounds, even those intrinsically colored.[36c] By using the new conditions with the Panvera substrate, the IC_{50} value of the rhein–huprine hybrid was 1.50 μM. Thus, the novel *O*-benzylated hybrids **11a-c**,**e** were still less potent than the rhein–huprine hybrid when using the same assay conditions, with 5-fold lower potencies in the best cases (**11b** and **11c**).

In Cellulo Aβ42 and Tau Antiaggregating Activity. The evaluation of the antiaggregating activity of several classes of (chloro)tacrine- or related huprine-based hybrids developed over the years in our group has shown that many of them display moderate to good potencies,[19] with percentages of inhibition up to 70–80% when tested at a 10 μM concentration in vitro or in a simplified in vivo model, namely intact *Escherichia coli* cells that overexpress the amyloidogenic protein, either Aβ42 or tau.[39] Interestingly, this antiaggregating activity was extensive to other completely unrelated amyloidogenic proteins associated with other neurologic and non-neurologic disorders and to fungal, yeast, and bacterial proteins. These findings made us hypothesize that common mechanisms exist that mediate the aggregation of amyloidogenic proteins, thereby making it possible the development of amyloid aggregation pan-inhibitors.[20]

To further characterize the biological effects of the novel CR-6–(chloro)tacrine hybrids, their Aβ42 and tau antiaggregating activities were assessed in *E. coli* cells. The series of 6-chlorotacrine- and tacrine-based amides and reverse amides were found to be inactive. Similarly, the parent compounds 6-chlorotacrine, tacrine, and the CR-6-derived carboxylic acid **7** and amine **14** were not active. Moderate antiaggregating potencies were found for the longer homologs of the series of amines (**6b** and **6c**) and *O*-benzylated amides (**11b** and **11c**), with percentages of inhibition around 30–50% at 10 μM (Table 1). Even if these activities were only

moderate, they seem to arise from the molecular hybridization, because, separately, none of the parent compounds is active in this assay. These results are in line with our hypothesis that hybrid compounds bearing two aromatic systems separated by linkers of suitable length display antiaggregating activity against amyloidogenic proteins, such as Aβ42 and tau.

In Vitro Brain Permeability. The ability to cross the BBB and enter the brain is a necessary condition for all drugs and candidates developed to treat central nervous system (CNS) diseases, such as AD. Indeed, poor brain permeability seems to be behind the failure of antioxidants in clinical trials against AD, in general, and is one of the major flaws of the antioxidant lead CR-6, in particular. When designing CR-6-based multitarget compounds we had anticipated that its hybridization with the lipophilic AChE inhibitor 6-chlorotacrine should result in sufficiently increased lipophilicity to make the hybrids brain permeable through passive diffusion. To validate our hypothesis and assess the suitability of the novel CR-6–chlorotacrine hybrids as potential anti-Alzheimer agents, their brain permeability was evaluated using the well-established PAMPA-BBB assay.[40] The permeability (P_e) of the novel hybrids, the parent compounds 6-chlorotacrine, tacrine, and the CR-6-derived carboxylic acid **7** and amine **14**, and fourteen commercial drugs, used for assay validation, was measured through a lipid extract of porcine brain membrane. Based on the linear correlation between the reported and experimentally determined P_e values of the commercial drugs and the limits established by Di et al. for BBB permeation,[40] the threshold for high BBB permeation (CNS+) was set at P_e (10^{-6} cm s^{-1}) > 5.2, whereas low BBB permeation (CNS–) was expected for compounds with P_e (10^{-6} cm s^{-1}) < 2.0.

Gratifyingly, all the novel CR-6–chlorotacrine hybrids displayed PAMPA-BBB permeabilities well over the threshold for high permeation and between the P_e values of the parent polar CR-6-

based intermediates **7** and **14** [P_e (10^{-6} cm s^{-1}) = 0.4 and 1.0, respectively, both CNS–] and those of the lipophilic 6-chlorotacrine and tacrine [P_e (10^{-6} cm s^{-1}) = 26.1 and 22.5, respectively, both CNS+]. Thus, P_e (10^{-6} cm s^{-1}) values in the range 7.0–12.5 were found for 6-chlorotacrine-based hybrids (**4a-d**, **5a-c**, **6a-d**, and *O*-benzylated hybrids **11a-c**,**e**) and in the range 6.6–8.9 for tacrine-based hybrids (**12a-c**). Only the shorter homolog of the tacrine-based series, **12e**, showed an uncertain brain permeability (CNS±) with a P_e value slightly lower than that of the CNS+ threshold. Overall, these results suggested that molecular hybridization of CR-6 and 6-chlorotacrine resulted in brain permeable compounds.

In Vivo Studies. Selection of Compounds. The antioxidant lead CR-6 had been found to exert, at some extent, neuroprotective effects in in vivo studies, despite its poor brain permeation.[15] After having assessed in vitro the success of the hybridization strategy of CR-6 with 6-chlorotacrine, in terms of both multitarget profile and brain permeation, we decided to further advance to in vivo efficacy studies with selected compounds. Several compounds out of the 19 novel CR-6–(chloro)tacrine hybrids displayed an interesting in vitro multitarget profile and could be suitably selected for the in vivo studies. Indeed, many of the compounds displayed very potent hAChE and hBChE inhibitory activities and retained the antioxidant potency of the lead CR-6. This was certainly the case of the amines **6a-c**, which were overall the most potent anticholinesterase compounds, with IC_{50} values in the subnanomolar range for hAChE inhibition (0.12–0.44 nM) and low nanomolar range for hBChE inhibition (13.4–18.3 nM). However, these effects were largely disbalanced with their other activities, namely antioxidant, BACE-1 inhibition, and antiaggregating potencies in the micromolar range. This might render difficult the selection of a proper dose for in vivo studies that could lead to antioxidant or anti-amyloid effects without the risk of cholinergic side-effects. In contrast, the *O*-benzylated compounds **11a**-

c were devoid of antioxidant activity but endowed with the best BACE-1 and Aβ42 and tau antiaggregating activities. Even if in the micromolar range, these activities were not so markedly disbalanced with their 1−2-digit nanomolar anticholinesterase potencies as they were in amines **6a-c**. Moreover, we speculated with the possibility that the *O*-benzylated hybrids **11** could be metabolically transformed, at least in part, into the *O*-debenzylated compounds, i.e. the corresponding hybrids of the amide series **4**, through a CYP-mediated *O*-dealkylation. This is a conceivable metabolic process as it would involve a benzylic position that, *per se*, is prone to CYP-mediated oxidation. This metabolic conversion would restore the free hydroxyl group at position 6 of the chroman scaffold. Thus, the generated metabolite would be able to exert antioxidant effects.

In the light of these considerations and also taking into consideration that they have the same total linker length and very similar anticholinesterase and antiaggregating potencies as the so far in vivo best-performing huprine-based multitarget compound developed in our group,[19a] we selected hybrid **11b** and its *O*-debenzylated counterpart, **4b**, to be further advanced to in vivo efficacy studies. Each of these compounds displayed an interesting and distinct, complementary mutitarget profile: **4b**, displayed the initially pursued anticholinesterase/antioxidant/brain permeable profile, while **11b** was devoid of antioxidant effect but exhibited additional moderate BACE-1 and Aβ42 and tau antiaggregating effects (Figure 5).

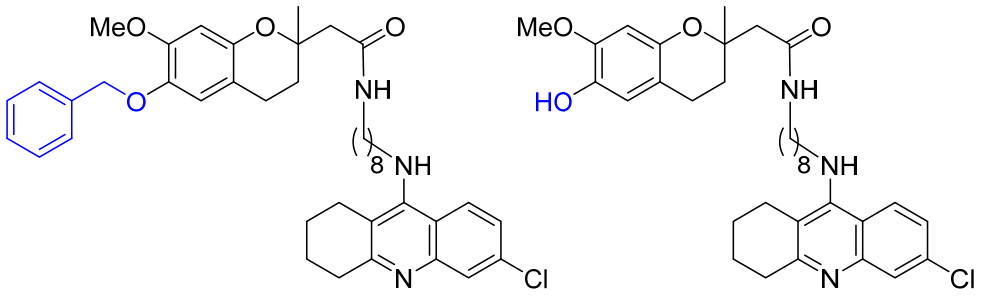

	11b	**4b**
IC_{50} hAChE:	**10.4 nM**	**3.7 nM**
IC_{50} hBChE:	**100 nM**	**170 nM**
IC_{50} DPPH:	**not active**	**19.1 μM**
IC_{50} hBACE-1:	**8.31 μM**	**19% at 5 μM**
Inh. Aβ42 aggreg:	**24% at 10 μM**	**7% at 10 μM**
Inh. tau aggreg:	**40% at 10 μM**	**15% at 10 μM**
P_e (10^{-6} cm s^{-1}):	**12.3 (CNS+)**	**9.6 (CNS+)**

Figure 5. In vitro biological profile of the selected compounds for in vivo efficacy studies.

In Vivo Assessment of Acute Toxicity and Dose Selection. The in vivo studies were performed as depicted in Figure 6. First, a preliminary assessment of acute toxicity was carried out for the selection of the dose to be used in the chronic efficacy studies. For this purpose, three doses (5, 10, and 15 mg/kg) of the selected hybrids **4b** and **11b** were injected intraperitoneally to wild-type (WT) C57BL6/J mice, and their general health status based on the appearance of physical signs was monitored from 5 min to 24 h after injection (time points: 5 min, 10 min, 15 min, 30 min, 1 h, 2 h, 3 h, 6 h, 8 h, 24 h). The doses of 5 and 10 mg/kg of both hybrids were well tolerated. After ip injection of the highest dose of 15 mg/kg of **4b**, some side effects appeared, with the animals showing reduced locomotor activity, piloerection, ptosis, and tremor. All these effects started disappearing 30 min later, and 3 h after administration the animals were normally active, without any physical sign of unhealthy status. The highest dose of 15 mg/kg of the *O*-benzylated hybrid **11b** produced the same side effects but delayed in time, as they appeared 10-15 min after

ip injection. Like with **4b**, the animals looked completely normal 3 h after the administration of **11b**. The delayed appearance of the same side effects could be related to the speculated metabolic conversion of **11b** into **4b**, which might be responsible for the transient side effects, with the delay of their appearance resulting from the time needed for the metabolic debenzylation process.

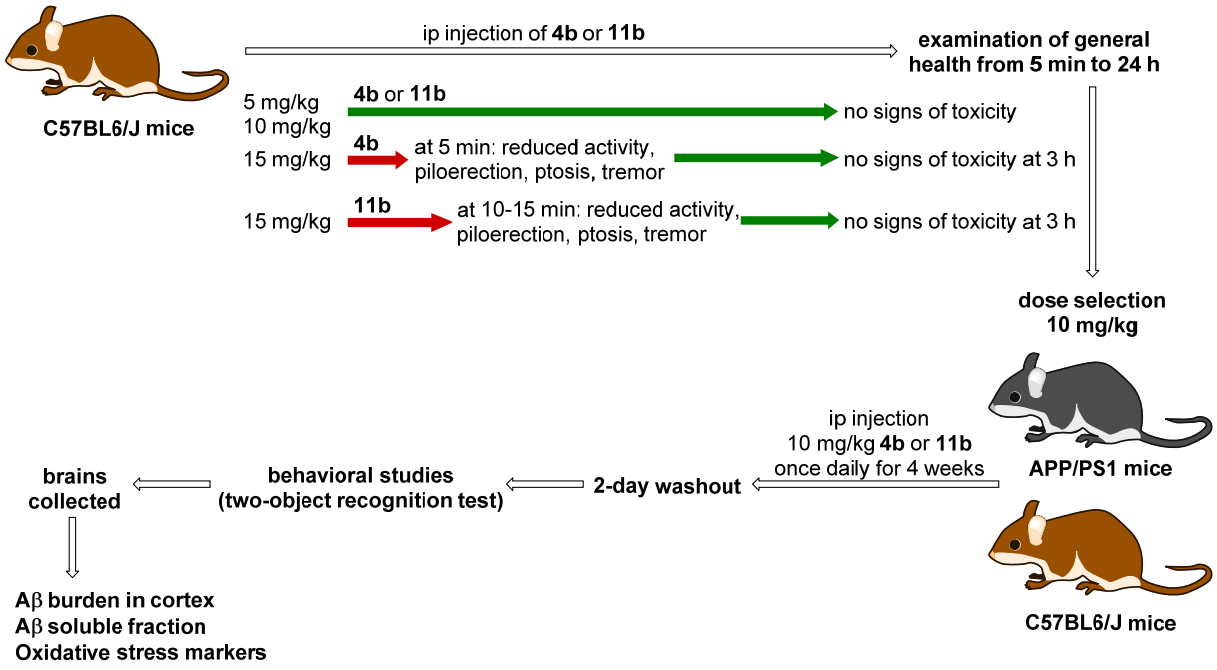

Figure 6. Flow diagram of in vivo efficacy studies with the novel CR-6–chlorotacrine hybrids **4b** and **11b**.

Chronic In Vivo Efficacy Studies. Behavioral Studies. The in vivo proof-of-concept for the novel class of CR-6-based hybrids was performed using double transgenic APP/PS1 mice, a well-established mouse model of AD. The main purpose of these studies was to determine whether the multiple activities found in vitro for the novel hybrids would impact the progression of the neurodegenerative process in vivo, i.e. to assess potential disease-modifying effects. To this end,

6-month-old WT and transgenic mice were daily administered with vehicle, **4b** (10 mg/kg, ip), or **11b** (10 mg/kg, ip) for 4 weeks. Following the chronic treatment, a 2-day washout period was applied,[41] before animals' cognitive performance evaluation.

To assess the effects of **4b** and **11b** on cognitive performance, the two-object recognition test was used. One day after letting mice explore for 9 min a V-maze with two identical objects situated at the ends of the arms, one of the two familiar objects was replaced by a novel one and the mice were placed again for 9 min in the V-maze. The time spent exploring both objects was recorded, to calculate an object recognition index (RI) as the difference between the time spent exploring the novel and the familiar object, divided by the total time spent exploring the two objects. Low object RI values are indicative of memory impairment. Two-way ANOVA revealed a genotype effect ($F_{(1, 24)} = 8.241$, $p < 0.01$) but no treatment effect or interaction between both factors. Subsequent *post hoc* analysis indicated a significant memory impairment in vehicle-treated APP/PS1 mice ($p < 0.05$, Figure 7) when compared to corresponding WT littermates, but not in hybrid **4b**- and **11b**-treated APP/PS1 mice. Indeed, **4b**- and **11b**-treated APP/PS1 mice did not worsen their cognitive performance compared to treated WT littermates. Notably, although not statistically significant, hybrid **4b** showed a tendency to increase the RI in APP/PS1 relative to vehicle-treated mice, which might suggest cognitive enhancing properties for this compound (Figure 7).

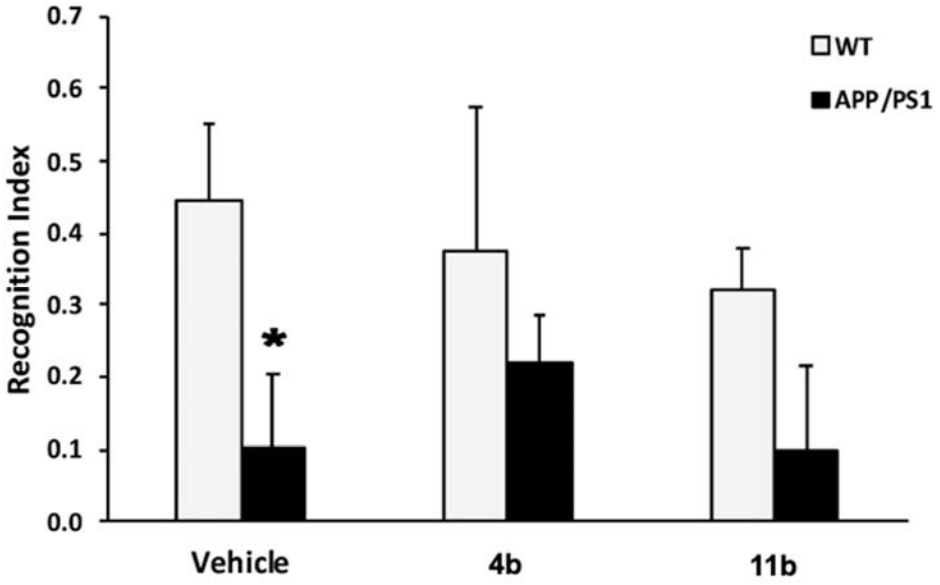

Figure 7. Memory performance in the two-object recognition test of male wild-type (WT Vehicle, n = 6; WT **4b**, n = 5; WT **11b**, n = 6) and male APP/PS1 (APP/PS1 Vehicle, n = 5; APP/PS1 **4b**, n = 7; APP/PS1 **11b**, n = 6) mice after chronic treatment with the novel hybrids **4b** and **11b** (10 mg/kg/day, 4 weeks, ip). APP/PS1 mice chronically treated with vehicle, but not with **4b** or **11b**, exhibit a significant reduction in the recognition index when compared to corresponding WT littermates. Data are expressed as the mean values ± SEM. Data were analyzed by two-way ANOVA with genotype ($p < 0.01$) and treatment as between factors, followed by two-tail Student's *t*-test to compare between genotypes (* $p < 0.05$).

Effects on Cortical APP/PS1 Mouse Amyloid Pathology. APP/PS1 mice already present amyloid plaques at the age of six months.[42] The effects of treatment with hybrids **4b** and **11b** on the amyloidogenic and non-amyloidogenic pathways were assessed. To this end, once the behavioral experiments were finished, the animals were sacrificed and their brains collected and processed for the quantification of several markers of amyloid pathology, namely cortical amyloid burden and cortical soluble Aβ40 and Aβ42 levels. Gene expression of *Adam10* (*α-secretase*) and

Bace1 (*β-secretase*), and brain levels of ADAM10, BACE-1, sAPPα (a product resulting from APP cleavage by α-secretase, non-amyloidogenic pathway) and sAPPβ (a product resulting from APP cleavage by β-secretase, amyloidogenic pathway) were also quantified.

First, the analysis of Aβ burden in the cortex of APP/PS1 mice treated with the novel hybrids, especially **4b**, indicated a tendency to decrease the Aβ content, although one-way ANOVA revealed that the changes were not statistically significant (Figure 8A,B). Similarly, no significant difference was observed between vehicle and **4b**- or **11b**-treated APP/PS1 mice in the cortical soluble Aβ40 or Aβ42 levels, two of the most toxic forms of Aβ peptide (Figure 8C).

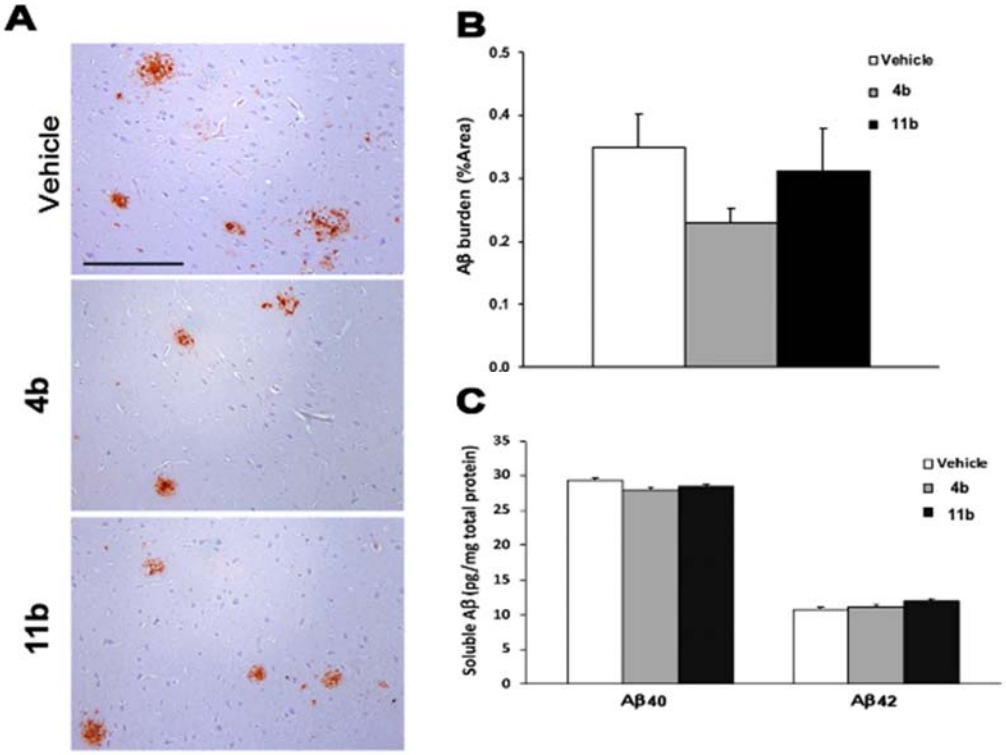

Figure 8. (A) Representative images of Aβ immunoreactivity in cortical sections of male APP/PS1 mice subjected to chronic vehicle (n = 5), **4b (**n = 7), or **11b** (n = 6) treatment. Scale bar represents 200 μm. (B) Aβ burden quantification reveals a tendency to decrease in the cortex of **4b**-treated APP/PS1 mice. (C) Soluble $A\beta_{40}$ and $A\beta_{42}$ levels are not significantly modified by

chronic **4b** or **11b** treatment in cortical homogenates of APP/PS1 mice. Data are expressed as the mean values ± SEM and were analyzed by one-way ANOVA with treatment as between factor (not significant in any case).

Next, while evaluation of *Adam10* in vehicle-treated animals revealed a reduction in APP/PS1 when compared with WT littermate mice, *Bace1* gene expression was higher in APP/PS1 mice (Figure 9A,B). These results agreed with the expected preponderance of the amyloidogenic pathway of APP processing in APP/PS1 transgenic mice, leading to amyloid pathology. However, when evaluating the corresponding protein levels (ADAM10 and BACE-1) we could observe only a tendency, which not fully confirmed gene expression results (Figure 9C,D). In **11b**-treated APP/PS1 mice, it was found a significant increase of gene expression of *Adam10*, whereas in **4b**-treated mice the increase was not statistically significant. In contrast, both compounds were found to be able to significantly reduce *Bace1* gene expression (Figure 9A,B). However, these promising results regarding gene expression of *Adam10* (increased by hybrids **4b** and **11b**) and *Bace1* (decreased by **4b** and **11b**) did not correlate with the brain levels of the corresponding proteins ADAM10 and BACE-1, except in the case of hybrid **11b**, which also led to increased protein levels of ADAM10 (Figure 9C,D). Overall, these results could be indicative that hybrids **4b** and **11b** might impinge into ADAM10 and BACE-1 expression processes (i.e. post-transcriptional, translational and protein degradation regulation) controlling steady-state protein abundances, thus making it difficult to establish any correlation between mRNA expression and protein density, as suggested for some perturbed systems.[43]

Finally, regarding the soluble fragments arising from APP cleavage via α-secretase (non-amyloidogenic pathway, sAPPα) or via BACE-1 (amyloidogenic pathway, sAPPβ), non-

significant differences were found among groups, except for **11b**, which significantly reduced sAPPβ protein levels in WT and APP/PS1 relative to vehicle-treated animals (Figure 9E-F). Collectively, these results might point to a possible beneficial effect of **4b** and **11b** pushing up the non-amyloidogenic pathway, thus overcoming the deleterious effects of the amyloidogenic one.

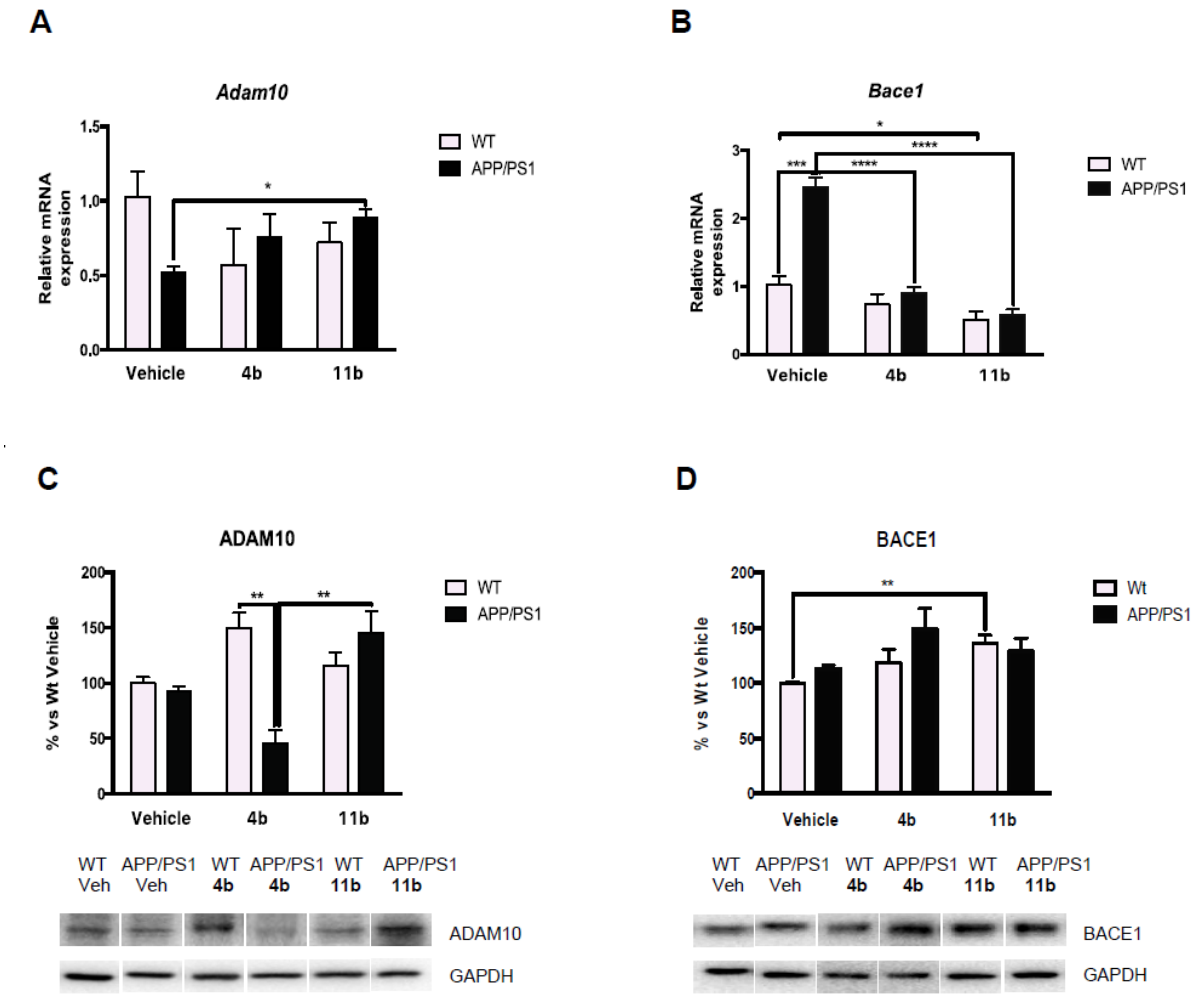

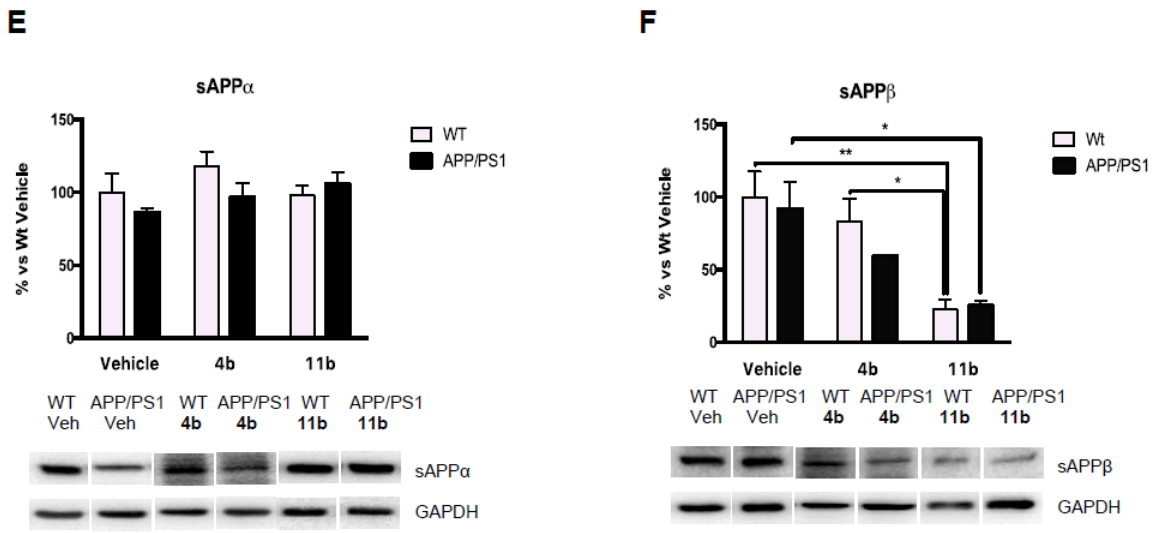

Figure 9. (A) Gene expression of *Adam10 (α-secretase)* and (B) *Bace1 (β-secretase);* (C) Representative Western blot and quantification for ADAM10, (D) BACE1, (E) sAPPα and (F) sAPPβ in cortical samples from treated male mice (WT Vehicle, n = 6; WT **4b**, n = 5; WT **11b**, n = 6; APP/PS1 Vehicle, n = 5; APP/PS1 **4b**, n = 7; APP/PS1 **11b**, n = 6). Data are expressed as the mean values ± SEM. Data were analyzed by two-way ANOVA with genotype and as between factors, followed by two-tail Student's *t*-test to compare between genotypes or Tukey's *post hoc* test to compare between treatments. *p<0.05, **p<0.01, ***p<0.001; ****p<0.0001.

Effects on Oxidative Stress Markers in Cortex of APP/PS1 Mice. Antioxidants can exert their effects in vivo by directly preventing the formation or scavenging radicals and oxidant species and by upregulating the expression of antioxidant enzymes or inhibiting pro-oxidant enzymes.[9a] Several of these markers of oxidative stress were evaluated in cortical samples of treated mice. Increased levels of markers of protein oxidation, such as protein carbonyls, are found in brains of AD and MCI patients. The level of carbonylated proteins generated by oxidative reactions was measured. Two-way ANOVA revealed a genotype effect ($F_{(1, 24)} = 3.784$, $p < 0.05$), with APP/PS1

mice having clearly higher levels of oxidized proteins in cortex than WT littermates (Figure 10). Treatment of transgenic mice with the novel hybrids **4b** and **11b** led to a tendency to reduce the levels of oxidized proteins compared with the vehicle-treated group, but the decrease was not statistically significant (Figure 10).

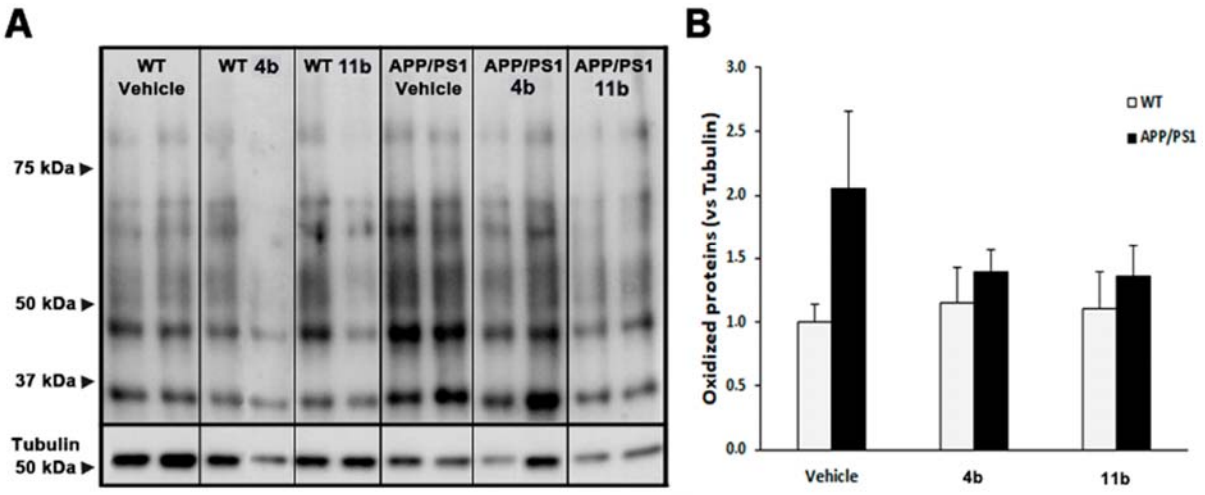

Figure 10. (A) Representative immunoblot for oxidized proteins (upper panel) and corresponding β-tubulin loading control (lower panel) from cortical samples of treated male mice (WT Vehicle, n = 6; WT **4b**, n = 5; WT **11b**, n = 6; APP/PS1 Vehicle, n = 5; APP/PS1 **4b**, n = 7; APP/PS1 **11b**, n = 6). Black triangles indicate the molecular weight of proteins. (B) Optical density quantification of the immunoblots normalized with respect to WT-vehicle group. Data are expressed as the mean values ± SEM and were analyzed by two-way ANOVA with genotype ($p < 0.05$) and treatment as between factors, followed by two-tail Student's *t*-test to compare between genotypes.

The enzyme superoxide dismutase 2 (SOD2) is involved in scavenging ROS produced by mitochondrial electron transport chain, which are markedly overproduced in the surrounding Aβ

deposition areas.[44] The levels of SOD2 around Aβ plaques were analyzed by double immunostaining in brain tissue of APP/PS1 mice. A tendency to increase the levels of the antioxidative enzyme SOD2 was found in **11b**-treated animals, even though it did not reach statistical significance (Figure 11).

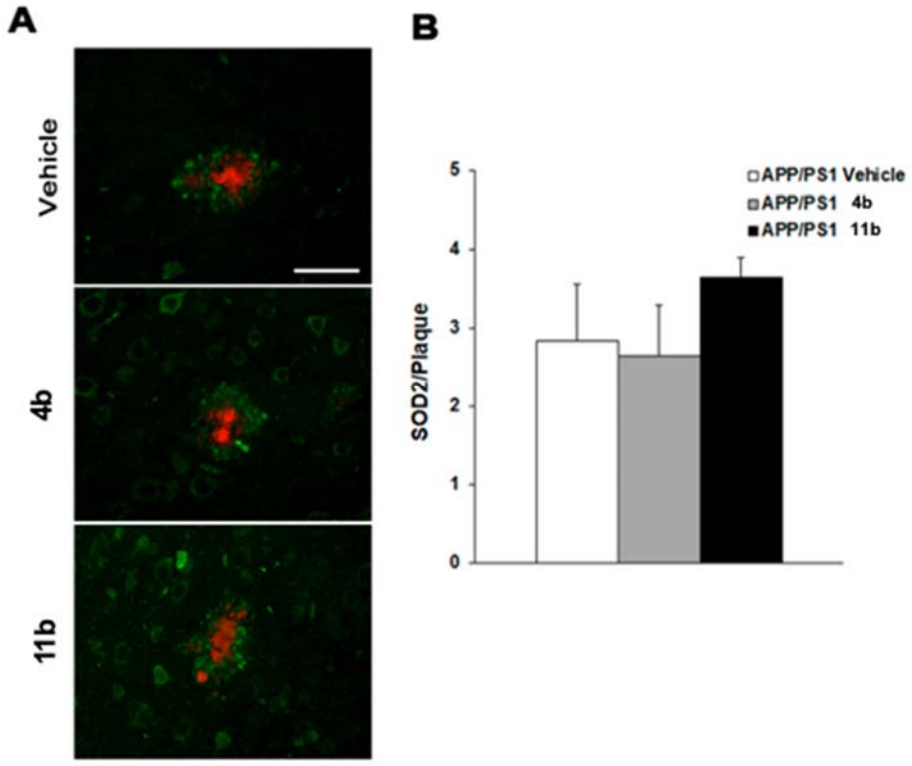

Figure 11. (A) Representative images of double SOD2 (green) and Aβ (red) immunostaining in cortical sections of male APP/PS1 mice chronically treated with vehicle (n = 5), **4b (**n = 7), or **11b** (n = 6). Scale bar represents 50 μm. (B) Quantification of the SOD2 staining around the Aβ plaques reveals a tendency to increase the levels of this enzyme involved in ROS neutralization in **11b**-treated APP/PS1 respect to vehicle-treated mice, but this increase does not reach the statistical significance. Data are expressed as the mean values ± SEM and were analyzed by one-way ANOVA with treatment as between factor (not significant).

Despite the lack of statistical significance, we observed a tendency to decrease oxidized proteins in both **4b**- and **11b**-treated APP/PS1 mice and to increase the antioxidant enzyme SOD2 after treatment with **11b.** The nuclear factor-erythroid 2-related factor 2 (Nrf2) is an emerging regulator of cellular oxidative stress as it controls the expression of an array of antioxidant genes, such as heme oxigenase 1 (Hmox1) and several genes related to glutathione production and regeneration, among others. To shed light into the mechanisms behind the in vivo antioxidant effects of the novel hybrids, Nrf2 protein levels in the cortex of treated animals were determined (Figure 12A). Interestingly, treatment with hybrid **11b** led to significantly increased total levels of the transcription factor Nrf2 in APP/PS1 mice. The enzymes catalase and glutathione peroxidase 1 (GPX1) are also part of the protective antioxidant system. The levels of the antioxidant enzyme catalase increased after treatment with both **4b** and **11b**, although it did not reach significance (Figure 12B), whereas GPX1 protein levels were significantly increased in **4b**-treated APP/PS1 mice (Fig 12C). Moreover, gene expression for inducible nitric oxide synthase (*iNOS*) and *Hmox1* was evaluated. *iNOS* gene expression was not modified with treatments, but *Hmox1* expression was significantly increased in **4b**-treated animals (Figure 12D,E).

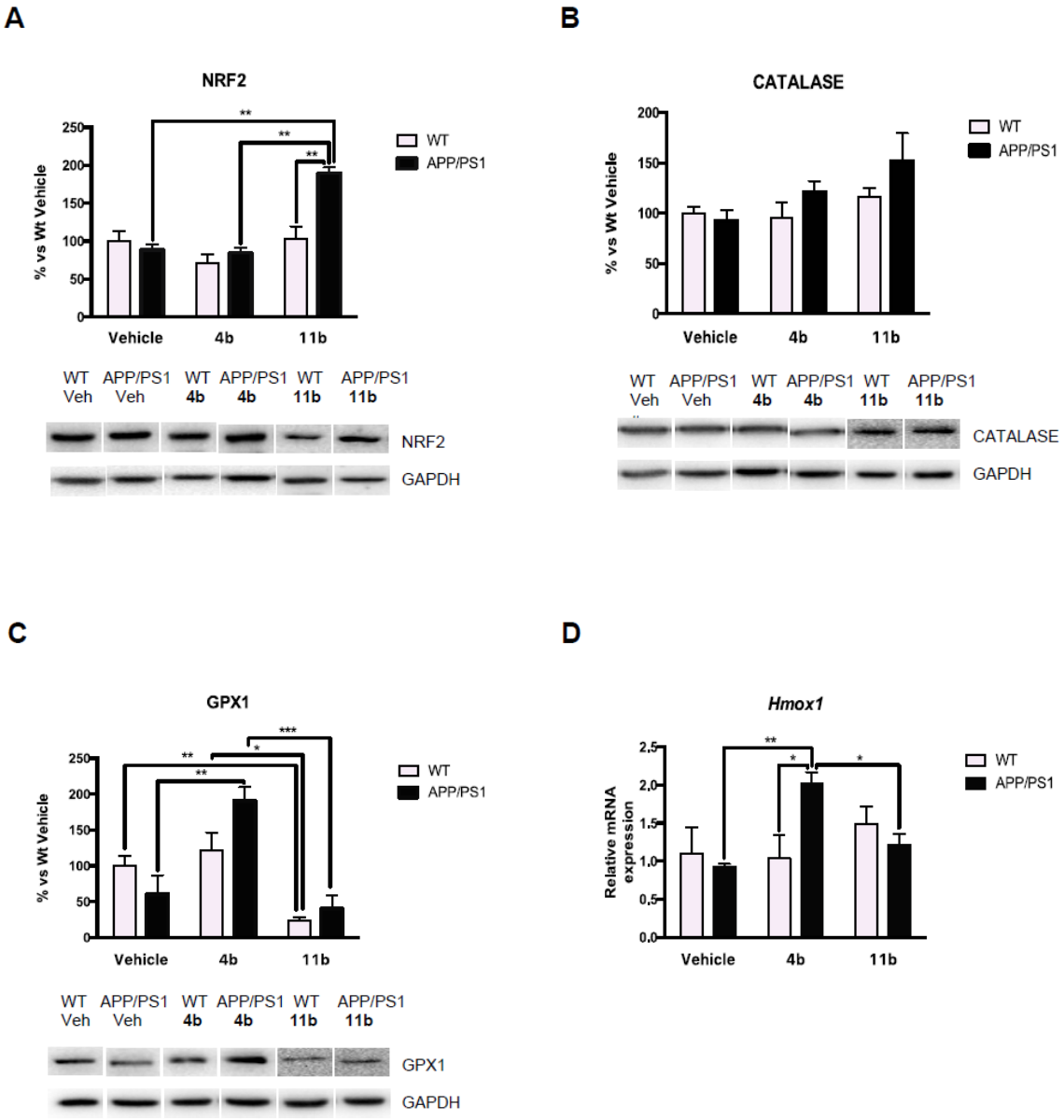
A
NRF2
% vs Wt Vehicle
250
200
150
100
50
0
**
**
**
WT
APP/PS1
Vehicle
4b
11b
WT Veh
APP/PS1 Veh
WT 4b
APP/PS1 4b
WT 11b
APP/PS1 11b
NRF2
GAPDH
B
CATALASE
% vs Wt Vehicle
200
150
100
50
0
WT
APP/PS1
Vehicle
4b
11b
WT Veh
APP/PS1 Veh
WT 4b
APP/PS1 4b
WT 11b
APP/PS1 11b
CATALASE
GAPDH
C
GPX1
% vs Wt Vehicle
250
200
150
100
50
0
***
**
*
**
WT
APP/PS1
Vehicle
4b
11b
WT Veh
APP/PS1 Veh
WT 4b
APP/PS1 4b
WT 11b
APP/PS1 11b
GPX1
GAPDH
D
Hmox1
Relative mRNA expression
2.5
2.0
1.5
1.0
0.5
0.0
**
*
*
WT
APP/PS1
Vehicle
4b
11b

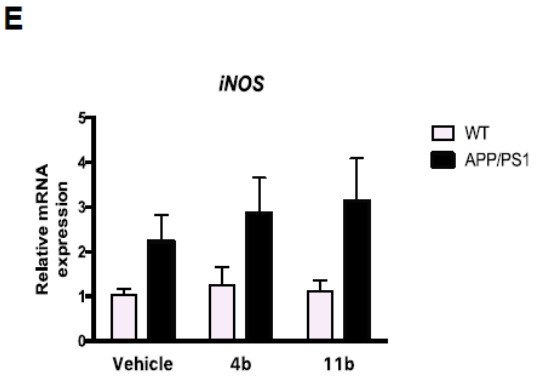

Figure 12. Representative Western blot and quantification for Nrf2 (A), catalase (B), and GPX1 (C) in cortical samples from treated male mice (WT Vehicle, n = 6; WT **4b**, n = 5; WT **11b**, n = 6; APP/PS1 Vehicle, n = 5; APP/PS1 **4b**, n = 7; APP/PS1 **11b**, n = 6). Data show a tendency to increase in antioxidant defense markers in APP/PS1 mice treated with the novel hybrids **4b** or **11b**. Moreover, **4b** treatment increases GPX1 levels in APP/PS1 mice compared to vehicle group. Representative gene expression of *Hmox1* (D) and *iNOS* (E). Hybrids **4b** and **11b** seem to increase *Hmox1* and *iNOS* gene expression, but only **4b** in the first case reaches statistical significance. Data are expressed as the mean values ± SEM and were analyzed by two-way ANOVA with genotype and as between factors, followed by two-tail Student's *t*-test to compare between genotypes or Tukey's *post hoc* test to compare between treatments. *p<0.05, **p<0.01, ***p<0.001.

While non-significant positive tendencies were found for several oxidative stress markers in treated APP/PS1 mice, compound **4b** did significantly increase GPX1 protein levels and *Hmox1* expression, whereas **11b** treatment led to a significant increase of Nrf2 protein levels. These results might suggest that **4b** and **11b** exert antioxidant effects in vivo either directly increasing

detoxifying enzymes against redox misbalance or inducing a slow antioxidant response by modulation of Nrf2 pathway.

Plasma and Microsomal Stability Studies and Metabolite Identification. Metabolism of drugs, while increasing their polarity to speed clearance from the organism, can lead to active metabolites that contribute to the final biological effect or to reactive metabolites that can cause harmful effects. The latter seems to be the case for tacrine, the first drug approved for the treatment of AD, which was withdrawn from the market due to induction of hepatotoxicity in 30% of patients. Its toxic effect seems to be largely dependent on the formation of toxic metabolites. Indeed, some metabolites arising from microsomal hydroxylation at position 1, 2, 4, and 7 of tacrine have been suggested to account for its hepatotoxic effects.[45] However, these toxic effects are not shared by all tacrine derivatives. For example, a recently reported family of trolox−tacrine hybrids, featuring a chroman-based trolox moiety, a tacrine or 6-chlorotacrine unit, and oligomethylene linkers functionalized with an amide group were found to be in general less toxic to human hepatoma HepG2 cells than tacrine and 6-chlorotacrine.[46] The almost negligible toxicity on human hepatic cells of some of these compounds could be ascribed to the formation of nontoxic metabolites, as suggested by in vitro microsomal stability studies. After 1 h of incubation of one of these trolox−chlorotacrine hybrids (Figure 13) with human liver microsomes, no significant metabolic changes in the 6-chlorotacrine unit of the hybrid were found, i.e. potentially toxic hydroxylated tacrine metabolites were not formed.[46] Instead, the main metabolite resulted from the reactivity of the chroman trolox moiety, namely a *p*-benzoquinone arising from oxidative ring opening (Figure 13).[46] The oxidative opening of the chroman ring might be another potential focus of reactive metabolites, and, hence, of toxicity, as the benzoquinone could react as a Michael acceptor with

nucleophilic protein residues. However, this did not seem to be the case, in the light of the reported negligible toxicity of the trolox–tacrine hybrid both in vitro against human hepatocytes and also in acute toxicity studies in rats.[46]

This type of *p*-benzoquinone metabolites has been also reported for other chroman derivatives, such as the naturally occurring ɣ-tocopherol and α-tocopherol. Actually, in the latter case the *p*-benzoquinone has been found to be the major metabolite in vivo (Figure 13).[47] Interestingly, not only does the *p*-benzoquinone metabolite of α-tocopherol not cause toxicity but it is efficiently reduced by several biological systems, including rat liver microsomal, mitochondrial, and cytosolic preparations, to form the corresponding hydroquinone metabolite, which is indeed more important for antioxidant activity than α-tocopherol itself.[48]

Likewise, it has been reported that incubation of CR-6 with rat liver microsomes leads to the formation of the *p*-benzoquinone metabolite, in equilibrium with its ring-closed spiro derivative arising from a nonenzymatically-promoted cyclization, and the corresponding hydroquinone (Figure 13).[49] Also in this case, the formation of the potentially toxic benzoquinone did not seem to be an issue, as the in vivo toxicity of CR-6 is very low.

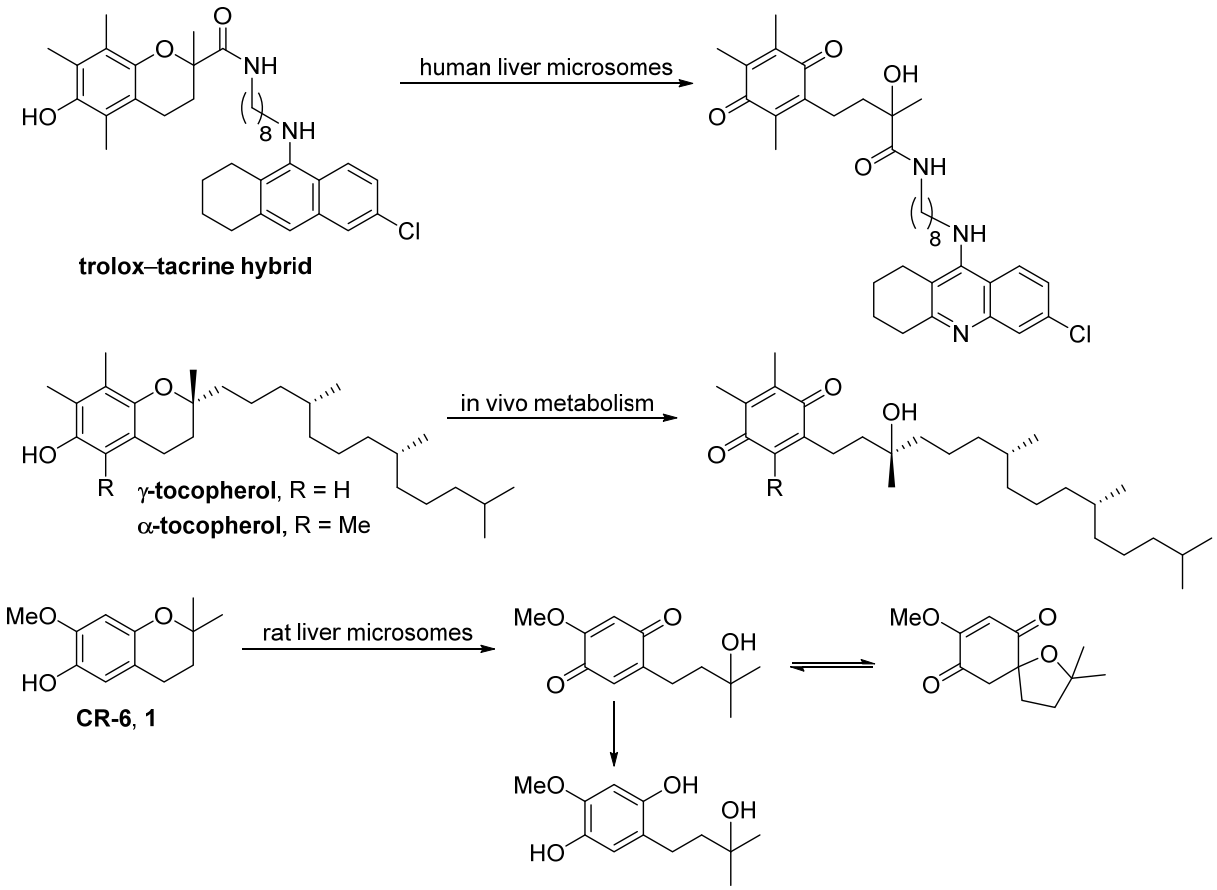

Figure 13. Reported metabolic transformation of chroman derivatives.[46–49]

In the light of these precedents, it seemed quite likely that the structurally related CR6–chlorotacrine hybrids could undergo a similar metabolic fate. Notwithstanding that, the stability of the CR6–chlorotacrine hybrid **4b** in biological media was assessed. In particular, we determined its stability in human, mouse, and rat plasma and liver microsomes, and we performed a qualitative determination of its metabolites after incubation with human, mouse, and rat liver microsomes.

The plasma stability of compound **4b** was assessed by incubating it at 37 ºC at different times (0, 60, 180, and 360 min) in human, mouse, and rat plasma, and determining the residual amount of

compound (expressed as residual percentage over starting amount) by UPLC-MS/MS. Compound **4b** turned out to be fully stable up to 6 h in human, mouse, and rat plasma (Table 2).

Table 2. Stability of Compound 4b in Human, Mouse, and Rat Plasma at 37 ºC[a]

	Remaining percentage of compound **4b**			
	0 min	60 min	180 min	360 min
Human plasma	100%	100%	100%	100%
Mouse plasma	100%	100%	100%	100%
Rat plasma	100%	100%	100%	98%

[a] Values are expressed as the mean of two independent experiments, each performed in triplicate.

Next, the microsomal stability of compound **4b** was assessed by incubating it at 37 ºC at different times (0, 10, 20, 40, and 60 min) with human, mouse, and rat liver microsomes, using testosterone as a reference compound of known short half-life. The stability parameters are summarized in Table 3.

Compound **4b** was apparently transformed to a great extent upon incubation with human liver microsomes, with a 44.0%, 18.6%, and a 3.6% of the initial amount of compound remaining unaltered after 20 min, 40 min, and 1 h, respectively. These results imply a short half-life (12.6 min) and a high microsomal intrinsic clearance (CL_{int}). In contrast, compound **4b** turned out to be much more stable after incubation with mouse and rat liver microsomes, where half-lives of 50.5 and 42.4 min, respectively, were found, with a significant amount of **4b**, 55.2% and 36.5%, respectively, remaining unchanged after 1 h (Table 3). The stability of **4b** was particularly favorable in mouse liver microsomes, from which it can be categorized as a low clearance compound (CL_{int} < 15 μL/min /mg protein).[50]

Table 3. Stability of Compound 4b in Human, Mouse, and Rat Liver Microsomes at 37 ºC[a]

	Human microsomes			Mouse microsomes			Rat microsomes		
Compound	Residual amount (%)	$t_{1/2}$ (min)	CL_{int} (μL/min /mg prot)	Residual amount (%)	$t_{1/2}$ (min)	CL_{int} (μL/min /mg prot)	Residual amount (%)	$t_{1/2}$ (min)	CL_{int} (μL/min /mg prot)
4b	3.6%	12.6	55.2	55.2%	50.5	13.7	36.5%	42.4	16.3
testosterone	6.1%	9.9	69.7	14.7%	13.7	50.7	2.9%	2.4	286.2

[a] Values are expressed as the mean of two independent experiments, each performed in triplicate.

Finally, the supernatants of the microsomal stability assays with human, mouse, and rat liver microsomes were qualitatively analyzed by using a UPLC-MS/MS system to identify potential metabolites of **4b**. As expected, the *p*-benzoquinone metabolite **M1** resulting from oxidative opening of the chroman ring, likely together with its ring-closed spiro derivative **M2** seemed to have been formed (Figure 14). Interestingly, the hydroquinone metabolite **M3** resulting from reduction of **M1** was also found, as it was 6-chlorotacrine (**M4**), whereas, as it had been reported for the trolox–tacrine hybrids, potentially toxic hydroxylated tacrine metabolites were not detected.

Compound **4b** and metabolites **M1**-**M3** have similar structures, and, all of them, as well as metabolite **M4** should have a very similar degree of ionization. Even though the analysis was only qualitative, a roughly comparison of the MS peak areas of **4b** and its metabolites seems to indicate that i) compound **4b** was more abundant than any metabolite at all the tested times in mouse and rat liver microsomes, but not in human liver microsomes after 40 min incubation, and ii) metabolite **M4** (6-chlorotacrine) seemed to be clearly less abundant than **M1**-**M2** and **M3** (Table S4 in Supporting Information).

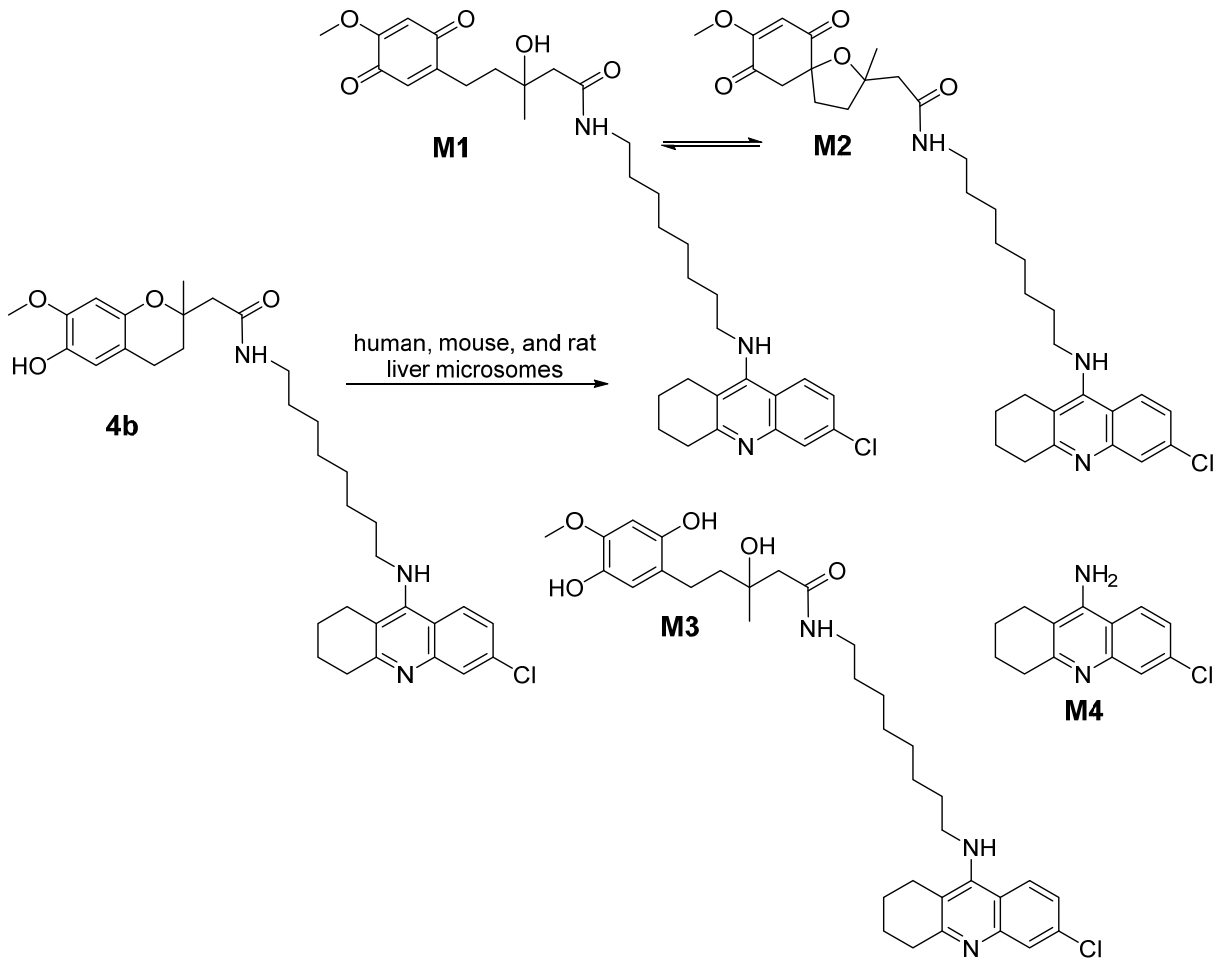

Figure 14. Metabolites of compound **4b** found after incubation with human, mouse, and rat liver microsomes.

The favorable stability of compound **4b** found in mouse plasma and mouse liver microsomes might suggest that the effects observed in the in vivo efficacy studies in mice should mostly derive from **4b** itself. Like for other chroman derivatives (Figure 13), the *p*-benzoquinone resulting from oxidative ring opening seems to be a major metabolite, which could contribute to the biological activity. Thus, we cannot rule out the possibility that this metabolite, after reduction to the corresponding hydroquinone, can be, in part, responsible for the in vivo effects

on oxidative stress markers, as reported for α-tocopherol. By contrast, it is not very likely that this metabolite retains the anticholinesterase activity of the parent compound **4b**, because its benzoquinone ring should protrude from the mouth of the gorge of hAChE (see Figure S5, in Supporting Information). Finally, the fact that hydroxylated tacrine metabolites are not formed from **4b** seems to be in line with its apparent lack of toxicity in mice after 4 weeks of treatment.

CONCLUSIONS

Because oxidative stress has a prominent role in the multifactorial pathogenesis of AD, antioxidant agents are regarded as a promising therapeutic strategy. However, antioxidants have failed to demonstrate efficacy in clinical trials so far. These failures could be ascribed to the poor brain permeability of antioxidants and to the fact that other pathogenic mechanisms of AD should be hit additionally to oxidative stress to efficiently cope with the multifactorial nature of this disease. Here we have shown that molecular hybridization of the promising but non-brain permeable antioxidant lead CR-6 with the potent lipophilic AChE inhibitor 6-chlorotacrine is a good approach to overcome both limitations. On the one hand, the resulting CR-6–chlorotacrine hybrids displayed favorable brain permeabilities, as measured in the in vitro PAMPA-BBB assay. On the other hand, the novel hybrids displayed multiple biological activities in vitro, including picomolar to nanomolar hAChE and nanomolar hBChE inhibitory activities, apart from the antioxidant effect. Indeed, combination of the CR-6 and 6-chlorotacrine scaffolds had a synergistic effect, with the hybrids being up to 120- and 40-fold more potent towards hAChE and hBChE than the parent 6-chlorotacrine, while retaining or displaying slightly improved antioxidant activity relative to the lead CR-6. Interestingly, some hybrids exhibited moderate in vitro activities against other key targets, such as BACE-1 and Aβ42 and tau aggregation. Chronic in vivo efficacy studies

with two selected compounds in double transgenic APP/PS1 mice have shown positive tendencies in improving cognition, amyloid pathology (reduction of amyloid burden and potentiation of the non-amyloidogenic APP processing pathway), and oxidative stress (reduction of the levels of oxidized proteins and increase of the levels of antioxidant enzymes). Even though most of the observed in vivo effects did not reach statistical significance, it was found that compounds **4b** and **11b** significantly reduced *Bace1* gene expression, with the latter compound also reducing brain sAPPβ protein levels and increasing *Adam10* gene expression. Significant in vivo effects were also found regarding some oxidative stress markers, namely increased brain GPX1 protein levels and *Hmox1* expression, and increased Nrf2 protein levels upon treatment with **4b** and **11b**, respectively. By virtue of their moderate in vivo effects, these compounds constitute interesting brain permeable multitarget anti-Alzheimer leads.

EXPERIMENTAL SECTION

Chemistry. All reagents and solvents were obtained from commercial suppliers and used without further purification. The progress of the reactions was monitored by thin-layer chromatography (TLC) on aluminum-backed sheets with silica gel 60 F_{254} (Merck, ref 1.05554) using CH_2Cl_2 / MeOH / 50% aq NH_4OH 95:5:1 (**4a**–**d**, **12a**–**c**,**e**, and **5a**–**c**) or 90:10:1 (**6a**–**d**, **11a**–**c**,**e**) as solvent system. The spots were visualized by UV irradiation and / or 1% aq. $KMnO_4$, followed by charring with a heat-gun. Column chromatography was performed on silica gel 60 AC.C (35−70 mesh, SDS, ref 2000027). Melting points were determined in open capillary tubes with a MFB 595010M Gallenkamp melting point apparatus. IR spectra were run on a Perkin Elmer Spectrum RX I spectrophotometer. Absorption values are expressed as wavenumbers (cm^{-1}); only significant absorption bands are given. 400 MHz ^1H / 100.6 MHz ^{13}C NMR spectra were

recorded on a Varian Mercury 400 spectrometer, at the Centres Científics i Tecnològics of the University of Barcelona (CCiTUB). The chemical shifts are reported in ppm (δ scale) relative to solvent signals (CD_3OD at 3.31 and 49.0 ppm in the ^1H and ^{13}C NMR spectra, respectively), and coupling constants are reported in Hertz (Hz). Assignments given for the NMR spectra of the new compounds have been carried out by comparison with the NMR data of compounds **4b**, **4d**, **5b**, **6b**, **6d**, and **11b**, which in turn, were assigned on the basis of COSY $^1H/^1H$ (standard procedures) and COSY $^1H/^{13}C$ (gHSQC and gHMBC sequences) experiments. High resolution mass spectra were carried out at the CCiTUB with a LC/MSD TOF Agilent Technologies spectrometer. Analytical RP-HPLC was performed with a Hewlett Packard Series 110 modular system equipped with a UV detector 1315A, using a RP Kromasil 100 C18 (15×0.46 cm, 5 μm) column, CH_3CN / H_2O mixtures containing 0.1% TFA (gradient from 20% to 100% CH_3CN in 20 min) as the eluent, a flow of 1 mL/min, λ = 254 nm. The analytical samples of all of the compounds that were subjected to pharmacological evaluation possessed a purity ≥95% as evidenced by HPLC measurements.

***N*-{7-[(6-Chloro-1,2,3,4-tetrahydroacridin-9-yl)amino]heptyl}-2-(6-hydroxy-7-methoxy-2-methylchroman-2-yl)acetamide (4a).** A solution of carboxylic acid **7** (166 mg, 0.66 mmol) in in a mixture of EtOAc (9.7 mL) and DMF (0.5 mL) was treated with *N*-(3-dimethylaminopropyl)-*N'*-ethylcarbodiimide hydrochloride (EDC·HCl, 153 mg, 0.80 mmol), Et_3N (0.18 mL, 131 mg, 1.30 mmol), and 1-hydroxy-1*H*-benzotriazole (HOBt, 134 mg, 0.99 mmol). The resulting mixture was stirred at rt for 15 min and then treated with a suspension of amine **10a** (250 mg, 0.72 mmol) in a mixture of EtOAc (10 mL) and DMF (1.5 mL). The reaction mixture was stirred at rt for 1 day and was concentrated *in vacuo*, to give a dark brown solid (763 mg), which was purified by column chromatography (35−70 μm silica gel, hexane /

EtOAc / Et_3N mixtures, gradient elution). On elution with hexane / EtOAc / Et_3N 20:80:0.2, amide **4a** (254 mg, 67% yield) was isolated as a white solid; R_f 0.62 (CH_2Cl_2 / MeOH / 50% aq NH_4OH 95:5:1).

A solution of **4a** (237 mg, 0.41 mmol) in CH_2Cl_2 (2 mL) was filtered through a 0.22 μm PVDF filter, treated with HCl / Et_2O (1.35 N, 0.9 mL) and evaporated under reduced pressure. The resulting solid was washed with pentane (3 × 2 mL) to give, after drying at 40 ºC/30 Torr for 48 h, **4a**·HCl (232 mg) as a yellowish solid: mp 122–126 °C; IR (ATR) *v* 3600–2200 (max at 3244, 3065, 2927, 2852, N–H, N^+–H, O–H, C–H st), 1632, 1573, 1509 (C=O, Ar–C–C, Ar–C–N st) cm^{-1}; ^1H NMR (400 MHz, CD_3OD) δ 1.31 (s, 3H, 2-CH_3), 1.31–1.41 (complex signal, 6H, 3'-H_2, 4'-H_2, 5'-H_2), 1.49 (tt, $J = J' = 6.8$ Hz, 2H, 2'-H_2), superimposed in part 1.77 (dt, $J = 13.2$ Hz, $J' = 6.8$ Hz, 1H, 3-H_A), 1.79 (m, 2H, 6'-H_2), 1.89 (dt, $J = 13.2$ Hz, $J' = 7.2$ Hz, 1H, 3-H_B), 1.91–2.00 (complex signal, 4H, 2"-H_2, 3"-H_2), 2.44 (d, $J = 13.6$ Hz, 1H, 2-CH_A-CO), 2.48 (d, $J = 13.6$ Hz, 1H, 2-CH_B-CO), 2.61 (dd, $J = 7.2$ Hz, $J' = 6.8$ Hz, 2H, 4-H_2), 2.65 (t, $J = 6.4$ Hz, 2H, 1"-H_2), 2.99 (t, $J = 5.6$ Hz, 2H, 4"-H_2), 3.16 (dt, $J = 13.6$ Hz, $J' = 6.8$ Hz, 1H, 1'-H_A), 3.20 (dt, $J = 13.6$ Hz, $J' = 6.8$ Hz, 1H, 1'-H_B), 3.73 (s, 3H, 7-OCH_3), 3.89 (t, $J = 7.2$ Hz, 2H, 7'-H_2), 4.85 (s, NH, $^+$NH, OH), 6.31 (s, 1H, 8-H), 6.44 (s, 1H, 5-H), 7.55 (dd, $J = 9.2$ Hz, $J' = 2.0$ Hz, 1H, 7"-H), 7.77 (d, $J = 2.0$ Hz, 1H, 5"-H), 8.36 (d, $J = 9.2$ Hz, 1H, 8"-H); ^{13}C NMR (100.6 MHz, CD_3OD) δ 21.7 (CH_2, C3"), 22.4 (CH_2, C4), 22.8 (CH_2, C2"), 24.5 (CH_3, 2-CH_3), 24.7 (CH_2, C1"), 27.6 (CH_2, C5'), 27.7 (CH_2, C4'), 29.3 (CH_2, C4"), 29.9 (CH_2, C3'), 30.3 (CH_2, C2'), 31.3 (CH_2, C6'), 32.3 (CH_2, C3), 40.1 (CH_2, C1'), 47.5 (CH_2, 2-*C*H_2-CO), 49.3 (CH_2, C7'), 56.4 (CH_3, 7-OCH_3), 75.6 (C, C2), 102.2 (CH, C8), 113.3 (C, C9a"), 113.4 (C, C4a), 115.4 (C, C8a"), 116.1 (CH, C5), 119.1 (CH, C5"), 126.8 (CH, C7"), 128.7 (CH, C8"), 140.1 (C, C6"), 140.5 (C, C10a"), 141.1 (C, C6), 147.4 (C, C8a), 148.3 (C, C7), 152.1 (C, C4a"), 157.8 (C, C9"), 172.4 (C,

CONH); HRMS (ESI) calcd for ($C_{33}H_{42}{}^{35}ClN_3O_4$ + H^+): 580.2937, found 580.2927; HPLC purity 100%.

***N*-{8-[(6-Chloro-1,2,3,4-tetrahydroacridin-9-yl)amino]octyl}-2-(6-hydroxy-7-methoxy-2-methylchroman-2-yl)acetamide (4b).** It was prepared as described for **4a**. From carboxylic acid **7** (120 mg, 0.48 mmol) and amine **10b** (188 mg, 0.52 mmol), a brown sticky solid (624 mg) was obtained and subjected to column chromatography purification (35−70 μm silica gel, hexane / EtOAc / Et_3N mixtures, gradient elution). On elution with hexane / EtOAc / Et_3N 20:80:0.2, amide **4b** (189 mg, 67% yield) was isolated as a yellowish solid; R_f 0.63 (CH_2Cl_2 / MeOH / 50% aq NH_4OH 95:5:1).

4b·HCl: beige solid; mp 127–130 °C; IR (ATR) *v* 3600–2200 (max at 3244, 3059, 2927, 2854, N–H, N^+–H, O–H, C–H st), 1632, 1573, 1510 (C=O, Ar–C–C, Ar–C–N st) cm^{-1}; ^1H NMR (400 MHz, CD_3OD) δ 1.27–1.34 (complex signal, 6H, 3'-H_2, 4'-H_2, 5'-H_2), 1.31 (s, 3H, 2-CH_3), 1.39 (tt, $J = J' = 6.8$ Hz, 2H, 6'-H_2), 1.48 (tt, $J = J' = 6.8$ Hz, 2H, 2'-H_2), superimposed in part 1.75 (dt, $J = 13.6$ Hz, $J' = 6.8$ Hz, 1H, 3-H_A), 1.80 (tt, $J = 7.2$ Hz, $J' = 6.8$ Hz, 2H, 7'-H_2), 1.89 (dt, $J = 13.6$ Hz, $J' = 6.8$ Hz, 1H, 3-H_B), 1.92–2.00 (complex signal, 4H, 2"-H_2, 3"-H_2), 2.44 (d, $J = 13.6$ Hz, 1H, 2-CH_A-CO), 2.48 (d, $J = 13.6$ Hz, 1H, 2-CH_B-CO), 2.62 (t, $J = 6.8$ Hz, 2H, 4-H_2), 2.66 (t, $J = 5.6$ Hz, 2H, 1"-H_2), 2.99 (t, $J = 6.0$ Hz, 2H, 4"-H_2), 3.16 (dt, $J = 13.6$ Hz, $J' = 6.8$ Hz, 1H, 1'-H_A), 3.20 (dt, $J = 13.6$ Hz, $J' = 6.8$ Hz, 1H, 1'-H_B), 3.75 (s, 3H, 7-OCH_3), 3.90 (t, $J = 7.2$ Hz, 2H, 8'-H_2), 4.85 (s, NH, $^+$NH, OH), 6.32 (s, 1H, 8-H), 6.44 (s, 1H, 5-H), 7.55 (dd, $J = 9.2$ Hz, $J' = 2.4$ Hz, 1H, 7"-H), 7.76 (d, $J = 2.4$ Hz, 1H, 5"-H), 8.36 (d, $J = 9.2$ Hz, 1H, 8"-H); ^{13}C NMR (100.6 MHz, CD_3OD) δ 21.8 (CH_2, C3"), 22.4 (CH_2, C4), 22.8 (CH_2, C2"), 24.62 (CH_3, 2-CH_3), 24.64 (CH_2, C1"), 27.5 (CH_2, C6'), 27.7 (CH_2, C5'), 29.3 (CH_2, C4"), 30.1 (CH_2), 30.2 (CH_2) (C3', C4'), 30.4 (CH_2, C2'), 31.3 (CH_2, C7'), 32.3 (CH_2, C3), 40.2 (CH_2, C1'), 47.4

(CH_2, 2-*C*H_2-CO), 49.3 (CH_2, C8'), 56.4 (CH_3, 7-OCH_3), 75.6 (C, C2), 102.2 (CH, C8), 113.3 (C, C9a"), 113.4 (C, C4a), 115.4 (C, C8a"), 116.1 (CH, C5), 119.1 (CH, C5"), 126.7 (CH, C7"), 128.8 (CH, C8"), 140.1 (C, C6"), 140.5 (C, C10a"), 141.1 (C, C6), 147.4 (C, C8a), 148.3 (C, C7), 152.0 (C, C4a"), 157.8 (C, C9"), 172.4 (C, CONH); HRMS (ESI) calcd for ($C_{34}H_{44}{}^{35}ClN_3O_4$ + H^+): 594.3093, found 594.3096; HPLC purity 96%.

***N*-{9-[(6-Chloro-1,2,3,4-tetrahydroacridin-9-yl)amino]nonyl}-2-(6-hydroxy-7-methoxy-2-methylchroman-2-yl)acetamide (4c).** It was prepared as described for **4a**. From carboxylic acid **7** (163 mg, 0.65 mmol) and amine **10c** (266 mg, 0.71 mmol), a brown sticky solid (828 mg) was obtained and subjected to column chromatography purification (35−70 μm silica gel, hexane / EtOAc / Et_3N mixtures, gradient elution). On elution with hexane / EtOAc / Et_3N 20:80:0.2, amide **4c** (338 mg, 86% yield) was isolated as a white solid; R_f 0.66 (CH_2Cl_2 / MeOH / 50% aq NH_4OH 95:5:1).

4c·HCl: light yellow solid; mp 104–106 °C; IR (ATR) ν 3600–2200 (max at 3244, 3065, 2924, 2852, N–H, N^+–H, O–H, C–H st), 1632, 1573, 1510 (C=O, Ar–C–C, Ar–C–N st) cm^{-1}; ^1H NMR (400 MHz, CD_3OD) δ 1.23–1.33 (complex signal, 8H, 3'-H_2, 4'-H_2, 5'-H_2, 6'-H_2), 1.32 (s, 3H, 2-CH_3), 1.40 (tt, $J = J' = 7.2$ Hz, 2H, 7'-H_2), 1.48 (tt, $J = J' = 6.8$ Hz, 2H, 2'-H_2), superimposed in part 1.77 (dt, $J = 13.6$ Hz, $J' = 6.8$ Hz, 1H, 3-H_A), 1.80 (tt, $J = J' = 7.2$ Hz, 2H, 8'-H_2), 1.90 (dt, $J = 13.6$ Hz, $J' = 7.2$ Hz, 1H, 3-H_B), 1.92–2.00 (complex signal, 4H, 2"-H_2, 3"-H_2), 2.44 (d, $J = 13.2$ Hz, 1H, 2-CH_A-CO), 2.49 (d, $J = 13.2$ Hz, 1H, 2-CH_B-CO), 2.63 (dd, $J = 7.2$ Hz, $J' = 6.8$ Hz, 2H, 4-H_2), 2.67 (t, $J = 5.2$ Hz, 2H, 1"-H_2), 2.99 (t, $J = 5.2$ Hz, 2H, 4"-H_2), 3.16 (dt, $J = 13.6$ Hz, $J' = 6.8$ Hz, 1H, 1'-H_A), 3.20 (dt, $J = 13.6$ Hz, $J' = 6.8$ Hz, 1H, 1'-H_B), 3.75 (s, 3H, 7-OCH_3), 3.92 (t, $J = 7.2$ Hz, 2H, 9'-H_2), 4.85 (s, NH, $^+$NH, OH), 6.34 (s, 1H, 8-H), 6.45 (s, 1H, 5-H), 7.56 (dd, $J = 9.2$ Hz, $J' = 2.0$ Hz, 1H, 7"-H), 7.76 (d, $J = 2.0$ Hz, 1H, 5"-H),

8.38 (d, J = 9.2 Hz, 1H, 8”-H); ^{13}C NMR (100.6 MHz, CD_3OD) δ 21.7 (CH_2, C3”), 22.4 (CH_2, C4), 22.8 (CH_2, C2”), 24.6 (CH_3, 2-CH_3), 24.7 (CH_2, C1”), 27.6 (CH_2, C7’), 27.8 (CH_2, C6’), 29.3 (CH_2, C4”), 30.1 (CH_2), 30.2 (CH_2) (C3’, C4’), 30.38 (CH_2), 30.42 (CH_2) (C2’, C5’), 31.3 (CH_2, C8’), 32.3 (CH_2, C3), 40.2 (CH_2, C1’), 47.4 (CH_2, 2-*C*H_2-CO), 49.3 (CH_2, C9’), 56.4 (CH_3, 7-OCH_3), 75.6 (C, C2), 102.2 (CH, C8), 113.31 (C, C9a”), 113.35 (C, C4a), 115.4 (C, C8a”), 116.1 (CH, C5), 119.1 (CH, C5”), 126.7 (CH, C7”), 128.8 (CH, C8”), 140.1 (C, C6”), 140.5 (C, C10a”), 141.1 (C, C6), 147.4 (C, C8a), 148.3 (C, C7), 152.0 (C, C4a”), 157.8 (C, C9”), 172.4 (C, CONH); HRMS (ESI) calcd for ($C_{35}H_{46}{}^{35}ClN_3O_4 + H^+$): 608.3250, found 608.3243; HPLC purity 99%.

***N*-{8-[(6-Chloro-1,2,3,4-tetrahydroacridin-9-yl)amino]-3,6-dioxaoctyl}-2-(6-hydroxy-7-methoxy-2-methylchroman-2-yl)acetamide (4d).** It was prepared as described for **4a**. From carboxylic acid **7** (130 mg, 0.52 mmol) and amine **10d** (206 mg, 0.57 mmol), a brown sticky solid (617 mg) was obtained and subjected to column chromatography purification (35−70 μm silica gel, hexane / EtOAc / Et_3N mixtures, gradient elution). On elution with hexane / EtOAc / Et_3N 10:90:0.2 to 0:100:0.2, amide **4d** (281 mg, 91% yield) was isolated as a light brown sticky solid; R_f 0.79 (CH_2Cl_2 / MeOH / 50% aq NH_4OH 95:5:1).

4d·HCl: brown solid; mp 55–57 °C; IR (ATR) ν 3600–2400 (max at 3362, 3250, 3068, 2921, 2860, N–H, N^+–H, O–H, C–H st), 1630, 1572, 1509 (C=O, Ar–C–C, Ar–C–N st) cm^{-1}; ^{1}H NMR (400 MHz, CD_3OD) δ 1.28 (s, 3H, 2-CH_3), 1.68 (dt, J = 13.6 Hz, $J’$ = 6.8 Hz, 1H, 3-H_A), 1.81 (dt, J = 13.6 Hz, $J’$ = 6.8 Hz, 1H, 3-H_B), 1.89–2.00 (complex signal, 4H, 2”-H_2, 3”-H_2), 2.36 (d, J = 13.6 Hz, 1H, 2-CH_A-CO), 2.46 (d, J = 13.6 Hz, 1H, 2-CH_B-CO), 2.53 (t, J = 6.8 Hz, 2H, 4-H_2), 2.63 (t, J = 6.0 Hz, 2H, 1”-H_2), 2.98 (t, J = 5.6 Hz, 2H, 4”-H_2), 3.33 (dt, J = 14.0 Hz, $J’$ = 5.2 Hz, 1H, 1’-H_A), 3.40 (dt, J = 14.0 Hz, $J’$ = 5.2 Hz, 1H, 1’-H_B), 3.53 (t, J = 5.2 Hz, 2H, 2’-

H_2), 3.62 (m, 2H), 3.66 (m, 2H) (4'-H_2, 5'-H_2), 3.71 (s, 3H, 7-OCH_3), 3.84 (t, J = 5.2 Hz, 2H, 7'-H_2), 4.10 (t, J = 5.2 Hz, 2H, 8'-H_2), 4.85 (s, NH, $^+$NH, OH), 6.33 (s, 1H, 8-H), 6.35 (s, 1H, 5-H), 7.52 (dd, J = 9.2 Hz, J' = 2.0 Hz, 1H, 7"-H), 7.74 (d, J = 2.0 Hz, 1H, 5"-H), 8.41 (d, J = 9.2 Hz, 1H, 8"-H); ^{13}C NMR (100.6 MHz, CD_3OD) δ 21.7 (CH_2, C3"), 22.2 (CH_2, C4), 22.7 (CH_2, C2"), 24.4 (CH_3 + CH_2, 2-CH_3, C1"), 29.3 (CH_2, C4"), 32.6 (CH_2, C3), 40.2 (CH_2, C1'), 46.7 (CH_2, 2-*C*H_2-CO), 49.3 (CH_2, C8'), 56.5 (CH_3, 7-OCH_3), 70.2 (CH_2, C7'), 70.4 (CH_2, C2'), 71.0 (CH_2), 71.3 (CH_2) (C4', C5'), 75.4 (C, C2), 102.5 (CH, C8), 113.4 (C, C4a), 113.6 (C, C9a"), 115.6 (C, C8a"), 116.0 (CH, C5), 119.1 (CH, C5"), 126.7 (CH, C7"), 128.9 (CH, C8"), 140.0 (C, C6"), 140.4 (C, C10a"), 141.2 (C, C6), 146.9 (C, C8a), 148.2 (C, C7), 152.3 (C, C4a"), 158.3 (C, C9"), 172.7 (C, CONH); HRMS (ESI) calcd for ($C_{32}H_{40}{}^{35}ClN_3O_6$ + H^+): 598.2678, found 598.2692; HPLC purity 96%.

7-[(6-Chloro-1,2,3,4-tetrahydroacridin-9-yl)amino]-*N*-[2-(6-hydroxy-7-methoxy-2-methylchroman-2-yl)ethyl]heptanamide (5a). To a solution of nitrile **13a** (462 mg, 1.35 mmol) in MeOH (2 mL) a 40% methanolic solution of KOH (3.7 mL) was added. The resulting suspension was stirred under reflux for 3 h, then treated with H_2O (4.7 mL), and stirred under reflux overnight. The resulting solution was cooled to rt and evaporated under reduced pressure. The residue was treated with HCl / dioxane (4 M, 6.8 mL) and the solution was concentrated *in vacuo* to give crude 7-[(6-chloro-1,2,3,4-tetrahydroacridin-9-yl)amino]heptanoic acid, in the form of hydrochloride salt, as a yellow solid (2.46 g) which was used in the following step without further purification.

From this crude carboxylic acid, the target amide **5a** was prepared as described for **4a**. From crude carboxylic acid (2.46 g) and amine **14** (159 mg, 0.68 mmol), a brown sticky solid (3.30 g) was obtained and subjected to column chromatography purification (35−70 μm silica gel, hexane

/ EtOAc / Et_3N mixtures, gradient elution). On elution with hexane / EtOAc / Et_3N 0:100:0.2, amide **5a** (337 mg, 87% overall yield) was isolated as a light yellow solid; R_f 0.57 (CH_2Cl_2 / MeOH / 50% aq NH_4OH 95:5:1).

5a·HCl: yellow solid; mp 121–123 °C; IR (ATR) *v* 3600–2400 (max at 3245, 3068, 2926, 2850, N–H, N^+–H, O–H, C–H st), 1630, 1572, 1509 (C=O, Ar–C–C, Ar–C–N st) cm^{-1}; ^1H NMR (400 MHz, CD_3OD) δ 1.25 (s, 3H, 2”-CH_3), superimposed in part 1.35 (tt, $J = J' = 7.2$ Hz, 2H), 1.43 (tt, $J = J' = 7.2$ Hz, 2H) (4-H_2, 5-H_2), 1.59 (tt, $J = J' = 7.2$ Hz, 2H, 3-H_2), 1.70 (dt, $J = 13.6$ Hz, $J' = 6.8$ Hz, 1H, 3”-H_A), 1.72–1.86 (complex signal, 5H, 6-H_2, 2”-CH_2, 3”-H_B), 1.90–2.00 (complex signal, 4H, 2’-H_2, 3’-H_2), 2.16 (t, $J = 7.2$ Hz, 2H, 2-H_2), 2.60 (t, $J = 6.8$ Hz, 2H, 4”-H_2), 2.66 (br t, $J = 5.6$ Hz, 2H, 1’-H_2), 2.99 (br t, $J = 5.6$ Hz, 2H, 4’-H_2), 3.27 (ddd, $J = 13.2$ Hz, $J' = 9.2$ Hz, $J'' = 6.0$ Hz, 1H, CH_A-NHCO), 3.39 (ddd, $J = 13.2$ Hz, $J' = 9.2$ Hz, $J'' = 6.0$ Hz, 1H, CH_B-NHCO), 3.74 (s, 3H, 7”-OCH_3), 3.90 (t, $J = 7.2$ Hz, 2H, 7-H_2), 4.86 (s, NH, $^+$NH, OH), 6.30 (s, 1H, 8”-H), 6.42 (s, 1H, 5”-H), 7.55 (dd, $J = 9.2$ Hz, $J' = 2.0$ Hz, 1H, 7’-H), 7.76 (d, $J = 2.0$ Hz, 1H, 5’-H), 8.36 (d, $J = 9.2$ Hz, 1H, 8’-H); ^{13}C NMR (100.6 MHz, CD_3OD) δ 21.7 (CH_2, C3’), 22.3 (CH_2, C4”), 22.8 (CH_2, C2’), 24.3 (CH_3, 2”-CH_3), 24.7 (CH_2, C1’), 26.7 (CH_2, C3), 27.4 (CH_2, C5), 29.3 (CH_2, C4’), 29.7 (CH_2, C4), 31.1 (CH_2, C6), 32.6 (CH_2, C3”), 35.9 (CH_2, *C*H_2-NHCO), 36.9 (CH_2, C2), 39.4 (CH_2, 2”-CH_2), 49.1 (CH_2, C7), 56.3 (CH_3, 7”-OCH_3), 75.8 (C, C2”), 102.2 (CH, C8”), 113.3 (C, C9a’), 113.4 (C, C4a”), 115.4 (C, C8a’), 116.1 (CH, C5”), 119.1 (CH, C5’), 126.8 (CH, C7’), 128.8 (CH, C8’), 140.1 (C, C6’), 140.5 (C, C10a’), 140.8 (C, C6”), 147.7 (C, C8a”), 148.3 (C, C7”), 152.0 (C, C4a’), 157.8 (C, C9’), 175.9 (C, C1); HRMS (ESI) calcd for ($C_{33}H_{42}{}^{35}ClN_3O_4 + H^+$): 580.2937, found 580.2946; HPLC purity 96%.

8-[(6-Chloro-1,2,3,4-tetrahydroacridin-9-yl)amino]-*N*-[2-(6-hydroxy-7-methoxy-2-methylchroman-2-yl)ethyl]octanamide (5b). It was prepared as described for **5a**. From nitrile

13b (367 mg, 1.03 mmol), crude 8-[(6-chloro-1,2,3,4-tetrahydroacridin-9-yl)amino]octanoic acid, in the form of hydrochloride salt, was obtained as a yellow solid (1.93 g) and used in the following step without further purification. From crude carboxylic acid (1.93 g) and amine **14** (100 mg, 0.43 mmol), a brown sticky solid (2.29 g) was obtained and subjected to column chromatography purification (35−70 μm silica gel, hexane / EtOAc / Et_3N mixtures, gradient elution). On elution with hexane / EtOAc / Et_3N 20:80:0.2, amide **5b** (139 mg, 55% overall yield) was isolated as a yellow solid; R_f 0.67 (CH_2Cl_2 / MeOH / 50% aq NH_4OH 95:5:1).

5b·HCl: yellow solid; mp 72–74 °C; IR (ATR) ν 3600–2200 (max at 3245, 3063, 2921, 2850, N–H, N^+–H, O–H, C–H st), 1630, 1572, 1509 (C=O, Ar–C–C, Ar–C–N st) cm^{-1}; ^1H NMR (400 MHz, CD_3OD) δ 1.25 (s, 3H, 2”-CH_3), 1.28–1.44 (complex signal, 6H, 4-H_2, 5-H_2, 6-H_2), 1.57 (tt, $J = J' = 7.2$ Hz, 2H, 3-H_2), 1.69 (dt, $J = 13.2$ Hz, $J' = 6.4$ Hz, 1H, 3”-H_A), 1.71–1.86 (complex signal, 5H, 7-H_2, 2”-CH_2, 3”-H_B), 1.92–2.00 (complex signal, 4H, 2’-H_2, 3’-H_2), 2.16 (t, $J = 7.2$ Hz, 2H, 2-H_2), 2.61 (t, $J = 6.4$ Hz, 2H, 4”-H_2), 2.66 (br t, $J = 5.6$ Hz, 2H, 1’-H_2), 2.99 (br t, $J = 5.6$ Hz, 2H, 4’-H_2), 3.29 (ddd, $J = 13.6$ Hz, $J' = 8.8$ Hz, $J'' = 6.4$ Hz, 1H, CH_A-NHCO), 3.40 (ddd, $J = 13.6$ Hz, $J' = 9.2$ Hz, $J'' = 6.0$ Hz, 1H, CH_B-NHCO), 3.75 (s, 3H, 7”-OCH_3), 3.91 (t, $J = 7.2$ Hz, 2H, 8-H_2), 4.87 (s, NH, $^+$NH, OH), 6.30 (s, 1H, 8”-H), 6.43 (s, 1H, 5”-H), 7.56 (dd, $J = 9.2$ Hz, $J' = 2.0$ Hz, 1H, 7’-H), 7.77 (d, $J = 2.0$ Hz, 1H, 5’-H), 8.37 (d, $J = 9.2$ Hz, 1H, 8’-H); ^{13}C NMR (100.6 MHz, CD_3OD) δ 21.8 (CH_2, C3’), 22.3 (CH_2, C4”), 22.8 (CH_2, C2’), 24.2 (CH_3, 2”-CH_3), 24.7 (CH_2, C1’), 26.7 (CH_2, C3), 27.5 (CH_2, C6), 29.3 (CH_2, C4’), 29.9 (CH_2), 30.0 (CH_2) (C4, C5), 31.4 (CH_2, C7), 32.6 (CH_2, C3”), 36.0 (CH_2, *C*H_2-NHCO), 37.0 (CH_2, C2), 39.4 (CH_2, 2”-CH_2), 49.3 (CH_2, C8), 56.3 (CH_3, 7”-OCH_3), 75.8 (C, C2”), 102.2 (CH, C8”), 113.3 (C, C9a’), 113.4 (C, C4a”), 115.4 (C, C8a’), 116.1 (CH, C5”), 119.1 (CH, C5’), 126.8 (CH, C7’), 128.8 (CH, C8’), 140.1 (C, C6’), 140.5 (C, C10a’), 140.8 (C, C6”), 147.7

(C, C8a"), 148.3 (C, C7"), 152.1 (C, C4a'), 157.8 (C, C9'), 176.1 (C, C1); HRMS (ESI) calcd for ($C_{34}H_{44}{}^{35}ClN_3O_4$ + H^+): 594.3093, found 594.3092; HPLC purity 97%.

9-[(6-Chloro-1,2,3,4-tetrahydroacridin-9-yl)amino]-*N*-[2-(6-hydroxy-7-methoxy-2-methylchroman-2-yl)ethyl]nonanamide (5c). It was prepared as described for **5a**. From nitrile **13c** (315 mg, 0.85 mmol), crude 9-[(6-chloro-1,2,3,4-tetrahydroacridin-9-yl)amino]nonanoic acid, in the form of hydrochloride salt, was obtained as a light yellow solid (1.55 g) and used in the following step without further purification. From crude carboxylic acid (1.55 g) and amine **14** (133 mg, 0.57 mmol), a brown oily residue (2.21 g) was obtained and subjected to column chromatography purification (35−70 μm silica gel, hexane / EtOAc / Et_3N mixtures, gradient elution). On elution with hexane / EtOAc / Et_3N 10:90:0.2, amide **5c** (189 mg, 52% overall yield) was isolated as a light yellow solid; R_f 0.69 (CH_2Cl_2 / MeOH / 50% aq NH_4OH 95:5:1).

5c·HCl: yellow solid; mp 107–111 °C; IR (ATR) ν 3600–2200 (max at 3314, 3242, 3057, 2921, 2849, N–H, N^+–H, O–H, C–H st), 1625, 1571, 1518 (C=O, Ar–C–C, Ar–C–N st) cm^{-1}; ^1H NMR (400 MHz, CD_3OD) δ 1.26 (s, 3H, 2"-CH_3), 1.26–1.38 (complex signal, 6H, 4-H_2, 5-H_2, 6-H_2), superimposed in part 1.42 (tt, $J = J' = 7.2$ Hz, 2H, 7-H_2), 1.57 (tt, $J = J' = 7.2$ Hz, 2H, 3-H_2), 1.72 (dt, $J = 13.6$ Hz, $J' = 6.8$ Hz, 1H, 3"-H_A), 1.74–1.87 (complex signal, 5H, 8-H_2, 2"-CH_2, 3"-H_B), 1.91–2.00 (complex signal, 4H, 2'-H_2, 3'-H_2), 2.16 (t, $J = 7.2$ Hz, 2H, 2-H_2), 2.61 (t, $J = 6.8$ Hz, 2H, 4"-H_2), 2.66 (br t, $J = 6.0$ Hz, 2H, 1'-H_2), 2.99 (br t, $J = 6.0$ Hz, 2H, 4'-H_2), 3.29 (ddd, $J = 13.2$ Hz, $J' = 9.2$ Hz, $J'' = 6.4$ Hz, 1H, CH_A-NHCO), 3.41 (ddd, $J = 13.2$ Hz, $J' = 9.2$ Hz, $J'' = 6.4$ Hz, 1H, CH_B-NHCO), 3.75 (s, 3H, 7"-OCH_3), 3.91 (t, $J = 7.2$ Hz, 2H, 9-H_2), 4.87 (s, NH, $^+$NH, OH), 6.30 (s, 1H, 8"-H), 6.44 (s, 1H, 5"-H), 7.56 (dd, $J = 9.2$ Hz, $J' = 2.4$ Hz, 1H, 7'-H), 7.77 (d, $J = 2.4$ Hz, 1H, 5'-H), 8.37 (d, $J = 9.2$ Hz, 1H, 8'-H); ^{13}C NMR (100.6 MHz, CD_3OD) δ 21.8 (CH_2, C3'), 22.3 (CH_2, C4"), 22.8 (CH_2, C2'), 24.2 (CH_3, 2"-CH_3), 24.7 (CH_2, C1'), 26.8

(CH_2, C3), 27.6 (CH_2, C7), 29.3 (CH_2, C4'), 30.00 (CH_2), 30.02 (CH_2), 30.1 (CH_2) (C4, C5, C6), 31.3 (CH_2, C8), 32.6 (CH_2, C3"), 36.1 (CH_2, *C*H_2-NHCO), 37.0 (CH_2, C2), 39.4 (CH_2, 2"-CH_2), 49.3 (CH_2, C9), 56.3 (CH_3, 7"-OCH_3), 75.8 (C, C2"), 102.2 (CH, C8"), 113.3 (C, C9a'), 113.4 (C, C4a"), 115.4 (C, C8a'), 116.1 (CH, C5"), 119.1 (CH, C5'), 126.8 (CH, C7'), 128.8 (CH, C8'), 140.1 (C, C6'), 140.5 (C, C10a'), 140.8 (C, C6"), 147.7 (C, C8a"), 148.3 (C, C7"), 152.0 (C, C4a'), 157.8 (C, C9'), 176.2 (C, C1); HRMS (ESI) calcd for ($C_{35}H_{46}{}^{35}ClN_3O_4 + H^+$): 608.3250, found 608.3259; HPLC purity 99%.

***N*-(6-Chloro-1,2,3,4-tetrahydroacridin-9-yl)-*N'*-[2-(6-hydroxy-7-methoxy-2-methylchroman-2-yl)ethyl]heptane-1,7-diamine (6a).** A solution of tosylate **15** (175 mg, 0.44 mmol) in dry CH_3CN (1.5 mL) was added to a suspension of amine **10a** (461 mg, 1.33 mmol) and anhyd Et_3N (0.07 mL, 51 mg, 0.50 mmol) in dry CH_3CN (2 mL). The reaction mixture was stirred at 80 ºC for 48 h and then concentrated *in vacuo*, to give a dark brown oil (789 mg), which was purified by column chromatography (35−70 μm silica gel, CH_2Cl_2 / MeOH / 50% aq NH_4OH mixtures, gradient elution). On elution with CH_2Cl_2 / MeOH / 50% aq NH_4OH 99:1:0.4 to 98:2:0.4, amine **6a** (61 mg, 24% yield) was isolated as a beige solid; R_f 0.76 (CH_2Cl_2 / MeOH / 50% aq NH_4OH 90:10:1).

A solution of **6a** (37 mg, 0.07 mmol) in CH_2Cl_2 (1 mL) was filtered through a 0.2 μm PTFE filter, treated with HCl / Et_2O (1.35 N, 0.4 mL) and evaporated under reduced pressure. The resulting solid was washed with pentane (3 × 2 mL) to give, after drying at 40 ºC/30 Torr for 48 h, **6a**·2HCl (34 mg) as a beige solid: mp 160–163 °C; IR (ATR) ν 3600–2200 (max at 3240, 2930, 2852, 2780, 2604, 2496, N–H, N^+–H, O–H, C–H st), 1628, 1573, 1509 (Ar–C–C, Ar–C–N st) cm^{-1}; ^1H NMR (400 MHz, CD_3OD) δ 1.30 (s, 3H, 2"-CH_3), 1.39–1.51 (complex signal, 6H, 3-H_2, 4-H_2, 5-H_2), 1.71 (m, 2H, 6-H_2), superimposed in part 1.80 (dt, J = 13.6 Hz, J' = 6.8 Hz,

1H, 3”-H_A), 1.82–1.88 (complex signal, 3H, 2-H_2, 3”-H_B), 1.90–2.00 (complex signal, 5H, 2’-H_2, 3’-H_2, 2”-C*H*$_A$-CH_2-NH), 2.07 (dt, *J* = 14.4 Hz, *J’* = 6.8 Hz , 1H, 2”-C*H*$_B$-CH_2-NH), 2.64–2.72 (complex signal, 4H, 1’-H_2, 4”-H_2), 2.97–3.05 (complex signal, 4H, 7-H_2, 4’-H_2), 3.21 (t, *J* = 7.6 Hz, 2H, 2”-CH_2-C*H*$_2$-NH), 3.76 (s, 3H, 7”-OCH_3), 3.94 (t, *J* = 7.6 Hz, 2H, 1-H_2), 4.86 (s, NH, $^+$NH, $^+NH_2$, OH), 6.35 (s, 1H, 8”-H), 6.48 (s, 1H, 5”-H), 7.56 (dd, *J* = 9.2 Hz, *J’* = 1.6 Hz, 1H, 7’-H), 7.79 (d, *J* = 1.6 Hz, 1H, 5’-H), 8.39 (d, *J* = 9.2 Hz, 1H, 8’-H); ^{13}C NMR (100.6 MHz, CD_3OD) δ 21.7 (CH_2, C3’), 22.2 (CH_2, C4”), 22.9 (CH_2, C2’), 23.7 (CH_3, 2”-CH_3), 24.8 (CH_2, C1’), 27.2 (CH_2, C6), 27.4 (CH_2), 27.5 (CH_2) (C3, C5), 29.3 (CH_2, C4’), 29.7 (CH_2, C4), 31.3 (CH_2, C2), 32.6 (CH_2, C3”), 36.4 (CH_2, 2”-*C*H_2-CH_2-NH), 44.7 (CH_2, 2”-CH_2-*C*H_2-NH), 48.9 (CH_2, C7), 49.1 (CH_2, C1), 56.4 (CH_3, 7”-OCH_3), 75.3 (C, C2”), 102.2 (CH, C8”), 113.32 (C), 113.34 (C) (C9a’, C4a”), 115.4 (C, C8a’), 116.2 (CH, C5”), 119.1 (CH, C5’), 126.8 (CH, C7’), 128.8 (CH, C8’), 140.0 (C, C6’), 140.5 (C, C10a’), 141.3 (C, C6”), 147.2 (C, C8a”), 148.4 (C, C7”), 152.1 (C, C4a’), 157.8 (C, C9’); HRMS (ESI) calcd for ($C_{33}H_{44}{}^{35}ClN_3O_3$ + H^+): 566.3144, found 566.3138; HPLC purity 98%.

***N*-(6-Chloro-1,2,3,4-tetrahydroacridin-9-yl)-*N’*-[2-(6-hydroxy-7-methoxy-2-methylchroman-2-yl)ethyl]octane-1,8-diamine (6b).** It was prepared as described for **6a**. From tosylate **15** (170 mg, 0.43 mmol) and amine **10b** (467 mg, 1.30 mmol), a brown oily residue (678 mg) was obtained and subjected to column chromatography purification (35−70 μm silica gel, CH_2Cl_2 / MeOH / 50% aq NH_4OH mixtures, gradient elution). On elution with CH_2Cl_2 / MeOH / 50% aq NH_4OH 99:1:0.4, amine **6b** (143 mg, 57% yield) was isolated as a beige solid; R_f 0.74 (CH_2Cl_2 / MeOH / 50% aq NH_4OH 90:10:1).

6b·2HCl: light yellow solid; mp 147–149 °C; IR (ATR) *v* 3600–2200 (max at 3240, 2930, 2852, 2780, N–H, N^+–H, O–H, C–H st), 1630, 1573, 1511 (Ar–C–C, Ar–C–N st) cm^{-1}; ^{1}H NMR

(400 MHz, CD_3OD) δ 1.30 (s, 3H, 2”-CH_3), 1.36–1.52 (complex signal, 8H, 3-H_2, 4-H_2, 5-H_2, 6-H_2), 1.69 (m, 2H, 7-H_2), superimposed in part 1.78 (dt, J = 13.6 Hz, J' = 6.8 Hz, 1H, 3”-H_A), 1.80–1.88 (complex signal, 3H, 2-H_2, 3”-H_B), 1.92–2.00 (complex signal, 5H, 2’-H_2, 3’-H_2, 2”-CH_A-CH_2-NH), 2.07 (dt, J = 13.6 Hz, J' = 7.2 Hz , 1H, 2”-CH_B-CH_2-NH), 2.65–2.72 (complex signal, 4H, 1’-H_2, 4”-H_2), 2.96–3.04 (complex signal, 4H, 8-H_2, 4’-H_2), 3.21 (t, J = 8.0 Hz, 2H, 2”-CH_2-CH_2-NH), 3.76 (s, 3H, 7”-OCH_3), 3.94 (t, J = 6.8 Hz, 2H, 1-H_2), 4.86 (s, NH, $^+$NH, $^+NH_2$, OH), 6.36 (s, 1H, 8”-H), 6.49 (s, 1H, 5”-H), 7.56 (dd, J = 9.2 Hz, J' = 2.4 Hz, 1H, 7’-H), 7.79 (d, J = 2.4 Hz, 1H, 5’-H), 8.39 (d, J = 9.2 Hz, 1H, 8’-H); ^{13}C NMR (100.6 MHz, CD_3OD) δ 21.8 (CH_2, C3’), 22.2 (CH_2, C4”), 22.9 (CH_2, C2’), 23.7 (CH_3, 2”-CH_3), 24.8 (CH_2, C1’), 27.2 (CH_2, C7), 27.5 (CH_2), 27.6 (CH_2) (C3, C6), 29.3 (CH_2, C4’), 30.0 (CH_2), 30.1 (CH_2) (C4, C5), 31.4 (CH_2, C2), 32.6 (CH_2, C3”), 36.4 (CH_2, 2”-CH$_2$-CH_2-NH), 44.7 (CH_2, 2”-CH_2-CH$_2$-NH), 49.2 (CH_2, C8), 49.3 (CH_2, C1), 56.4 (CH_3, 7”-OCH_3), 75.4 (C, C2”), 102.2 (CH, C8”), 113.3 (2C, C9a’, C4a”), 115.4 (C, C8a’), 116.2 (CH, C5”), 119.1 (CH, C5’), 126.8 (CH, C7’), 128.8 (CH, C8’), 140.1 (C, C6’), 140.5 (C, C10a’), 141.3 (C, C6”), 147.2 (C, C8a”), 148.4 (C, C7”), 152.1 (C, C4a’), 157.8 (C, C9’); HRMS (ESI) calcd for ($C_{34}H_{46}{}^{35}ClN_3O_3$ + H^+): 580.3300, found 580.3302; HPLC purity 98%.

***N*-(6-Chloro-1,2,3,4-tetrahydroacridin-9-yl)-*N’*-[2-(6-hydroxy-7-methoxy-2-methylchroman-2-yl)ethyl]nonane-1,9-diamine (6c).** It was prepared as described for **6a**. From tosylate **15** (142 mg, 0.36 mmol) and amine **10c** (403 mg, 1.08 mmol), a brown oily residue (544 mg) was obtained and subjected to column chromatography purification (35−70 μm silica gel, CH_2Cl_2 / MeOH / 50% aq NH_4OH mixtures, gradient elution). On elution with CH_2Cl_2 / MeOH / 50% aq NH_4OH 99.3:0.7:0.4 to 99:1:0.4, amine **6c** (125 mg, 59% yield) was isolated as a beige sticky solid; R_f 0.76 (CH_2Cl_2 / MeOH / 50% aq NH_4OH 90:10:1).

6c·2HCl: beige solid; mp 153–157 °C; IR (ATR) *v* 3600–2200 (max at 3229, 2925, 2852, 2785, N–H, N^+–H, O–H, C–H st), 1628, 1571, 1509 (Ar–C–C, Ar–C–N st) cm^{-1}; ^1H NMR (400 MHz, CD_3OD) δ 1.30 (s, 3H, 2”-CH_3), 1.32–1.50 (complex signal, 10H, 3-H_2, 4-H_2, 5-H_2, 6-H_2, 7-H_2), 1.68 (m, 2H, 8-H_2), superimposed in part 1.79 (dt, J = 13.2 Hz, J' = 6.4 Hz, 1H, 3”-H_A), 1.80–1.90 (complex signal, 3H, 2-H_2, 3”-H_B), 1.90–2.01 (complex signal, 5H, 2’-H_2, 3’-H_2, 2”-CH_A-CH_2-NH), 2.06 (dt, J = 13.6 Hz, J' = 7.6 Hz , 1H, 2”-CH_B-CH_2-NH), 2.64–2.74 (complex signal, 4H, 1’-H_2, 4”-H_2), 2.97–3.03 (complex signal, 4H, 9-H_2, 4’-H_2), 3.22 (t, J = 7.6 Hz, 2H, 2”-CH_2-CH_2-NH), 3.77 (s, 3H, 7”-OCH_3), 3.94 (t, J = 7.6 Hz, 2H, 1-H_2), 4.85 (s, NH, $^+$NH, $^+NH_2$, OH), 6.36 (s, 1H, 8”-H), 6.50 (s, 1H, 5”-H), 7.56 (dd, J = 9.2 Hz, J' = 2.0 Hz, 1H, 7’-H), 7.79 (d, J = 2.0 Hz, 1H, 5’-H), 8.39 (d, J = 9.2 Hz, 1H, 8’-H); ^{13}C NMR (100.6 MHz, CD_3OD) δ 21.8 (CH_2, C3’), 22.2 (CH_2, C4”), 22.9 (CH_2, C2’), 23.7 (CH_3, 2”-CH_3), 24.7 (CH_2, C1’), 27.3 (CH_2, C8), 27.5 (CH_2), 27.7 (CH_2) (C3, C7), 29.3 (CH_2, C4’), 30.1 (CH_2), 30.2 (CH_2), 30.4 (CH_2) (C4, C5, C6), 31.4 (CH_2, C2), 32.6 (CH_2, C3”), 36.5 (CH_2, 2”-*C*H_2-CH_2-NH), 44.7 (CH_2, 2”-CH_2-*C*H_2-NH), 48.9 (CH_2), 49.1 (CH_2) (C1, C9), 56.4 (CH_3, 7”-OCH_3), 75.4 (C, C2”), 102.2 (CH, C8”), 113.4 (2C, C9a’, C4a”), 115.5 (C, C8a’), 116.2 (CH, C5”), 119.2 (CH, C5’), 126.8 (CH, C7’), 128.8 (CH, C8’), 140.1 (C, C6’), 140.6 (C, C10a’), 141.3 (C, C6”), 147.2 (C, C8a”), 148.4 (C, C7”), 152.2 (C, C4a’), 157.8 (C, C9’); HRMS (ESI) calcd for ($C_{35}H_{48}{}^{35}ClN_3O_3$ + H^+): 594.3457, found 594.3461; HPLC purity 97%.

***N*-(6-Chloro-1,2,3,4-tetrahydroacridin-9-yl)-*N’*-[2-(6-hydroxy-7-methoxy-2-methylchroman-2-yl)ethyl]-3,6-dioxaoctane-1,8-diamine (6d).** It was prepared as described for **6a**. From tosylate **15** (200 mg, 0.51 mmol) and amine **10d** (553 mg, 1.52 mmol), a brown sticky solid (763 mg) was obtained and subjected to column chromatography purification (35−70 μm silica gel, CH_2Cl_2 / MeOH / 50% aq NH_4OH mixtures, gradient elution). On elution with

CH_2Cl_2 / MeOH / 50% aq NH_4OH 99.3:0.7:0.4 to 99:1:0.4, amine **6d** (90 mg, 30% yield) was isolated as a brown solid; R_f 0.77 (CH_2Cl_2 / MeOH / 50% aq NH_4OH 90:10:1).

6d·2HCl: brown sticky solid; IR (ATR) *v* 3600–2200 (max at 3369, 3250, 2919, 2857, 2790, N–H, N^+–H, O–H, C–H st), 1630, 1576, 1509 (Ar–C–C, Ar–C–N st) cm^{-1}; ^1H NMR (400 MHz, CD_3OD) δ 1.27 (s, 3H, 2”-CH_3), 1.74 (dt, J = 14.0 Hz, J' = 6.4 Hz, 1H, 3”-H_A), 1.79 (dt, J = 14.0 Hz, J' = 6.4 Hz, 1H, 3”-H_B), 1.92–2.00 (complex signal, 5H, 2’-H_2, 3’-H_2, 2”-CH_A-CH_2-NH), 2.05 (dt, J = 14.0 Hz, J' = 6.8 Hz, 1H, 2”-CH_B-CH_2-NH), 2.56 (dt, J = 12.0 Hz, J' = 6.4 Hz, 1H, 4”-H_A), 2.60–2.70 (complex signal, 3H, 1’-H_2, 4”-H_B), 3.01 (br t, J = 5.6 Hz, 2H, 4’-H_2), 3.25 (t, J = 4.8 Hz, 2H, 8-H_2), superimposed in part 3.31 (m, 2H, 2”-CH_2-CH_2-NH), 3.66–3.73 (complex signal, 4H, 4-H_2, 7-H_2), 3.71 (s, 3H, 7”-OCH_3), 3.77 (t, J = 4.8 Hz, 2H, 5-H_2), 3.88 (m, 2H, 2-H_2), 4.11 (t, J = 4.8 Hz, 2H, 1-H_2), 4.85 (s, NH, $^+$NH, $^+NH_2$, OH), 6.31 (s, 1H, 8”-H), 6.40 (s, 1H, 5”-H), 7.54 (dd, J = 9.2 Hz, J' = 2.0 Hz, 1H, 7’-H), 7.78 (d, J = 2.0 Hz, 1H, 5’-H), 8.43 (d, J = 9.2 Hz, 1H, 8’-H); ^{13}C NMR (100.6 MHz, CD_3OD) δ 21.7 (CH_2, C3’), 22.1 (CH_2, C4”), 22.8 (CH_2, C2’), 23.4 (CH_3, 2”-CH_3), 24.6 (CH_2, C1’), 29.3 (CH_2, C4’), 32.6 (CH_2, C3”), 36.4 (CH_2, 2”-*C*H_2-CH_2-NH), 44.8 (CH_2, 2”-CH_2-*C*H_2-NH), 48.5 (CH_2, C8), 49.1 (CH_2, C1), 56.5 (CH_3, 7”-OCH_3), 66.8 (CH_2, C4), 70.4 (CH_2, C2), 71.3 (CH_2), 71.4 (CH_2) (C5, C7), 75.9 (C, C2”), 102.3 (CH, C8”), 113.4 (C, C9a’), 113.7 (C, C4a”), 115.6 (C, C8a’), 116.1 (CH, C5”), 119.2 (CH, C5’), 126.8 (CH, C7’), 128.8 (CH, C8’), 140.1 (C, C6’), 140.4 (C, C10a’), 141.4 (C, C6”), 146.8 (C, C8a”), 148.3 (C, C7”), 152.4 (C, C4a’), 158.2 (C, C9’); HRMS (ESI) calcd for ($C_{32}H_{42}{}^{35}ClN_3O_5$ + H^+): 584.2886, found 584.2879; HPLC purity 98%.

***N*-{7-[(6-Chloro-1,2,3,4-tetrahydroacridin-9-yl)amino]heptyl}-2-(6-benzyloxy-7-methoxy-2-methylchroman-2-yl)acetamide (11a).** It was prepared as described for **4a**. From carboxylic acid **8** (200 mg, 0.58 mmol) and amine **10a** (222 mg, 0.64 mmol), a brown solid (784 mg) was

obtained and subjected to column chromatography purification (35−70 μm silica gel, CH_2Cl_2 / MeOH / 50% aq NH_4OH mixtures, gradient elution). On elution with CH_2Cl_2 / MeOH / 50% aq NH_4OH 100:0:0.4 to 95:5:0.4, amide **11a** (326 mg, 83% yield) was isolated as a light yellow solid; R_f 0.73 (CH_2Cl_2 / MeOH / 50% aq NH_4OH 90:10:1).

11a·HCl: light yellow solid; mp 107–109 °C; IR (ATR) ν 3600–2200 (max at 3255, 3053, 2929, 2852, N–H, N^+–H, C–H st), 1632, 1568, 1512 (C=O, Ar–C–C, Ar–C–N st) cm^{-1}; ^1H NMR (400 MHz, CD_3OD) δ 1.27–1.38 (complex signal, 6H, 3'-H_2, 4'-H_2, 5'-H_2), 1.33 (s, 3H, 2-CH_3), 1.48 (tt, $J = J' = 6.8$ Hz, 2H, 2'-H_2), superimposed in part 1.75 (tt, $J = J' = 6.4$ Hz, 2H, 6'-H_2), 1.80 (dt, $J = 13.6$ Hz, $J' = 5.6$ Hz, 1H, 3-H_A), superimposed in part 1.90 (dt, $J = 13.6$ Hz, $J' = 5.6$ Hz, 1H, 3-H_B), 1.88–1.98 (complex signal, 4H, 2"-H_2, 3"-H_2), 2.45 (d, $J = 13.6$ Hz, 1H, 2-CH_A-CO), 2.53 (d, $J = 13.6$ Hz, 1H, 2-CH_B-CO), 2.61 (t, $J = 6.0$ Hz, 2H, 1"-H_2), 2.67 (m, 2H, 4-H_2), 2.94 (t, $J = 5.6$ Hz, 2H, 4"-H_2), 3.14 (dt, $J = 13.6$ Hz, $J' = 6.4$ Hz, 1H, 1'-H_A), 3.25 (dt, $J = 13.6$ Hz, $J' = 6.4$ Hz, 1H, 1'-H_B), 3.76 (s, 3H, 7-OCH_3), 3.86 (t, $J = 7.6$ Hz, 2H, 7'-H_2), 4.85 (s, NH, $^+$NH), 4.89 (d, $J = 11.6$ Hz, 1H, 6-OCH_A), 4.93 (d, $J = 11.6$ Hz, 1H, 6-OCH_B), 6.41 (s, 1H, 8-H), 6.67 (s, 1H, 5-H), 7.22–7.32 [complex signal, 3H, benzyl 3(5)-H, benzyl 4-H], 7.35 [dd, $J = 8.4$ Hz, $J' = 1.6$ Hz, 2H, benzyl 2(6)-H], 7.53 (dd, $J = 9.2$ Hz, $J' = 2.0$ Hz, 1H, 7"-H), 7.71 (d, $J = 2.0$ Hz, 1H, 5"-H), 8.33 (d, $J = 9.2$ Hz, 1H, 8"-H); ^{13}C NMR (100.6 MHz, CD_3OD) δ 21.7 (CH_2, C3"), 22.4 (CH_2, C4), 22.8 (CH_2, C2"), 24.63 (CH_2, C1"), 24.64 (CH_3, 2-CH_3), 27.7 (CH_2), 27.8 (CH_2) (C4', C5'), 29.3 (CH_2, C4"), 30.0 (CH_2, C3'), 30.3 (CH_2, C2'), 31.3 (CH_2, C6'), 32.0 (CH_2, C3), 40.1 (CH_2, C1'), 47.7 (CH_2, 2-*C*H_2-CO), 49.3 (CH_2, C7'), 56.5 (CH_3, 7-OCH_3), 73.5 (CH_2, 6-OCH_2), 75.9 (C, C2), 103.1 (CH, C8), 113.2 (2C, C9a", C4a), 115.4 (C, C8a"), 117.7 (CH, C5), 119.1 (CH, C5"), 126.7 (CH, C7"), 128.7 [3CH, benzyl C2(6), benzyl C4], 128.8 (CH, C8"), 129.3 [2CH, benzyl C3(5)], 138.9 (C, benzyl C1), 140.1 (C, C6"), 140.5 (C, C10a"), 143.3

(C, C6), 149.3 (C, C8a), 151.0 (C, C7), 151.9 (C, C4a"), 157.6 (C, C9"), 172.3 (C, CONH); HRMS (ESI) calcd for ($C_{40}H_{48}{}^{35}ClN_3O_4$ + H^+): 670.3406, found 670.3400; HPLC purity 97%.

***N*-{8-[(6-Chloro-1,2,3,4-tetrahydroacridin-9-yl)amino]octyl}-2-(6-benzyloxy-7-methoxy-2-methylchroman-2-yl)acetamide (11b).** It was prepared as described for **4a**. From carboxylic acid **8** (100 mg, 0.29 mmol) and amine **10b** (116 mg, 0.32 mmol), a brown solid (462 mg) was obtained and subjected to column chromatography purification (35−70 μm silica gel, CH_2Cl_2 / MeOH / 50% aq NH_4OH mixtures, gradient elution). On elution with CH_2Cl_2 / MeOH / 50% aq NH_4OH 100:0:0.4, amide **11b** (183 mg, 92% yield) was isolated as a yellow solid; R_f 0.73 (CH_2Cl_2 / MeOH / 50% aq NH_4OH 90:10:1).

11b·HCl: light yellow solid; mp 127–129 °C; IR (ATR) ν 3600–2200 (max at 3261, 3053, 2924, 2852, N–H, N^+–H, C–H st), 1632, 1571, 1510 (C=O, Ar–C–C, Ar–C–N st) cm^{-1}; ^1H NMR (400 MHz, CD_3OD) δ 1.20–1.34 (complex signal, 6H, 3'-H_2, 4'-H_2, 5'-H_2), 1.33 (s, 3H, 2-CH_3), 1.37 (tt, $J = J' = 6.8$ Hz, 2H, 6'-H_2), 1.48 (tt, $J = J' = 6.8$ Hz, 2H, 2'-H_2), superimposed in part 1.77 (tt, $J = 7.2$ Hz, $J' = 6.8$ Hz, 2H, 7'-H_2), 1.79 (dt, $J = 13.6$ Hz, $J' = 6.8$ Hz, 1H, 3-H_A), superimposed in part 1.90 (dt, $J = 13.6$ Hz, $J' = 6.8$ Hz, 1H, 3-H_B), 1.87–1.99 (complex signal, 4H, 2"-H_2, 3"-H_2), 2.45 (d, $J = 13.6$ Hz, 1H, 2-CH_A-CO), 2.53 (d, $J = 13.6$ Hz, 1H, 2-CH_B-CO), 2.61 (t, $J = 5.6$ Hz, 2H, 1"-H_2), 2.67 (m, 2H, 4-H_2), 2.94 (t, $J = 6.0$ Hz, 2H, 4"-H_2), 3.14 (dt, $J = 13.6$ Hz, $J' = 6.8$ Hz, 1H, 1'-H_A), 3.25 (dt, $J = 13.6$ Hz, $J' = 6.8$ Hz, 1H, 1'-H_B), 3.77 (s, 3H, 7-OCH_3), 3.85 (t, $J = 7.2$ Hz, 2H, 8'-H_2), 4.85 (s, NH, $^+$NH), 4.89 (d, $J = 12.0$ Hz, 1H, 6-OCH_A), 4.93 (d, $J = 12.0$ Hz, 1H, 6-OCH_B), 6.42 (s, 1H, 8-H), 6.67 (s, 1H, 5-H), 7.18–7.30 [complex signal, 3H, benzyl 3(5)-H, benzyl 4-H], 7.35 [dm, $J = 8.0$ Hz, 2H, benzyl 2(6)-H], 7.52 (dd, $J = 9.2$ Hz, $J' = 2.0$ Hz, 1H, 7"-H), 7.72 (d, $J = 2.0$ Hz, 1H, 5"-H), 8.33 (d, $J = 9.2$ Hz, 1H, 8"-H); ^{13}C NMR (100.6 MHz, CD_3OD) δ 21.7 (CH_2, C3"), 22.4 (CH_2, C4), 22.8 (CH_2, C2"), 24.62

(CH_2, C1”), 24.63 (CH_3, 2-CH_3), 27.6 (CH_2, C6’), 27.8 (CH_2, C5’), 29.3 (CH_2, C4”), 30.2 (CH_2), 30.3 (CH_2) (C3’, C4’), 30.4 (CH_2, C2’), 31.4 (CH_2, C7’), 32.0 (CH_2, C3), 40.2 (CH_2, C1’), 47.7 (CH_2, 2-*C*H_2-CO), 49.3 (CH_2, C8’), 56.5 (CH_3, 7-OCH_3), 73.4 (CH_2, 6-OCH_2), 75.9 (C, C2), 103.0 (CH, C8), 113.17 (C), 113.20 (C) (C4a, C9a”), 115.3 (C, C8a”), 117.5 (CH, C5), 119.1 (CH, C5”), 126.7 (CH, C7”), 128.7 [3CH, benzyl C2(6), benzyl C4], 128.8 (CH, C8”), 129.3 [2CH, benzyl C3(5)], 138.9 (C, benzyl C1), 140.0 (C, C6”), 140.5 (C, C10a”), 143.3 (C, C6), 149.3 (C, C8a), 150.9 (C, C7), 151.9 (C, C4a”), 157.6 (C, C9”), 172.3 (C, CONH); HRMS (ESI) calcd for ($C_{41}H_{50}{}^{35}ClN_3O_4 + H^+$): 684.3562, found 684.3563; HPLC purity 99%.

***N*-{9-[(6-Chloro-1,2,3,4-tetrahydroacridin-9-yl)amino]nonyl}-2-(6-benzyloxy-7-methoxy-2-methylchroman-2-yl)acetamide (11c).** It was prepared as described for **4a**. From carboxylic acid **8** (128 mg, 0.37 mmol) and amine **10c** (154 mg, 0.41 mmol), a brown oily residue (521 mg) was obtained and subjected to column chromatography purification (35−70 μm silica gel, CH_2Cl_2 / MeOH / 50% aq NH_4OH mixtures, gradient elution). On elution with CH_2Cl_2 / MeOH / 50% aq NH_4OH 100:0:0.4 to 99:1:0.4, amide **11c** (236 mg, 90% yield) was isolated as a light yellow solid; R_f 0.74 (CH_2Cl_2 / MeOH / 50% aq NH_4OH 90:10:1).

11c·HCl: light yellow solid; mp 107–109 °C; IR (ATR) ν 3600–2200 (max at 3244, 3053, 2924, 2852, N–H, N^+–H, C–H st), 1633, 1573, 1510 (C=O, Ar–C–C, Ar–C–N st) cm^{-1}; ^1H NMR (400 MHz, CD_3OD) δ 1.18–1.36 (complex signal, 8H, 3’-H_2, 4’-H_2, 5’-H_2, 6’-H_2), 1.33 (s, 3H, 2-CH_3), 1.39 (tt, J = 7.6 Hz, J' = 6.8 Hz, 2H, 7’-H_2), 1.48 (tt, $J = J'$ = 6.8 Hz, 2H, 2’-H_2), superimposed in part 1.77 (tt, J = 7.6 Hz, J' = 7.2 Hz, 2H, 8’-H_2), 1.80 (dt, J = 13.2 Hz, J' = 6.0 Hz, 1H, 3-H_A), superimposed in part 1.90 (dt, J = 13.2 Hz, J' = 6.0 Hz, 1H, 3-H_B), 1.87–1.98 (complex signal, 4H, 2”-H_2, 3”-H_2), 2.45 (d, J = 13.6 Hz, 1H, 2-CH_A-CO), 2.52 (d, J = 13.6 Hz, 1H, 2-CH_B-CO), 2.63 (t, J = 5.2 Hz, 2H, 1”-H_2), 2.69 (m, 2H, 4-H_2), 2.95 (t, J = 6.0 Hz, 2H, 4”-

H_2), 3.14 (dt, *J* = 13.2 Hz, *J'* = 6.8 Hz, 1H, 1'-H_A), 3.23 (dt, *J* = 13.2 Hz, *J'* = 6.8 Hz, 1H, 1'-H_B), 3.77 (s, 3H, 7-OCH_3), 3.87 (t, *J* = 7.2 Hz, 2H, 9'-H_2), 4.85 (s, NH, $^+$NH), 4.91 (d, *J* = 12.4 Hz, 1H, 6-OCH_A), 4.94 (d, *J* = 12.4 Hz, 1H, 6-OCH_B), 6.42 (s, 1H, 8-H), 6.68 (s, 1H, 5-H), 7.22 (br t, *J* = 7.2 Hz, 1H, benzyl 4-H), 7.27 [dd, *J* = *J'* = 7.2 Hz, 2H, benzyl 3(5)-H], 7.36 [br d, *J* = 7.2 Hz, 2H, benzyl 2(6)-H], 7.53 (dd, *J* = 9.2 Hz, *J'* = 2.0 Hz, 1H, 7"-H), 7.73 (d, *J* = 2.0 Hz, 1H, 5"-H), 8.34 (d, *J* = 9.2 Hz, 1H, 8"-H); ^{13}C NMR (100.6 MHz, CD_3OD) δ 21.8 (CH_2, C3"), 22.5 (CH_2, C4), 22.8 (CH_2, C2"), 24.56 (CH_3, 2-CH_3), 24.63 (CH_2, C1"), 27.7 (CH_2, C7'), 27.9 (CH_2, C6'), 29.3 (CH_2, C4"), 30.2 (CH_2), 30.3 (CH_2), 30.4 (CH_2), 30.5 (CH_2) (C2', C3', C4', C5'), 31.3 (CH_2, C8'), 32.1 (CH_2, C3), 40.2 (CH_2, C1'), 47.7 (CH_2, 2-*C*H_2-CO), 49.3 (CH_2, C9'), 56.4 (CH_3, 7-OCH_3), 73.5 (CH_2, 6-OCH_2), 75.9 (C, C2), 103.0 (CH, C8), 113.2 (C, C9a"), 113.3 (C, C4a), 115.4 (C, C8a"), 117.6 (CH, C5), 119.2 (CH, C5"), 126.7 (CH, C7"), 128.78 (CH, C8"), 128.81 [3CH, benzyl C2(6), benzyl C4], 129.3 [2CH, benzyl C3(5)], 139.0 (C, benzyl C1), 140.1 (C, C6"), 140.6 (C, C10a"), 143.4 (C, C6), 149.3 (C, C8a), 150.9 (C, C7), 152.0 (C, C4a"), 157.7 (C, C9"), 172.3 (C, CONH); HRMS (ESI) calcd for ($C_{42}H_{52}{}^{35}ClN_3O_4$ + H^+): 698.3719, found 698.3714; HPLC purity 97%.

***N*-{6-[(6-Chloro-1,2,3,4-tetrahydroacridin-9-yl)amino]hexyl}-2-(6-benzyloxy-7-methoxy-2-methylchroman-2-yl)acetamide (11e).** It was prepared as described for **4a**. From carboxylic acid **8** (100 mg, 0.29 mmol) and amine **10e** (107 mg, 0.32 mmol), a brown solid (463 mg) was obtained and subjected to column chromatography purification (35−70 μm silica gel, CH_2Cl_2 / MeOH / 50% aq NH_4OH mixtures, gradient elution). On elution with CH_2Cl_2 / MeOH / 50% aq NH_4OH 100:0:0.4, amide **11e** (191 mg, quantitative yield) was isolated as a light yellow solid; R_f 0.73 (CH_2Cl_2 / MeOH / 50% aq NH_4OH 90:10:1).

11e·HCl: light yellow solid; mp 126–128 °C; IR (ATR) *v* 3600–2200 (max at 3250, 3048, 2928, 2852, N–H, N^+–H, C–H st), 1632, 1573, 1510 (C=O, Ar–C–C, Ar–C–N st) cm^{-1}; ^1H NMR (400 MHz, CD_3OD) δ 1.31 (s, 3H, 2-CH_3), 1.34–1.44 (complex signal, 4H, 3'-H_2, 4'-H_2), 1.51 (tt, $J = J' = 6.8$ Hz, 2H, 2'-H_2), 1.70 (tt, $J = 7.2$ Hz, $J' = 6.8$ Hz, 2H, 5'-H_2), 1.80 (dt, $J = 13.6$ Hz, $J' = 6.0$ Hz, 1H, 3-H_A), superimposed in part 1.93 (dt, $J = 13.6$ Hz, $J' = 6.0$ Hz, 1H, 3-H_B), 1.85–1.96 (complex signal, 4H, 2"-H_2, 3"-H_2), 2.45 (d, $J = 13.6$ Hz, 1H, 2-CH_A-CO), 2.53 (d, $J = 13.6$ Hz, 1H, 2-CH_B-CO), superimposed in part 2.61 (m, 2H, 4-H_2), 2.65 (br t, $J = 6.4$ Hz, 2H, 1"-H_2), 2.90 (t, $J = 5.6$ Hz, 2H, 4"-H_2), 3.14 (dt, $J = 13.6$ Hz, $J' = 6.8$ Hz, 1H, 1'-H_A), 3.28 (dt, $J = 13.6$ Hz, $J' = 6.8$ Hz, 1H, 1'-H_B), 3.75 (s, 3H, 7-OCH_3), 3.80 (t, $J = 7.2$ Hz, 2H, 6'-H_2), 4.83 (d, $J = 12.0$ Hz, 1H, 6-OCH_A), 4.85 (s, NH, $^+$NH), 4.91 (d, $J = 12.0$ Hz, 1H, 6-OCH_B), 6.40 (s, 1H, 8-H), 6.62 (s, 1H, 5-H), 7.22–7.31 [complex signal, 3H, benzyl 3(5)-H, benzyl 4-H], 7.35 [dd, $J = 8.0$ Hz, $J' = 1.6$ Hz, 2H, benzyl 2(6)-H], 7.52 (dd, $J = 9.2$ Hz, $J' = 2.0$ Hz, 1H, 7"-H), 7.71 (d, $J = 2.0$ Hz, 1H, 5"-H), 8.28 (d, $J = 9.2$ Hz, 1H, 8"-H); ^{13}C NMR (100.6 MHz, CD_3OD) δ 21.7 (CH_2, C3"), 22.4 (CH_2, C4), 22.8 (CH_2, C2"), 24.56 (CH_2, C1"), 24.64 (CH_3, 2-CH_3), 27.36 (CH_2), 27.39 (CH_2) (C3', C4'), 29.2 (CH_2, C4"), 30.3 (CH_2, C2'), 31.3 (CH_2, C5'), 31.9 (CH_2, C3), 40.0 (CH_2, C1'), 47.8 (CH_2, 2-*C*H_2-CO), 49.3 (CH_2, C6'), 56.5 (CH_3, 7-OCH_3), 73.5 (CH_2, 6-OCH_2), 75.9 (C, C2), 103.1 (CH, C8), 113.2 (2C, C4a, C9a"), 115.3 (C, C8a"), 117.7 (CH, C5), 119.1 (CH, C5"), 126.7 (CH, C7"), 128.7 [3CH, benzyl C2(6), benzyl C4], 128.8 (CH, C8"), 129.3 [2CH, benzyl C3(5)], 138.9 (C, benzyl C1), 140.0 (C, C6"), 140.4 (C, C10a"), 143.3 (C, C6), 149.3 (C, C8a), 150.9 (C, C7), 151.9 (C, C4a"), 157.5 (C, C9"), 172.3 (C, CONH); HRMS (ESI) calcd for ($C_{39}H_{46}{}^{35}ClN_3O_4 + H^+$): 656.3249, found 656.3238; HPLC purity 99%.

***N*-{7-[(1,2,3,4-Tetrahydroacridin-9-yl)amino]heptyl}-2-(6-hydroxy-7-methoxy-2-methylchroman-2-yl)acetamide (12a).** A solution of amide **11a** (123 mg, 0.19 mmol) in

degassed EtOH (3 mL) was added to a suspension of 10% w/w Pd/C in EtOH (1.5 mL). The mixture was stirred at rt and atmospheric pressure of H_2 overnight. An additional portion of catalyst was added and the mixture was allowed to react under the same conditions overnight. The resulting mixture was filtered through a plug of Celite® and washed with EtOH (3 × 5 mL). The filtrate was evaporated in vacuo to afford hybrid **12a** (73 mg, 72% yield) as a light yellow solid; R_f 0.27 (CH_2Cl_2 / MeOH / 50% aq NH_4OH 95:5:1).

12a·HCl: light yellow solid; mp 115–118 °C; IR (ATR) ν 3600–2200 (max at 3248, 3092, 2930, 2852, N–H, N^+–H, O–H, C–H st), 1634, 1574, 1520 (C=O, Ar–C–C, Ar–C–N st) cm^{-1}; ^1H NMR (400 MHz, CD_3OD) δ 1.31 (s, 3H, 2-CH_3), 1.32–1.41 (complex signal, 6H, 3'-H_2, 4'-H_2, 5'-H_2), 1.49 (tt, $J = J' = 7.2$ Hz, 2H, 2'-H_2), 1.72–1.82 (complex signal, 3H, 3-H_A, 6'-H_2), 1.83–1.91 (m, 1H, 3-H_B), 1.92–2.00 (complex signal, 4H, 2"-H_2, 3"-H_2), 2.44 (d, $J = 13.6$ Hz, 1H, 2-CH_A-CO), 2.49 (d, $J = 13.6$ Hz, 1H, 2-CH_B-CO), 2.62 (t, $J = 6.0$ Hz, 2H, 4-H_2), 2.68 (t, $J = 5.6$ Hz, 2H, 1"-H_2), 3.00 (t, $J = 6.0$ Hz, 2H, 4"-H_2), 3.18 (m, 2H, 1'-H_2), 3.74 (s, 3H, 7-OCH_3), 3.91 (t, $J = 7.2$ Hz, 2H, 7'-H_2), 4.85 (s, NH, $^+$NH, OH), 6.33 (s, 1H, 8-H), 6.45 (s, 1H, 5-H), 7.58 (ddd, $J = 8.8$ Hz, $J' = 7.2$ Hz, $J'' = 1.2$ Hz, 1H, 7"-H), 7.74 (dd, $J = 8.4$ Hz, $J' = 1.2$ Hz, 1H, 5"-H), 7.84 (ddd, $J = 8.4$ Hz, $J' = 7.2$ Hz, $J'' = 1.2$ Hz, 1H, 6"-H), 8.37 (d, $J = 8.8$ Hz, 1H, 8"-H); ^{13}C NMR (100.6 MHz, CD_3OD) δ 21.8 (CH_2, C3"), 22.4 (CH_2, C4), 23.0 (CH_2, C2"), 24.4 (CH_3, 2-CH_3), 24.9 (CH_2, C1"), 27.6 (CH_2, C5'), 27.7 (CH_2, C4'), 29.3 (CH_2, C4"), 29.9 (CH_2, C3'), 30.2 (CH_2, C2'), 31.4 (CH_2, C6'), 32.3 (CH_2, C3), 40.4 (CH_2, C1'), 47.3 (CH_2, 2-*C*H_2-CO), 49.1 (CH, C7'), 56.4 (CH_3, 7-OCH_3), 75.5 (C, C2), 102.2 (CH, C8), 112.8 (C, C9a"), 113.3 (C, C4a), 116.1 (CH, C5), 117.0 (C, C8a"), 120.1 (CH, C5"), 126.3 (CH, C7"), 126.5 (CH, C8"), 134.0 (CH, C6"), 139.7 (C, C10a"), 141.1 (C, C6), 147.3 (C, C8a), 148.3 (C, C7), 151.6 (C, C4a"),

157.9 (C, C9”), 172.7 (C, CONH); HRMS (ESI) calcd for ($C_{33}H_{43}N_3O_4$+ H^+): 546.3332, found 546.3290; HPLC purity 100%.

***N*-{8-[(1,2,3,4-Tetrahydroacridin-9-yl)amino]octyl}-2-(6-hydroxy-7-methoxy-2-methylchroman-2-yl)acetamide (12b).** It was prepared as described for **12a**. From **11b** (56 mg, 0.08 mmol), amide **12b** (46 mg, 99% yield) was isolated as a light green solid; R_f 0.26 (CH_2Cl_2 / MeOH / 50% aq NH_4OH 95:5:1).

12b·HCl: light green solid; mp 104–107 °C; IR (ATR) *ν* 3600–2200 (max at 3249, 3090, 2927, 2852, N–H, N^+–H, O–H, C–H st), 1634, 1575, 1519 (C=O, Ar–C–C, Ar–C–N st) cm^{-1}; ^1H NMR (400 MHz, CD_3OD) *δ* 1.25–1.34 (complex signal, 9H, 2-CH_3, 3’-H_2, 4’-H_2, 5’-H_2), 1.38 (m, 2H, 6’-H_2), 1.47 (m, 2H, 2’-H_2), 1.72–1.84 (complex signal, 3H, 3-H_A, 7’-H_2), 1.87 (m, 1H, 3-H_B), 1.91–2.01 (complex signal, 4H, 2”-H_2, 3”-H_2), 2.44 (d, *J* = 13.2 Hz, 1H, 2-CH_A-CO), 2.48 (d, *J* = 13.2 Hz, 1H, 2-CH_B-CO), 2.62 (t, *J* = 6.4 Hz, 2H, 4-H_2), 2.69 (t, *J* = 5.6 Hz, 2H, 1”-H_2), 3.00 (t, *J* = 6.0 Hz, 2H, 4”-H_2), 3.17 (m, 2H, 1’-H_2), 3.75 (s, 3H, 7-OCH_3), 3.91 (t, *J* = 7.2 Hz, 2H, 8’-H_2), 4.85 (s, NH, $^+$NH, OH), 6.34 (s, 1H, 8-H), 6.45 (s, 1H, 5-H), 7.58 (ddd, *J* = 8.8 Hz, *J’* = 7.2 Hz, *J”* = 1.2 Hz, 1H, 7”-H), 7.74 (dd, *J* = 8.4 Hz, *J’* = 1.2 Hz, 1H, 5”-H), 7.84 (ddd, *J* = 8.4 Hz, *J’* = 7.2 Hz, *J”* = 1.2 Hz, 1H, 6”-H), 8.34 (br d, *J* = 8.8 Hz, 1H, 8”-H); ^{13}C NMR (100.6 MHz, CD_3OD) *δ* 21.8 (CH_2, C3”), 22.4 (CH_2, C4), 23.0 (CH_2, C2”), 24.5 (CH_3, 2-CH_3), 24.8 (CH_2, C1”), 27.6 (CH_2, C6’), 27.7 (CH_2, C5’), 29.3 (CH_2, C4”), 30.1 (CH_2), 30.2 (CH_2) (C3’, C4’), 30.3 (CH_2, C2’), 31.5 (CH_2, C7’), 32.3 (CH_2, C3), 40.3 (CH_2, C1’), 47.4 (CH_2, 2-*C*H_2-CO), 49.2 (CH, C8’), 56.4 (CH_3, 7-OCH_3), 75.6 (C, C2), 102.2 (CH, C8), 112.8 (C, C9a”), 113.3 (C, C4a), 116.1 (CH, C5), 117.0 (C, C8a”), 120.1 (CH, C5”), 126.3 (CH, C7”), 126.5 (CH, C8”), 134.1 (CH, C6”), 139.7 (C, C10a”), 141.1 (C, C6), 147.3 (C, C8a), 148.3 (C, C7), 151.6 (C,

C4a"), 157.9 (C, C9"), 172.6 (C, CONH); HRMS (ESI) calcd for ($C_{34}H_{45}N_3O_4$+ H^+): 560.3488, found 560.3496; HPLC purity 97%.

***N*-{9-[(1,2,3,4-Tetrahydroacridin-9-yl)amino]nonyl}-2-(6-hydroxy-7-methoxy-2-methylchroman-2-yl)acetamide (12c).** It was prepared as described for **12a**. From **11c** (65 mg, 0.09 mmol), amide **12c** (53 mg, 99% yield) was isolated as a light yellow solid; R_f 0.25 (CH_2Cl_2 / MeOH / 50% aq NH_4OH 95:5:1).

12c·HCl: light yellow solid; mp 105–108 °C; IR (ATR) *v* 3600–2200 (max at 3250, 3098, 2929, 2852, N–H, N^+–H, O–H, C–H st), 1633, 1572, 1515 (C=O, Ar–C–C, Ar–C–N st) cm^{-1}; ^1H NMR (400 MHz, CD_3OD) δ 1.21–1.35 (complex signal, 11H, 2-CH_3, 3'-H_2, 4'-H_2, 5'-H_2, 6'-H_2,), 1.39 (m, 2H, 7'-H_2), 1.47 (tt, $J = J' = 6.8$ Hz, 2H, 2'-H_2), 1.73–1.90 (complex signal, 4H, 3-H_2, 8'-H_2), 1.93–2.02 (complex signal, 4H, 2"-H_2, 3"-H_2), 2.44 (d, $J = 13.6$ Hz, 1H, 2-CH_A-CO), 2.49 (d, $J = 13.6$ Hz, 1H, 2-CH_B-CO), 2.63 (t, $J = 6.8$ Hz, 2H, 4-H_2), 2.70 (t, $J = 5.2$ Hz, 2H, 1"-H_2), 3.01 (t, $J = 6.8$ Hz, 2H, 4"-H_2), 3.18 (m, 2H, 1'-H_2), 3.76 (s, 3H, 7-OCH_3), 3.93 (t, $J = 7.2$ Hz, 2H, 9'-H_2), 4.85 (s, NH, $^+$NH, OH), 6.34 (s, 1H, 8-H), 6.45 (s, 1H, 5-H), 7.58 (ddd, $J = 8.8$ Hz, $J' = 6.8$ Hz, $J'' = 1.2$ Hz, 1H, 7"-H), 7.74 (dd, $J = 8.4$ Hz, $J' = 1.2$ Hz, 1H, 5"-H), 7.85 (ddd, $J = 8.4$ Hz, $J' = 6.8$ Hz, $J'' = 1.2$ Hz, 1H, 6"-H), 8.39 (br d, $J = 8.8$ Hz, 1H, 8"-H); ^{13}C NMR (100.6 MHz, CD_3OD) δ 21.8 (CH_2, C3"), 22.4 (CH_2, C4), 23.0 (CH_2, C2"), 24.4 (CH_3, 2-CH_3), 24.9 (CH_2, C1"), 27.6 (CH_2, C7'), 27.8 (CH_2, C6'), 29.3 (CH_2, C4"), 30.1 (CH_2), 30.2 (2CH_2) (C2', C3', C4'), 30.4 (CH_2, C5'), 31.5 (CH_2, C8'), 32.3 (CH_2, C3), 40.6 (CH_2, C1'), 47.2 (CH_2, 2-*C*H_2-CO), 49.2 (CH, C9'), 56.4 (CH_3, 7-OCH_3), 75.5 (C, C2), 102.2 (CH, C8), 112.8 (C, C9a"), 113.3 (C, C4a), 116.0 (CH, C5), 117.0 (C, C8a"), 120.1 (CH, C5"), 126.3 (CH, C7"), 126.5 (CH, C8"), 134.0 (CH, C6"), 139.7 (C, C10a"), 141.1 (C, C6), 147.2 (C, C8a), 148.3 (C,

C7), 151.6 (C, C4a"), 157.9 (C, C9"), 172.8 (C, CONH); HRMS (ESI) calcd for ($C_{35}H_{47}N_3O_4$+ H^+): 574.3645, found 574.3655; HPLC purity 99%.

***N*-{6-[(1,2,3,4-Tetrahydroacridin-9-yl)amino]hexyl}-2-(6-hydroxy-7-methoxy-2-methylchroman-2-yl)acetamide (12e).** It was prepared as described for **12a**. From **11e** (43 mg, 0.07 mmol), amide **12e** (35 mg, 99% yield) was isolated as a light yellow solid; R_f 0.27 (CH_2Cl_2 / MeOH / 50% aq NH_4OH 95:5:1).

12e·HCl: light yellow solid; mp 117–120 °C; IR (ATR) *v* 3600–2200 (max at 3236, 3081, 2930, 2856, N–H, N^+–H, O–H, C–H st), 1633, 1573, 1519 (C=O, Ar–C–C, Ar–C–N st) cm^{-1}; ^1H NMR (400 MHz, CD_3OD) δ 1.29 (s, 3H, 2-CH_3), 1.34–1.46 (complex signal, 4H, 3'-H_2, 4'-H_2), 1.52 (tt, $J = J' = 6.8$ Hz, 2H, 2'-H_2), 1.70–1.81 (complex signal, 3H, 3-H_A, 5'-H_2), 1.89 (m, 1H, 3-H_B), 1.93–2.01 (complex signal, 4H, 2"-H_2, 3"-H_2), 2.43 (d, $J = 13.2$ Hz, 1H, 2-CH_A-CO), 2.49 (d, $J = 13.2$ Hz, 1H, 2-CH_B-CO), 2.59 (m, 2H, 4-H_2), 2.68 (t, $J = 5.6$ Hz, 2H, 1"-H_2), 3.00 (t, $J = 6.0$ Hz, 2H, 4"-H_2), 3.20 (m, 2H, 1'-H_2), 3.72 (s, 3H, 7-OCH_3), 3.85 (t, $J = 7.6$ Hz, 2H, 6'-H_2), 4.85 (s, NH, $^+$NH, OH), 6.32 (s, 1H, 8-H), 6.41 (s, 1H, 5-H), 7.57 (ddd, $J = 8.8$ Hz, $J' = 7.2$ Hz, $J'' = 1.2$ Hz, 1H, 7"-H), 7.73 (dd, $J = 8.4$ Hz, $J' = 1.2$ Hz, 1H, 5"-H), 7.84 (ddd, $J = 8.4$ Hz, $J' = 7.2$ Hz, $J'' = 1.2$ Hz, 1H, 6"-H), 8.34 (br d, $J = 8.8$ Hz, 1H, 8"-H); ^{13}C NMR (100.6 MHz, CD_3OD) δ 21.8 (CH_2, C3"), 22.4 (CH_2, C4), 23.0 (CH_2, C2"), 24.5 (CH_3, 2-CH_3), 24.8 (CH_2, C1"), 27.3 (CH_2), 27.4 (CH_2) (C3', C4'), 29.3 (CH_2, C4"), 30.2 (CH_2, C2'), 31.4 (CH_2, C5'), 32.2 (CH_2, C3), 40.1 (CH_2, C1'), 47.5 (CH_2, 2-*C*H_2-CO), 49.0 (CH, C6'), 56.4 (CH_3, 7-OCH_3), 75.1 (C, C2), 102.2 (CH, C8), 112.8 (C, C9a"), 113.4 (C, C4a), 116.1 (CH, C5), 117.0 (C, C8a"), 120.1 (CH, C5"), 126.3 (CH, C7"), 126.5 (CH, C8"), 134.0 (CH, C6"), 139.8 (C, C10a"), 141.1 (C, C6), 147.4 (C, C8a), 148.3 (C, C7), 151.6 (C, C4a"), 157.9 (C, C9"), 172.6 (C, CONH); HRMS (ESI) calcd for ($C_{32}H_{41}N_3O_4$+ H^+): 532.3175, found 532.3165; HPLC purity 99%.

2-(6-Hydroxy-7-methoxy-2-methylchroman-2-yl)ethyl *p*-toluenesulfonate (15). A solution of *O*-benzyl-protected tosylate **16** (1.07 g, 2.22 mmol) in THF (15 mL) was added to a suspension of 10% w/w Pd/C (110 mg) in degassed THF (2 mL) under argon atmosphere. The resulting mixture was stirred under 1 atm of H_2 overnight, then filtered through a plug of Celite®, and washed with THF (3 × 5 mL). The filtrate was evaporated at reduced pressure to yield tosylate **15** (782 mg, 90% yield) as a light green solid; ^{1}H NMR (400 MHz, $CDCl_3$) δ 1.23 (s, 3H, 2-CH_3), 1.72 (m, 2H, 3-H_2), 1.91 (m, 1H), 1.99 (m, 1H) (2-C*H*$_2$-CH_2-OTs), 2.43 (s, 3H, tosyl CH_3), 2.62 (m, 2H, 4-H_2), 3.80 (s, 3H, 7-OCH_3), 3.97 (m, 2H, 2-CH_2-C*H*$_2$-OTs), 6.25 (s, 1H, 8-H), 6.56 (s, 1H, 5-H), 7.31 [d, *J* = 8.0 Hz, 2H, tosyl 3(5)-H], 7.76 [d, *J* = 8.0 Hz, 2H, tosyl 2(6)-H]; ^{13}C NMR (100.6 MHz, $CDCl_3$) δ 21.4 (CH_3, tosyl CH_3), 21.8 (CH_2, C4), 24.2 (CH_3, 2-CH_3), 31.7 (CH_2, C3), 38.2 (CH_2, 2-*C*H_2-CH_2-OTs), 56.0 (CH_3, 7-OCH_3), 67.6 (CH_2, 2-CH_2-*C*H_2-OTs), superimposed with solvent signal 76.7 (C, C2), 100.5 (CH, C8), 112.3 (C, C4a), 114.2 (CH, C5), 128.0 (CH), 129.9 (CH) (tosyl CH), 133.2 (C, tosyl C4), 139.4 (C, tosyl C1), 144.9 (C, C6), 145.9 (C), 146.3 (C) (C7, C8a); HRMS (ESI) calcd for ($C_{20}H_{24}O_6S$ + H^+): 393.1372, found 393.1336.

In Vitro Biological Studies

AChE and BChE Inhibition Assay. The inhibitory activity of the target CR6–chlorotacrine hybrids towards human recombinant AChE and human serum BChE (Sigma, Milan, Italy) was evaluated spectrophotometrically by the method of Ellman et al.[27] The enzyme stock solutions were prepared by dissolving enzyme lyophilized powders in 0.1% Triton X-100/0.1 M potassium phosphate, pH 8.0 (for hAChE) or in 0.1% aq. gelatin (for hBChE). The stock solutions of the target compounds (1 mM) were prepared in MeOH. The assay solution consisted of 340 μM 5,5'-dithiobis(2-nitrobenzoic acid) (DTNB), 0.02 unit/mL hAChE or hBChE, and 550 μM

acetylthiocholine iodide (substrate for hAChE) or butyrylthiocholine iodide (substrate for hBChE) in 0.1 M potassium phosphate, pH 8.0. Assay solutions with and without the target compounds were preincubated at 37 °C for 20 min, before the addition of the substrate. Blank solutions containing all components except the enzymes were prepared in parallel to correct for non-enzymatic hydrolysis of the substrates. Initial rates were monitored at 412 nm with a Jasco V-530 double beam spectrophotometer equipped with thermostated cuvette holders (37 °C). At least five increasing concentrations of the target compounds, which led to 20–80% inhibition of the enzymatic activities, were assayed. IC_{50} values were calculated using Microcal Origin 3.5 software (Microcal Software, Inc), and are expressed as mean ± standard error of the mean (SEM) of at least two experiments, each performed in triplicate.

Kinetic Analysis of AChE Inhibition. To estimate the mechanism of action of hybrid **6b**, Lineweaver-Burk double reciprocal plots were constructed at relatively low concentration of substrate (0.110-0.553 mM) using the same experimental conditions reported for the hAChE inhibition assay. The plots were assessed by a weighted least square analysis that assumed the variance of the velocity (v) to be a constant percentage of v for the entire data set. To confirm the mode of inhibition, Cornish-Bowden plot was obtained by plotting S/v (substrate/velocity ratio) versus inhibitor concentration.[51] Data analysis was performed with GraphPad Prism 4.03 software (GraphPad Software Inc.). The mechanism of inhibition was assessed by two independent experiments, each performed in triplicate.

Calculation of the inhibitor constant (K_i) value was carried out by re-plotting slopes of lines from the Lineweaver-Burk plot versus the inhibitor concentration and K_i was determined as the intersect on the negative x-axis. K'_i (dissociation constant for the enzyme–substrate–inhibitor complex) value was determined by plotting the apparent $1/v_{max}$ versus inhibitor concentration.[52]

Propidium Displacement Studies. The affinity of hybrid **6b** for the peripheral anionic site (PAS) of *Electrophorus electricus* AChE (EeAChE) (type VI-S, Sigma-Aldrich) was tested using propidium iodide (P) (Sigma-Aldrich), a known PAS-specific ligand as previously described by Taylor et al.[53] A shift in the excitation wavelength follows the complexation of propidium iodide and AChE.[53a] Fluorescence intensity was monitored by a Jasco 6200 spectrofluorometer (Jasco Europe, Italy) using a 0.5 mL quartz cuvette at rt. EeAChE (2 mM) was first incubated with 8 mM propidium iodide in 1 mM Tris-HCl, pH 8.0 at rt. The stock solution (4 mM) of the inhibitor was prepared in MeOH. In the back titration experiments of the propidium–AChE complex by **6b**, aliquots of the tested inhibitor (8–56 mM, final concentration) were added successively, and fluorescence emission was monitored at 635 nm upon excitation at 535 nm. Blanks containing propidium alone, inhibitor plus propidium and EeAChE alone were prepared and fluorescence emission was determined. Raw data were processed following the method of Taylor and Lappi[53b] to estimate K_D values assuming a dissociation constant value of propidium from EeAChE equals to 0.7 μM.[54] K_D values are expressed as mean ± standard deviation (SD) of three independent experiments.

Molecular Modeling Studies. The PDB codes 1Q83 and 5K5E, which correspond to the X-ray crystallographic structures of mouse AChE[55] and human BChE[56] enzymes were chosen to build up the initial models of the complexes with the selected target compounds (**6b**, **12a**). The 1Q83 structure was chosen for two reasons. First, the mouse enzyme is highly similar to the human AChE (97.5% sequence identity with hAChE), and, particularly, there is complete identity regarding the residues that shape the binding (catalytic, midgorge and peripheral) site. Second, the presence of the 3,8-diamino-6-phenyl-5-{6-{1-{2-[(1,2,3,4-tetrahydro-9-acridinyl)amino]ethyl}-1*H*-1,2,3-triazol-5-yl}hexyl}phenanthridinium (*syn*-TZ2PA6) ligand in

1Q83 widens the peripheral site, which thus permitted a better accommodation of the target hybrids in the enzyme. A similar rationale motivated the choice of the X-ray structure 5K5E, which contains the [(2*R*)-oxolan-2-yl]methyl-4-(9-ethylcarbazol-3-yl)-2-methyl-5-oxidanylidene-4,6,7,8 tetrahydro-1*H*-quinoline-3 carboxylate ligand, for BChE. The positioning of the chlorotacrine moiety of the selected hybrids in the catalytic site (and Tyr337, which exhibits a pronounced ligand-dependent conformation) was assisted by the X-ray structures 1E66, which corresponds to the complex of huprine X (containing a chlorotacrine moiety) bound to the *Torpedo californica* AChE enzyme,[35] and the complex of tacrine with human BChE (PDB entry 4BDS).[57]

To achieve a suitable binding mode, compounds **6b** and **12a** were manually docked into the binding site of the two proteins following the same protocol reported in previous works.[19c,58] Amber14[59] was used to perform MD simulations on the previously generated ligand–protein complexes previously generated by docking analysis. In this context, the general Amber force field (GAFF)[60] was used to parameterize the ligands, and the partial charges were derived at the HF/6-31G(d) level with Gaussian 09,[61] after preliminary optimization of the molecular structure, by using the restrained electrostatic potential (RESP)[62] fitting method implemented in Gaussian09 and Antechamber.

Classical MD simulations were carried out to explore the stability of the complexes for both enantiomers of hybrids **6b** and **12a**. To check the structural integrity of the binding mode, MD simulations were run in triplicate for each enantiomeric species. For simulations with AChE, the protonation state reported in previous works were adopted.[35,58] Protonation states for BChE at neutral pH were optimized in accordance with the pK_a values estimated by Propka.[63]

All complexes were solvated with a truncated octahedral (TIP3P)[64] water box with a layer of 20 Å and neutralized by adding Na^+ (for AChE) or Cl^- (for BChE) counterions. To maintain the protein structural integrity, the native water network around the chlorotacrine moiety, which mediates relevant interactions with the enzyme, was retained during generation of the starting protein–ligand models.

The complexes were energy minimized by following a three-stage protocol that involved firstly all hydrogen atoms, then water molecules, and finally all the system with a maximum number of minimization cycles of 10000 for the latter stage. Prior to MD simulation, a preliminary equilibration of the system from 0 to 300 K was accomplished in six steps, the first being performed at constant volume and the rest at constant pressure. Inspection of the X-ray crystallographic structures of several tacrine-based dual binding site AChEIs revealed that the tacrine unit shares a common binding mode, which in turn mimics the pose found for the AChE and BChE complexes with tacrine.[65] Accordingly, suitable restraints were imposed to the interactions formed by the chlorotacrine moiety in the catalytic site during equilibration in order to avoid artefactual structural changes due to the accommodation of the rest of the hybrid compound along the enzyme's gorge. These restraints were gradually reduced and finally eliminated during the first 15 ns of the MD production.

The SHAKE algorithm[66] was applied to constrain bonds involving hydrogen atoms. Periodic boundary conditions at constant volume were imposed on the system during the MD simulations. Cut-off for the non-bonded interactions was set to 10 Å. The electrostatic interactions beyond the cut-off within the periodic box were computed by applying the Particle Mesh Ewald (PME) method.[67] Langevin dynamics with a collision frequency of 1.0 was applied for temperature regulation during the heating. Finally, 50 ns of MD simulation at constant volume and

temperature (300 K) using the weak-coupling algorithm[68] with a time constant of 10.0 were run in triplicate for a total of 150 ns for AChE–(*R*)-**6b**, AChE–(*S*)-**6b**, BChE–(*R*)-**6b**, BChE–(*S*)-**6b**, BChE–(*R*)-**12a**, and BChE–(*S*)-**12a** complexes. The time step for saving of trajectory was set to 2 ps. Evaluation of complex stability during MD simulation by means of RMSD analysis for the protein backbone and heavy atoms and for the binding site (protein environment around 8.0 Å from ligand) as well as water electron density analysis (grid option in cpptraj module) were performed by using the CPPTRAJ module of Amber14.

DPPH Assay for Antioxidant Activity. 2,2-Diphenyl-1-picrylhydrazyl (DPPH) free radical assay[36,69] is a simple method to determine the antioxidant capacity. DPPH, trolox and MeOH were purchased from Sigma-Aldrich (Spain). Following the standard procedure, 2 mL of antioxidant solution at different concentrations (from 0 to 120 μM) in previously degassed MeOH were mixed with 2 mL of a 140 μM DPPH methanolic solution. After stirring at rt in the absence of light for 1 h, the absorbance was measured at 515 nm in a SpectraMax M5 (Molecular Devices, Sunnyvale, USA) using quartz cuvettes. CR-6 (**1**) was used as the positive control and the absorbance of MeOH was measured as a blank. Percentage of absorbance decrease of the DPPH radical (%I) was calculated using the following expression: $I\ (\%) = (A_0 – A_t / A_0) \times 100$, where A_0 and A_t represent the absorbance of DPPH in the absence of antioxidant and in the presence of a fixed antioxidant concentration after 60 min, respectively.

The IC_{50} (half maximal inhibitory concentration) values were estimated from the corresponding dose–response curves, using the computer software GraphPad Prism 5.03 for Windows (GraphPad Software, San Diego, USA), and are expressed as mean ± standard deviation of single experiments performed in triplicate.

BACE-1 Inhibition Assay. The inhibitory activity of the target CR6–chlorotacrine hybrids towards human recombinant BACE-1 (β-secretase, Invitrogen) was evaluated by employing Panvera peptide as the substrate.[70] The substrate (10 μL, 250 nM final concentration) was added to 10 μL of solution of the target compounds or buffer in control wells (20 mM NaOAc, pH 4.5, containing 0.1% w/v CHAPS). BACE-1 enzyme (10 μL, 12.91 mU) was added to start the reaction. The enzyme was left to react at 37 ºC for 1 h. The fluorescence signal was read at λ_{em} = 544 nm (λ_{ex} = 590 nm) after adding 10 μL of STOP solution (2.5 M NaOAc). The DMSO concentration in the final mixture was maintained below 5% (v/v) to guarantee no significant loss of enzyme activity. The fluorescence intensities with and without inhibitor were compared and the percent of inhibition due to the presence of the target compounds was calculated. The background signal was measured in control wells that contained all the reagents, except BACE-1, and was subtracted. The percent of inhibition due to the presence of increasing concentrations of the test compounds was calculated by the following expression: $100 – (IF_i/IF_o \times 100)$, where IF_i and IF_o are the fluorescence intensities obtained for BACE-1 in the presence and in the absence of inhibitor, respectively. The IC_{50} values were extrapolated from the corresponding dose–response curves. Results are expressed as mean ± standard error of the mean (SEM) of at least two experiments, each performed in triplicate. Data analysis was performed with GraphPad Prism 4.03 software (GraphPad Software Inc.).

Aβ42 and Tau Aggregation Inhibition Assay in *Escherichia coli* Cells. The Aβ42 and tau antiaggregating activities of the target compounds were assessed in *E. coli* cells, as previously described.[20,39] *E. coli* BL21 (DE3) competent cells were transformed with the pET28a vector (Novagen, Inc., Madison, WI, USA), which carries the DNA sequence of Aβ42, or with pTARA, which contains the RNA-polymerase gen of T7 phage (T7RP) under the control of the promoter

PBAD, and were then transformed with the pRKT42 vector, encoding four repeats of tau protein in two inserts. M9 minimal medium (10 mL) containing 50 μg/mL of kanamycin (for Aβ42 overexpression) or 0.5% of glucose, 50 μg/mL of ampicillin and 12.5 μg/mL of chloramphenicol (for tau overexpression) were inoculated with a colony of BL21 (DE3) cells bearing the plasmids. To fresh M9 minimal medium containing 50 μg/mL of kanamycin and 250 μM of Th-S (for Aβ42 assay) or 0.5% of glucose, 50 μg/mL of ampicillin, 12.5 μg/mL of chloramphenicol, and 250 μM of Th-S (for tau assay), the volume of overnight culture necessary to get a 1:500 dilution was added. The cultures were grown at 37 ºC and 250 rpm overnight until cell density reached OD_{600} = 0.6. A volume of 980 μL of the cultures was transferred into 1.5 mL eppendorf tubes that contained 10 μL of a solution of the target compound in DMSO and 10 μL of isopropyl 1-thio-β-D-galactopyranoside (IPTG) at 100 mM (for Aβ42 assay) or 10 μL of arabinose at 25% (for tau assay), leading to a final inhibitor concentration of 10 μM. The resulting cultures were grown at 37 °C and 1400 rpm with a Thermomixer (Eppendorf, Hamburg, Germany) overnight. The same amount of DMSO without the target compound was added to the sample as a negative control (maximal amount of Aβ42 or tau), whereas non-induced samples (in the absence of IPTG or arabinose) were prepared as positive controls (absence of Aβ42 or tau), and to assess the potential intrinsic toxicity of the target compounds.

The inhibitory activity of the target compounds on Aβ42 or tau aggregation was assessed by a previously reported fluorescence assay,[20,39] using a 2500 mM stock solution of thioflavin-S (Th-S, T1892, Sigma, St. Louis, MO, USA) in double-distilled water (Milli-Q system, Millipore, USA) and measuring the Th-S spectra on an Aminco Bowman Series 2 luminescence spectrophotometer (Aminco-Bowman AB2, SLM Aminco, Rochester, NY, USA) in the range 460–600 nm at 25 °C, with an excitation wavelength of 440 nm and slit widths of 4 nm, and an

emission wavelength of 485 nM. The results are the average of nine independent experiments, each performed in duplicate. As a positive control we used DP128, a known Aβ42 and tau antiaggregating compound,[20] for which percentages of inhibition of 68.2 ± 2.1 and 72.2 ± 2.1, respectively, were obtained.

PAMPA-BBB Assay for Brain Permeability. The brain permeability (P_e) of the target compounds was assessed by the in vitro parallel artificial membrane permeability assay for blood–brain barrier penetration of Di *et al*.,[40] using a lipid extract of porcine brain membrane in a mixture PBS/EtOH 70:30. After assay validation by comparison of the experimental and reported P_e values of a set of fourteen commercial drugs (Table S1 of Supporting Information), the following correlation was obtained: P_e (exp) = 1.5758 P_e (lit) – 1.1459 (R^2 = 0.9241). From this equation and considering the limits established by Di *et al.* for BBB permeation,[40] the threshold for high BBB permeation (CNS+) was set at *Pe* (10^{-6} cm s^{-1}) > 5.16; whereas the range for low BBB permeation (CNS–) was set at *Pe* (10^{-6} cm s^{-1}) < 2.01, and that for uncertain BBB permeation (CNS±) at 5.16 > *Pe* (10^{-6} cm s^{-1}) > 2.01. Three independent experiments, each performed in triplicate, were carried out for each compound.

In Vivo Efficacy Studies. Animals. The experiments were carried out on male APP/PS1 mice[42] and wild-type (WT) littermates (C57Bl6J background, bred in own colony located in the University of Barcelona animal facilities) aged 6 months at the beginning of the study. The University of Barcelona Committee on Animal Use and Care approved the protocol (number 411/18). Following the approved experimental protocol all animals were supervised daily to assess signs of adverse effects during treatment. A retrospective analysis of the protocol demonstrated that no corrective measures (i.e. use of analgesics) were needed. Animals were housed and tested in compliance with the guidelines provided by the Guide for the Care and Use

of Laboratory Animals[71] and following the European Union directives (2010/63/EU). Animals were maintained under standard animal housing conditions in a normal 12-h dark-light cycle with free access to food and water.

Acute Toxicity Studies and Dose Selection. A preliminary study was performed to evaluate the acute toxicity of the novel hybrids **4b** and **11b** and to select the dose to be used in the chronic efficacy studies. Three doses (5, 10, and 15 mg/kg) of **4b** and **11b** were prepared by dissolving the novel hybrids in 1% DMSO and 99% saline. Then, they were injected intraperitoneally (ip) in a volume of 10 mL/kg body weight to male WT mice aged 6 months (n = 4 per each compound and dose, total number of animals = 24). Animals were observed by experimented researchers blind to the treatment for the appearance of any physical sign 5 min, 10 min, 15 min, 30 min, 1 h, 2 h, 3 h, 6 h, 8 h, and 24 h after drug administration.

Chronic Pharmacological Treatment. The novel hybrids **4b** and **11b** (10 mg/kg) were dissolved in 1% DMSO and 99% saline and were injected intraperitoneally (ip) in a volume of 10 mL/kg body weight. Animals were treated once daily for 4 weeks with compounds **4b** and **11b** or the corresponding vehicle (WT Vehicle, n = 6; WT **4b**, n = 5; WT **11b**, n = 6; APP/PS1 Vehicle, n = 5; APP/PS1 **4b**, n = 7; APP/PS1 **11b**, n = 6). After 2 days of washing period, animals were subjected to behavioral evaluation.

Behavioral Evaluation of Cognitive Performance. Memory performance was evaluated with the two-object recognition test. On day 1, mice were placed for 9 min in a V-maze, in which two identical objects were situated at the ends of the arms; the time that the mice spent exploring each object was recorded. Then, 24 h after the training session, animals were placed again for 9 min in the V-maze, with one of the two familiar objects replaced by a novel object. The time that the animals spent exploring the two objects was recorded and an object recognition index (RI)

was calculated, as the difference between the time spent exploring the novel object (T_N) and the familiar object (T_F) divided by the total time spent exploring the two objects [$RI=(T_N-T_F)/(T_N+T_F)$]. Animals exhibiting memory impairments revealed a lower object recognition index.

Tissue Collection. At the end of the behavioral testing, the animals were sacrificed and their brains were removed. One brain hemisphere was dissected on ice, immediately frozen and stored at –80 ºC until processing for the protein or RNA quantification. The other brain hemisphere was fixed in 4% paraformaldehyde and processed for immunohistochemistry.

Aβ Immunohistochemistry. Tissue samples were embedded in paraffin and coronal sections (4 μm) were cut with a microtome. De-waxed sections were incubated with 98% formic acid (3 min) and then treated with citrate buffer (20 min) to enhance antigenicity. Then, the endogenous peroxidases were blocked by incubation in 10% MeOH-1% H_2O_2 solution (15 min). Sections were blocked with 3% normal horse serum solution and then incubated at 4 ºC overnight with the primary antibody against Aβ (1:50, Dako, Clone 6F/3D). Sections were subsequently rinsed and incubated with biotinylated secondary antibody (Dako), followed by EnVision+ system peroxidase (Dako) and finally with the chromogen diaminobenzidine and H_2O_2. Sections were lightly counterstained with haematoxylin. After staining, the sections were dehydrated and cover-slipped for microscopic observation. The Aβ burden in cortex was calculated as the percentage of the Aβ deposition area with respect to the total area in 9 representative pictures by each animal, corresponding to the main regions where Aβ deposition is observed in APP/PS1 mice. Sections from all the APP/PS1 animals were evaluated by using the Analysis tool of the software Adobe® Photoshop® CS4.

Aβ Soluble Quantification: Enzyme-Linked Immunosorbent Assay (ELISA). Fresh-frozen mouse brain cortex was homogenized in 4 volumes (wt:vol) of TBS extraction buffer (140 mM NaCl, 3 mM KCl, 25 mM Tris (pH 7.4), 5 mM EDTA, and protease inhibitor cocktail (Roche Molecular Systems, USA). Homogenate was spun 100,000 g × 1 h, and the supernatant was saved as the soluble fraction for Aβ quantification. $A\beta_{40}$ and $A\beta_{42}$ Human ELISA kits (Invitrogen™ Corporation, USA) were used to quantify the levels of $A\beta_{40}$ and $A\beta_{42}$ peptides in the brain soluble fractions. Quantitative determination was carried out according to the manufacturer's instructions. $A\beta_{40}$ and $A\beta_{42}$ levels were normalized to the total amount of protein from each individual sample (BCA method, Thermo Fisher Scientific, USA).

Protein Oxidation Quantification. The levels of the carbonyl groups introduced into proteins by oxidative reactions were measured by using the OxyBlot™ protein Oxidation Detection Kit (S7150, Merck Millipore, USA) following the manufacturer's instructions. Briefly, frozen samples of the cortex were homogenized in Laemmli buffer (62.5 mM Tris-Cl, pH 6.8 containing 2% SDS, 10% glycerol, 0.002% bromophenol blue and 50 mM DTT). Protein concentration was determined with the BCA method. Equal amounts of protein (20 μg) for each sample were prepared for derivatization. The carbonyl groups in the protein side chains were derivatized to 2,4-dinitrophenylhydrazone (DNP-hydrazone) by reaction with 2,4-dinitrophenylhydrazine (DNPH). The DNP-derivatized protein samples were loaded and separated by electrophoresis on sodium dodecyl sulfate polyacrylamide gel electrophoresis (SDS-PAGE) (10%) gels and transferred onto PVDF membranes (Amersham, Germany). Non-specific bindings were blocked by incubation in 3% non-fat milk in PBS containing 0.2% Tween for 1 h at room temperature. After washing, membranes were incubated overnight at 4 °C with the primary antibody against the DNP moiety of the proteins. Protein loading was monitored

using an antibody against β-tubulin (1:10,000, Abcam, UK). Membranes were then incubated for 1 h with an anti-rabbit HRP-conjugated secondary antibody (1:2,000, Dako), and immunocomplexes were revealed by chemiluminescence reagent (ECL, Amersham). Densitometric quantification was carried out with ImageJ software (NIH, USA). Bands were normalized to β-tubulin.

SOD2 and Aβ Double-Immunofluorescence. De-waxed sections were stained with a saturated solution of Sudan black B (Merck, USA) for 30 min to block the autofluorescence of lipofuscin granules present in cell bodies, then rinsed in 70% EtOH and washed in distilled water. The sections were treated with 98% formic acid (3 min) and with citrate buffer to enhance antigenicity, and then incubated at 4 ºC overnight with combinations of primary antibodies against Aβ (1:50, Dako) and the enzyme superoxide dismutase type 2 (SOD2, 1:500, Stressgen-Gentaur, Belgium). After washing, the sections were incubated with Alexa488 or Alexa546 (1:400, Molecular Probes) fluorescence secondary antibodies against the corresponding host species. After washing, the sections were mounted in Immuno-Fluore Mounting medium (ICN Biomedicals, USA), sealed, and dried overnight. Sections were examined with an Olympus BX51 microscope and 5 representative pictures taken from the cortex of each animal (n = 5 per group) were subjected to densitometric quantification by using the software Adobe® Photoshop® CS4. The SOD2 immunostaining was in reference to the Aβ plaque area in each picture.

Western Blotting Analysis. Tissue samples were homogenized in lysis buffer (Tris-HCl pH 7.4 50 mM, NaCl 150 mM, EDTA 5 mM, and 1X-Triton X-100) containing phosphatase and protease inhibitors (Cocktail II, Sigma). Protein concentration was determined by Bradford method. Aliquots of 15 μg of cortical protein extraction per sample were used. Protein samples were separated by SDS-PAGE (8-14%) and transferred onto polyvinylidene difluoride (PVDF)

membranes (Millipore). Afterwards, membranes were blocked in 5% non-fat milk in Tris-buffered saline (TBS) solution containing 0.1% Tween 20 for 1 h at room temperature, followed by overnight incubation at 4 °C with the primary antibody listed in Table S2 of Supporting Information. Then, membranes were washed and incubated with the secondary antibody (Table S2) for 1 h at room temperature. Immunoreactive proteins were visualized with the chemiluminiscence-based ChemiLucent^{TM} detection kit, following the manufacturer's protocol (ECL Kit, Millipore) and digital images were acquired using ChemiDoc XRS+System (BioRad). Semi-quantitative analyses were done using ImageLab software (BioRad) and results were expressed in Arbitrary Units, considering control protein levels as 100%. Protein loading was routinely monitored by immunodetection of glyceraldehyde-3-phosphate dehydrogenase (GAPDH) or β-tubulin.

RNA Extraction and Gene Expression Determination by q-PCR. Total RNA isolation was carried out using TRIsureTM reagent according to the manufacturer's instructions (Bioline Reagent, UK). The yield, purity, and quality of RNA were determined spectrophotometrically with a NanoDropTM ND-1000 (Thermo Scientific) apparatus. RNAs with A260/280 ratios higher than 1.9 were selected. Reverse Transcription-Polymerase Chain Reaction (RT-PCR) was performed as follows: 2 μg of messenger RNA (mRNA) was reverse-transcribed using High Capacity cDNA Reverse Transcription Kit (Applied Biosystems). Real-time quantitative PCR (qPCR) was used to quantify mRNA expression of oxidative stress and inflammatory genes listed in Table S3 of Supporting Information. SYBR®Green qPCR was performed in a Step One Plus Detection System (Applied Biosystems) employing SYBR®Green PCR Master Mix (Applied Biosystems). Each reaction mixture contained 2 μg of complementary DNA (cDNA). Data were analysed utilizing the comparative Cycle threshold (Ct) method (ΔΔCt), where the

housekeeping gene expression (β-actin) was used to normalize differences in sample loading and preparation. Each sample was analysed in duplicate and results represent the n-fold difference of transcription levels among different samples.

Statistical Analyses. Behavioral, western blotting, and qPCR data were analyzed by two-way ANOVA with genotype and treatment as between factors, followed by Tukey's *post hoc* test or two-tail Student's t-test when required. Aβ and SOD2 quantifications were analyzed by one-way ANOVA. The statistical outliers were determined with Grubbs' test and subsequently removed from the analysis. In all the experiments, the significance level was set at $p < 0.05$.

Stability at Human, Mouse, and Rat Plasma. Human, mouse, and rat plasma pooled from healthy donors, extracted in citrate tubes was employed in the assay. Plates containing 10 μM compound **4b** in plasma (total volume: 50 μL) were incubated at 37 ºC at different times (0, 60, 180, and 360 min). Then, acetonitrile (100 μL) was added for precipitating plasma protein, and the plate was centrifuged at 46,000 g for 60 min at 5 ºC. Supernatant was taken and analyzed by UPLC-MS/MS for sample quantification, using reverse phase Acquity UPLC® BEH C18 1.7 μm (2.1 mm x 50 mm, Waters) as the stationary phase, 0.1% formic acid in water (A) / 0.1% formic acid in acetonitrile (B) as the mobile phase, a flow of 0.6 mL/min, and the gradient indicated in Table 4.

Table 4. Gradient Used in the UPLC-MS/MS Analysis for Plasma Stability Studies

Time (min)	A (%)	B (%)
0	95	5
0.1	95	5
1	0	100

2	0	100
2.1	95	5
2.5	95	5

The chromatographic equipment employed was an UPLC QSM Waters Acquity. Compound concentrations were calculated from the MS peak areas. Values are expressed as the mean of two independent experiments, each performed in triplicate.

Stability at Human, Mouse, and Rat Liver Microsomes. Human, mouse, and rat microsomes from Tebu-Xenotech were employed in the assay, containing 20 mg/mL of protein.

The quantities of reagents, microsomes, and compound **4b** detailed in Table 5 were added to each well of a 96-well microplate.

Table 5. Quantities of Reagents, Microsomes, and Compound 4b Used in the Microsomal Stability Assays

	Blank (µL)	Human (µL)	Mouse (µL)	Rat (µL)
Phosphate buffer Na/K 50 mM pH 7.4	295	283.5	301.3	301.3
$MgCl_2$ 30 mM	50	50	50	50
NADP 10 mM	50	50	50	50
Glucose 6-P 100 mM	50	50	50	50
Glucose 6-P DH 20 U/mL	25	25	25	25
Water	25			
Human microsomes		36.5		
Mouse microsomes			18.7	

Rat microsomes				18.7
Compound **4b** 5 μM	5	5	5	5

Plates were incubated at 37 ºC and samples (75 μL) were taken at 0, 10, 20, 40, and 60 min. Samples were transferred to a microplate and acetonitrile (75 μL) and H_2O (30 μL) were successively added for inactivating the microsomes, and for improving the chromatographic conditions, respectively, and were kept at 4 ºC. When all the samples were taken, the plate was centrifuged at 46,000 g for 30 min at 15 ºC. Supernatant was taken and was analyzed in a UPLC-MS/MS system, using reverse phase Acquity UPLC® BEH C18 1.7 μm (2.1 mm x 50 mm, Waters) as the stationary phase, 0.1% formic acid in water (A) / 0.1% formic acid in acetonitrile (B) as the mobile phase, a flow of 0.6 mL/min, and the gradient indicated in Table 6.

Table 6. Gradient Used in the UPLC-MS/MS Analysis for Microsomal Stability Studies

Time (min)	A (%)	B (%)
0	95	5
0.1	95	5
1	0	100
2.5	0	100
2.6	95	5
3	95	5

The chromatographic equipment employed was an UPLC QSM Waters Acquity. Compound concentrations were calculated from the MS peak areas. Metabolic stability was calculated from

the logarithm of the remaining compound at each of the times evaluated. Values are expressed as the mean of two independent experiments, each performed in triplicate.

Metabolite Identification in Human, Mouse, and Rat Liver Microsomes. The supernatants of the microsomal stability assays with human, mouse, and rat liver microsomes were analyzed by using a UPLC-MS/MS system consisting of a Waters Acquity H-Class UPLC and a Xevo TQ-D triple quadrupole mass spectrometer, equipped with an electrospray ionization (ESI) source (Waters Corporation, Milford, MA, USA). Chromatographic separation was achieved using an Acquity UPLC BEH C18 (1.7 μm, 2.1 × 50 mm) column, with a UPLC mobile phase A consisting of 0.1% formic acid in water, a mobile phase B consisting of 0.1% formic acid in acetonitrile, the gradient indicated in Table 7, and an injection volume of 4 μL.

Table 7. Gradient Used in the UPLC-MS/MS Analysis for Metabolite Identification

Time (min)	A (%)	B (%)
0	95	5
0.1	95	5
1	0	100
2	0	100
2.1	95	5
3	95	5

ASSOCIATED CONTENT

Supporting Information. The following files are available free of charge.

RMSD analyses of the binding of **6b** to hAChE and hBChE, and of **12a** to hBChE, MD-averaged **6b**–hBChE complexes, PAMPA-BBB permeabilities of commercial drugs used for assay validation, antibodies and primers used in Western blot and qPCR studies, relative MS peak areas in the identification of metabolites in human, mouse, and rat liver microsomes, binding mode of the *p*-benzoquinone metabolite of **4b** within hAChE, copies of ^{1}H and ^{13}C NMR spectra and HPLC chromatograms of target compounds (PDF)

Molecular formula strings (CSV)

AUTHOR INFORMATION

Corresponding Author

Diego Muñoz-Torrero – *Laboratory of Medicinal Chemistry (CSIC Associated Unit), Faculty of Pharmacy and Food Sciences, and Institute of Biomedicine (IBUB), University of Barcelona (UB), E-08028 Barcelona, Spain*; orcid.org/0000-0002-8140-8555; Phone: (+34) 934024533; E-mail: dmunoztorrero@ub.edu

Author Contributions

The manuscript was written through contributions of all authors. All authors have given approval to the final version of the manuscript.

Notes

The authors declare no competing financial interest.

ACKNOWLEDGMENTS

This work was supported by Ministerio de Ciencia, Innovación y Universidades (MCIU), Agencia Estatal de Investigación (AEI) and FEDER (SAF2017-82771-R, MDM-2017-0767) and Generalitat de Catalunya (GC) (2017SGR106, 2017SGR1746). Fellowships from GC to F.J.P.-A. and from MCIU to D.P.-I. are gratefully acknowledged.

ABBREVIATIONS

Aβ, β-amyloid peptide; AChE, acetylcholinesterase; AD, Alzheimer's disease; APP, amyloid precursor protein; ATCh, acetylthiocholine; BACE-1, β-site APP cleaving enzyme; BChE, butyrylcholinesterase; CAS, catalytic anionic site; Cl-THA, 6-chlorotacrine; CNS, central nervous system; DNP, 2,4-dinitrophenyl; DPPH, 2,2-diphenyl-1-picrylhydrazyl; DTNB, 5,5'-dithiobis(2-nitrobenzoic acid); EeAChE, *Electrophorus electricus* acetylcholinesterase; ELISA, Enzyme-Linked Immunosorbent Assay; GAFF, general Amber force field; GAPDH, glyceraldehyde-3-phosphate dehydrogenase; GPX1, glutathione peroxidase 1; hAChE, human acetylcholinesterase; hBChE, human butyrylcholinesterase; Hmox1, heme oxigenase 1; HNE, 4-hydroxy-2-nonenal; iNOS, inducible nitric oxide synthase; ip, intraperitoneally; IPTG, isopropyl 1-thio-β-D-galactopyranoside; MCI, mild cognitive impairment; MD, molecular dynamics; Nrf2, nuclear factor-erythroid 2-related factor 2; PAMPA-BBB, parallel artificial membrane permeation assay for blood–brain barrier; PAS, peripheral anionic site; P_e, permeability; PME, Particle Mesh Ewald; qPCR, quantitative Polymerase Chain Reaction; RESP, restrained electrostatic potential; RI, recognition index; ROS, reactive oxygen species; RT-PCR, Reverse Transcription-Polymerase Chain Reaction; SD, standard deviation; SDS-PAGE, sodium dodecyl sulfate polyacrylamide gel electrophoresis; SOD2, superoxide dismutase 2; SEM, standard error

of the mean; TBS, Tris-buffered saline; THA, tacrine; Th-S, thioflavin-S; TLC, thin-layer chromatography; WT, wild type

REFERENCES

(1) Alzheimer's Disease International. 2018. World Alzheimer Report 2018: The State of the Art of Dementia Research: New Frontiers. London: Alzheimer's Disease International.

(2) Alzheimer's Disease International. 2019. World Alzheimer Report 2019: Attitudes to Dementia. London: Alzheimer's Disease International.

(3) Cavalli, A.; Bolognesi, M. L.; Minarini, A.; Rosini, M.; Tumiatti, V.; Recanatini, M.; Melchiorre, C. Multi-target-directed ligands to combat neurodegenerative diseases. *J. Med. Chem.* **2008**, *51*, 347–372.

(4) (a) Lemke, C.; Christmann, J.; Yin, J.; Alonso, J. M.; Serrano, E.; Chioua, M.; Ismaili, L.; Martínez-Grau, M. A.; Beadle, C. D.; Vetman, T.; Dato, F. M.; Bartz, U.; Elsinghorst, P. W.; Pietsch, M.; Müller, C. E.; Iriepa, I.; Wille, T.; Marco-Contelles, J.; Gütschow, M. Chromenones as multineurotargeting inhibitors of human enzymes. *ACS Omega* **2019**, *4*, 22161–22168. (b) Wang, Z.; Hu, J.; Yang, X.; Feng, X.; Li, X.; Huang, L.; Chan, A. S. C. Design, synthesis, and evaluation of orally bioavailable quinoline–indole derivatives as innovative multitarget-directed ligands: promotion of cell proliferation in the adult murine hippocampus for the treatment of Alzheimer's disease. *J. Med. Chem.* **2018**, *61*, 1871–1894.

(5) Muñoz-Torrero, D. Multitarget anti-Alzheimer Hybrid Compounds: Do They Work in Vivo?. In *Design of Hybrid Molecules for Drug Development*; Decker, M., Ed.; Elsevier: Amsterdam, 2017; pp 167–192.

(6) (a) Bajda, M.; Łażewska, D.; Godyń, J.; Zaręba, P.; Kuder, K.; Hagenow, S.; Łątka, K.; Stawarska, E.; Stark, H.; Kieć-Kononowicz, K.; Malawska, B. Search for new multi-target compounds against Alzheimer's disease among histamine H3 receptor ligands. *Eur. J. Med. Chem.* **2020**, *185*, 111785. (b) Mesiti, F.; Chavarria, D.; Gaspar, A.; Alcaro, S.; Borges, F. The chemistry toolbox of multitarget-directed ligands for Alzheimer's disease. *Eur. J. Med. Chem.* **2019**, *181*, 111572 (c) Wang, T.; Liu, X.; Guan, J.; Ge, S.; Wu, M.-B.; Lin, J.; Yang, L. Advancement of multi-target drug discoveries and promising applications in the field of Alzheimer's disease. *Eur. J. Med. Chem.* **2019**, *169*, 200–223 (d) Gontijo, V. S.; Viegas, F. P. D.; Ortiz, C. J. C.; de Freitas Silva, M.; Damasio, C. M.; Rosa, M. C.; Campos, T. G.; Couto, D. S.; Tranches Dias, K. S.; Viegas Jr., C. Molecular hybridization as a tool in the design of multi-target directed drug candidates for neurodegenerative diseases. *Curr. Neuropharmacol.* **2020**, *18*, 348–407 (e) Gandini, A.; Bartolini, M.; Tedesco, D.; Martinez-Gonzalez, L.; Roca, C.; Campillo, N. E.; Zaldivar-Diez, J.; Perez, C.; Zuccheri, G.; Miti, A.; Feoli, A.; Castellano, S.; Petralla, S.; Monti, B.; Rossi, M.; Moda, F.; Legname, G.; Martinez, A.; Bolognesi, M. L. Tau-centric multitarget approach for Alzheimer's disease: Development of first-in-class dual glycogen synthase kinase 3β and tau-aggregation inhibitors. *J. Med. Chem.* **2018**, *61*, 7640–7656.

(7) (a) Xu, A.; He, F.; Zhang, X.; Li, X.; Ran, Y.; Wei, C.; James Chou, C.; Zhang, R.; Wu, J. Tacrine-hydroxamate derivatives as multitarget-directed ligands for the treatment of Alzheimer's disease: design, synthesis, and biological evaluation. *Bioorg. Chem.* **2020**, *98*, 103721. (b) Duarte, Y.; Fonseca, A.; Gutiérrez, M.; Adasme-Carreño, F.; Muñoz-Gutierrez, C.; Alzate-Morales, J.; Santana, L.; Uriarte, E.; Álvarez, R.; Matos, M. J. Novel coumarin-quinoline hybrids: design of multitarget compounds for Alzheimer's disease. *Chem. Select*

2019, *4*, 551–558. (c) Zhang, P.; Xu, S.; Zhu, Z.; Xu, J. Multi-target design strategies for the improved treatment of Alzheimer's disease. *Eur. J. Med. Chem.* **2019**, *176*, 228–247. (d) Lalut, J.; Santoni, G.; Karila, D.; Lecoutey, C.; Davis, A.; Nachon, F.; Silman, I.; Sussman, J.; Weik, M.; Maurice, T.; Dallemagne, P.; Rochais, C. Novel multitarget-directed ligands targeting acetylcholinesterase and σ1 receptors as lead compounds for treatment of Alzheimer's disease: synthesis, evaluation, and structural characterization of their complexes with acetylcholinesterase. *Eur. J. Med. Chem.* **2019**, *162*, 234–248. (e) Pisani, L.; Iacobazzi, R. M.; Catto, M.; Rullo, M.; Farina, R.; Denora, N.; Cellamare, S.; Altomare, C. D. Investigating alkyl nitrates as nitric oxide releasing precursors of multitarget acetylcholinesterase-monoamine oxidase B inhibitors. *Eur. J. Med. Chem.* **2019**, *161*, 292–309. (f) Mezeiova, E.; Chalupova, K.; Nepovimova, E.; Gorecki, L.; Prchal, L.; Malinak, D.; Kuca, K.; Soukup, O.; Korabecny, J. Donepezil derivatives targeting amyloid-β cascade in Alzheimer's disease. *Curr. Alzheimer Res.* **2019**, *16*, 772–800. (g) Pérez-Areales, F. J.; Turcu, A. L.; Barniol-Xicota, M.; Pont, C.; Pivetta, D.; Espargaró, A.; Bartolini, M.; De Simone, A.; Andrisano, V.; Pérez, B.; Sabate, R.; Sureda, F. X.; Vázquez, S.; Muñoz-Torrero, D. A novel class of multitarget anti-Alzheimer benzohomoadamantane–chlorotacrine hybrids modulating cholinesterases and glutamate NMDA receptors. *Eur. J. Med. Chem.* **2019**, *180*, 613–626.

(8) Di Domenico, F.; Barone, E.; Perluigi, M.; Butterfield, D. A. Strategy to reduce free radical species in Alzheimer's disease: an update of selected antioxidants. *Expert Rev. Neurother.* **2015**, *15*, 19–40.

(9) (a) Rosini, M.; Simoni, E.; Milelli, A.; Minarini, A.; Melchiorre, C. Oxidative stress in Alzheimer's disease: are we connecting the dots? *J. Med. Chem.* **2014**, *57*, 2821–2831. (b)

von Bernhardi, R.; Eugenín, J. Alzheimer's disease: redox dysregulation as a common denominator for diverse pathogenic mechanisms. *Antiox. Redox Signal.* **2012**, *16*, 974–1031.

(10) Mecocci, P.; Polidori, M. C. Antioxidant clinical trials in mild cognitive impairment and Alzheimer's disease. *Biochim. Biophys. Acta* **2012**, *1822*, 631–638.

(11) Singh, A.; Kukreti, R.; Saso, L.; Kukreti, S. Oxidative stress: a key modulator in neurodegenerative diseases. *Molecules* **2019**, *24*, 1583.

(12) Casas, J.; Gorchs, G.; Sánchez-Baeza, F.; Teixidor, P.; Messeguer, A. Inhibition of rat liver microsomal lipid peroxidation elicited by simple 2,2-dimethylchromenes and chromans structurally related to precocenes. *J. Agric. Food Chem.* **1992**, *40*, 585–590.

(13) Montoliu, C.; Llansola, M.; Sáez, R.; Yenes, S.; Messeguer, A.; Felipo, V. Prevention of glutamate neurotoxicity in cultured neurons by 3,4-dihydro-6-hydroxy-7-methoxy-2,2-dimethyl-1(2*H*)-benzopyran (CR-6), a scavenger of nitric oxide. *Biochem. Pharmacol.* **1999**, *58*, 255–261.

(14) Sanvicens, N.; Gómez-Vicente, V.; Messeguer, A.; Cotter, T. G. The radical scavenger CR-6 protects SH-SY5Y neuroblastoma cells from oxidative stress-induced apoptosis: effect on survival pathways. *J. Neurochem.* **2006**, *98*, 735–747.

(15) Pérez-Asensio, F. J.; de la Rosa, X.; Jiménez-Altayó, F.; Gorina, R.; Martínez, E.; Messeguer, À.; Vila, E.; Chamorro, À.; Planas, A. M. Antioxidant CR-6 protects against reperfusion injury after a transient episode of focal brain ischemia in rats. *J. Cereb. Blood Flow Metab.* **2010**, *30*, 638–652.

(16) Vázquez-Jiménez, L.; Garrido, M.; Miceli, M.; Prats, E.; Ferrer-Montiel, A.; Teixidó, M.; Jimeno, C.; Messeguer, A. Synthesis and in vitro, ex-vivo and in vivo activity of hybrid compounds linking a potent ROS and RNS scavenger activity with diverse substrates addressed to pass across the blood-brain barrier. *Eur. J. Med. Chem.* **2016**, *123*, 788–802.

(17) (a) Patel, D. V.; Patel, N. R.; Kanhed, A. M.; Patel, S. P.; Sinha, A.; Kansara, D. D.; Mecwan, A. R.; Patel, S. B.; Upadhyay, P. N.; Patel, K. B.; Shah, D. B.; Prajapati, N. K.; Murumkar, P. R.; Patel, K. V.; Yadav, M. R. Novel multitarget directed triazinoindole derivatives as anti-Alzheimer agents. *ACS Chem. Neurosci.* **2019**, *10*, 3635–3661. (b) Nesi, G.; Sestito, S.; Digiacomo, M.; Rapposelli, S. Oxidative stress, mitochondrial abnormalities and proteins deposition: multitarget approaches in Alzheimer's disease. *Curr. Top. Med. Chem.* **2017**, *17*, 3062–3079. (c) Rodríguez-Franco, M. I.; Fernández-Bachiller, M. I.; Pérez, C.; Hernández-Ledesma, B.; Bartolomé, B. Novel tacrine−melatonin hybrids as dual-acting drugs for Alzheimer disease, with improved acetylcholinesterase inhibitory and antioxidant properties. *J. Med. Chem.* **2006**, *49*, 459–462. (d) Fernández-Bachiller, M. I.; Pérez, C.; Campillo, N. E.; Páez, J. A.; González-Muñoz, G. C.; Usán, P.; García-Palomero, E.; López, M. G.; Villarroya, M.; García, A. G.; Martínez, A.; Rodríguez-Franco, M. I. Tacrine-melatonin hybrids as multifunctional agents for Alzheimer's disease, with cholinergic, antioxidant, and neuroprotective properties. *ChemMedChem* **2009**, *4*, 828–841.

(18) Mishra, P.; Kumar, A.; Panda, G. Anti-cholinesterase hybrids as multi-target-directed ligands against Alzheimer's disease (1998–2018). *Bioorg. Med. Chem.* **2019**, *27*, 895–930.

(19) (a) Viayna, E.; Sola, I.; Bartolini, M.; De Simone, A.; Tapia-Rojas, C.; Serrano, F. G.; Sabaté, R.; Juárez-Jiménez, J.; Pérez, B.; Luque, F. J.; Andrisano, V.; Clos, M. V.; Inestrosa,

N. C.; Muñoz-Torrero, D. Synthesis and multitarget biological profiling of a novel family of rhein derivatives as disease-modifying anti-Alzheimer agents. *J. Med. Chem.* **2014**, *57*, 2549–2567. (b) Galdeano, C.; Viayna, E.; Sola, I.; Formosa, X.; Camps, P.; Badia, A.; Clos, M. V.; Relat, J.; Ratia, M.; Bartolini, M.; Mancini, F.; Andrisano, V.; Salmona, M.; Minguillón, C.; González-Muñoz, G. C.; Rodríguez-Franco, M. I.; Bidon-Chanal, A.; Luque, F. J.; Muñoz-Torrero, D. Huprine–tacrine heterodimers as anti-amyloidogenic compounds of potential interest against Alzheimer's and prion diseases. *J. Med. Chem.* **2012**, *55*, 661–669. (c) Camps, P.; Formosa, X.; Galdeano, C.; Muñoz-Torrero, D.; Ramírez, L.; Gómez, E.; Isambert, N.; Lavilla, R.; Badia, A.; Clos, M. V.; Bartolini, M.; Mancini, F.; Andrisano, V.; Arce, M. P.; Rodríguez-Franco, M. I.; Huertas, Ó.; Dafni, T.; Luque, F. J. Pyrano[3,2-*c*]quinoline−6-chlorotacrine hybrids as a novel family of acetylcholinesterase- and β-amyloid-directed anti-Alzheimer compounds. *J. Med. Chem.* **2009**, *52*, 5365–5379. (d) Di Pietro, O.; Pérez-Areales, F. J.; Juárez-Jiménez, J.; Espargaró, A.; Clos, M. V.; Pérez, B.; Lavilla, R.; Sabaté, R.; Luque, F. J.; Muñoz-Torrero, D. Tetrahydrobenzo[*h*][1,6]naphthyridine-6-chlorotacrine hybrids as a new family of anti-Alzheimer agents targeting β-amyloid, tau, and cholinesterase pathologies. *Eur. J. Med. Chem.* **2014**, *84*, 107–117.

(20) Espargaró, A.; Pont, C.; Gamez, P.; Muñoz-Torrero, D.; Sabate, R. Amyloid pan-inhibitors: one family of compounds to cope with all conformational diseases. *ACS Chem. Neurosci.* **2019**, *10*, 1311–1317.

(21) Di Pietro, O.; Juárez-Jiménez, J.; Muñoz-Torrero, D.; Laughton, C. A.; Luque, F. J. Unveiling a novel transient druggable pocket in BACE-1 through molecular simulations:

conformational analysis and binding mode of multisite inhibitors. *PLoS ONE* **2017**, *12*, e0177683.

(22) Muñoz-Ruiz, P.; Rubio, L.; García-Palomero, E.; Dorronsoro, I.; del Monte-Millán, M.; Valenzuela, R.; Usán, P.; de Austria, C.; Bartolini, M.; Andrisano, V.; Bidon-Chanal, A.; Orozco, M.; Luque, F. J.; Medina, M.; Martínez, A. Design, synthesis, and biological evaluation of dual binding site acetylcholinesterase inhibitors: new disease-modifying agents for Alzheimer's disease. *J. Med. Chem.* **2005**, *48*, 7223–7233.

(23) Pi, R.; Ye, M.; Cheng, Z.; Liu, P. Preparation of Tacrine-Ferulic Acid Containing Compounds for Treatment of Alzheimer's Disease. CN 101284812 A, **2008**.

(24) Hu, M.-K.; Lu, C.-F. A Facile synthesis of bis-tacrine isosteres. *Tetrahedron Lett.* **2000**, *41*, 1815–1818.

(25) Sola, I.; Artigas, A.; Taylor, M. C.; Pérez-Areales, F. J.; Viayna, E.; Clos, M. V.; Pérez, B.; Wright, C. W.; Kelly, J. M.; Muñoz-Torrero, D. Synthesis and biological evaluation of *N*-cyanoalkyl-, *N*-aminoalkyl-, and *N*-guanidinoalkyl-substituted 4-aminoquinoline derivatives as potent, selective, brain permeable antitrypanosomal agents. *Bioorg. Med. Chem.* **2016**, *24*, 5162–5171.

(26) (a) Camps, P.; Muñoz-Torrero, D.; Sánchez, L. Stereoselective synthesis of both enantiomers of *N*-Boc-α-aryl-γ-aminobutyric acids. *Tetrahedron Asymmetry* **2004**, *15*, 311–321. (b) Camps, P.; Muñoz-Torrero, D. Synthesis and applications of (*R*)- and (*S*)-pantolactone as chiral auxiliaries, *Curr. Org. Chem.* **2004**, *8*, 1339–1380.

(27) Ellman, G. L.; Courtney, K. D.; Andres, V., Jr.; Featherstone, R. M. A new and rapid colorimetric determination of acetylcholinesterase activity. *Biochem. Pharmacol.* **1961**, *7*, 88–95.

(28) Wlodek, S. T.; Antosiewicz, J.; McCammon, J. A.; Straatsma, T. P.; Gilson, M. K.; Briggs, J. M.; Humblet, C.; Sussman, J. L. Binding of tacrine and 6-chlorotacrine by acetylcholinesterase. *Biopolymers* **1996**, *38*, 109–117.

(29) (a) Scheiner, M.; Dolles, D.; Gunesch, S.; Hoffmann, M.; Nabissi, M.; Marinelli, O.; Naldi, M.; Bartolini, M.; Petralla, S.; Poeta, E.; Monti, B.; Falkeis, C.; Vieth, M.; Hübner, H.; Gmeiner, P.; Maitra, R.; Maurice, T.; Decker, M. Dual-acting cholinesterase–human cannabinoid receptor 2 ligands show pronounced neuroprotection in vitro and overadditive and disease-modifying neuroprotective effects in vivo. *J. Med. Chem.* **2019**, *62*, 9078–9102. (b) Maspero, M.; Volpato, D.; Cirillo, D.; Yuan Chen, N.; Messerer, R.; Sotriffer, C.; De Amici, M.; Holzgrabe, U.; Dallanoce, C. Tacrine-xanomeline and tacrine-iperoxo hybrid ligands: synthesis and biological evaluation at acetylcholinesterase and M1 muscarinic acetylcholine receptors. *Bioorg. Chem.* **2020**, *96*, 103633. (c) Fancellu, G.; Chand, K.; Tomás, D.; Orlandini, E.; Piemontese, L.; Silva, D. F.; Cardoso, S. M.; Chaves, S.; Santos, M. A. Novel tacrine–benzofuran hybrids as potential multi-target drug candidates for the treatment of Alzheimer's disease. *J. Enzyme Inhib. Med. Chem.* **2020**, *35*, 211–226. (d) Cheng, X.; Gu, J.; Pang, Y.; Liu, J.; Xu, T.; Li, X.; Hua, Y.; Newell, K. A.; Huang, X.-F.; Yu, Y.; Liu, Y. Tacrine–hydrogen sulfide donor hybrid ameliorates cognitive impairment in the aluminum chloride mouse model of Alzheimer's disease. *ACS Chem. Neurosci.* **2019**, *10*, 3500–3509.

(30) Savini, L.; Gaeta, A.; Fattorusso, C.; Catalanotti, B.; Campiani, G.; Chiasserini, L.; Pellerano, C.; Novellino, E.; McKissic, D.; Saxena, A. Specific targeting of acetylcholinesterase and butyrylcholinesterase recognition sites. Rational design of novel, selective, and highly potent cholinesterase inhibitors. *J. Med. Chem.* **2003**, *46*, 1–4.

(31) (a) Recanatini, M.; Cavalli, A.; Belluti, F.; Piazzi, L.; Rampa, A.; Bisi, A.; Gobbi, S.; Valenti, P.; Andrisano, V.; Bartolini, M., Cavrini, V. SAR of 9-amino-1,2,3,4-tetrahydroacridine-based acetylcholinesterase inhibitors: synthesis, enzyme inhibitory activity, QSAR, and structure-based CoMFA of tacrine analogues. *J. Med. Chem.* **2000**, *43*, 2007–2018. (b) Wlodek, S. T.; Antosiewicz, J.; McCammon, J. A.; Straatsma, T. P.; Gilson, M. K.; Briggs, J. M.; Humblet, C.; Sussman, J. L. Binding of tacrine and 6-chlorotacrine by acetylcholinesterase. *Biopolymers* **1996**, *38*, 109–117.

(32) (a) Hoffmann, M.; Stiller, C.; Endres, E.; Scheiner, M.; Gunesch, S.; Sotriffer, C.; Maurice, T.; Decker, M. Highly selective butyrylcholinesterase inhibitors with tunable duration of action by chemical modification of transferable carbamate units exhibit pronounced neuroprotective effect in an Alzheimer's disease mouse model. *J. Med. Chem.* **2019**, *62*, 9116–9140. (b) Darvesh, S. Butyrylcholinesterase as a diagnostic and therapeutic target for Alzheimer's disease. *Curr. Alzheimer Res.* **2016**, *13*, 1173–1177.

(33) Elsinghorst, P. W.; Cieslik, J. S.; Mohr, K.; Tränkle, C.; Gütschow, M. First gallamine–tacrine hybrid: design and characterization at cholinesterases and the M_2 muscarinic receptor. *J. Med. Chem.* **2007**, *50*, 5685–5695.

(34) (a) Camps, P.; Formosa, X.; Galdeano, C.; Gómez, T.; Muñoz-Torrero, D.; Scarpellini, M.; Viayna, E.; Badia, A.; Clos, M. V.; Camins, A.; Pallàs, M.; Bartolini, M.; Mancini, F.;

Andrisano, V.; Estelrich, J.; Lizondo, M.; Bidon-Chanal, A.; Luque, F. J. Novel donepezil-based inhibitors of acetyl- and butyrylcholinesterase and acetylcholinesterase-induced β-amyloid aggregation. *J. Med. Chem.* **2008**, *51*, 3588–3598. (b) Alonso, D.; Dorronsoro, I.; Rubio, L.; Muñoz, P.; García-Palomero, E.; Del Monte, M.; Bidon-Chanal, A.; Orozco, M.; Luque, F. J.; Castro, A.; Medina, M.; Martínez, A. Donepezil-tacrine hybrid related derivatives as new dual binding site inhibitors of AChE. *Bioorg Med Chem.* **2005**, *13*, 6588–6597.

(35) Dvir, H.; Wong, D. M.; Harel, M.; Barril, X.; Orozco, M.; Luque, F. J.; Muñoz-Torrero, D.; Camps, P.; Rosenberry, T. L.; Silman, I.; Sussman, J. L. 3D structure of *Torpedo californica* acetylcholinesterase complexed with huprine X at 2.1 Å resolution: kinetic and molecular dynamic correlates. *Biochemistry* **2002**, *41*, 2970–2981.

(36) (a) Blois, M. S. Antioxidant determinations by the use of a stable free radical. *Nature* **1958**, *181*, 1199–1200. (b) Brand-Williams, W.; Cuvelier, M. E.; Berset, C. Use of a free radical method to evaluate antioxidant activity. *LWT - Food Sci. Technol.* **1995**, *28*, 25–30.

(37) (a) Hu, H.; Chen, Z.; Xu, X.; Xu, Y. Structure-based survey of the binding modes of BACE1 inhibitors. *ACS Chem. Neurosci.* **2019**, *10*, 880–889. (b) Hsiao, C.-C.; Rombouts, F.; Gijsen, H. J. M. New evolutions in the BACE1 inhibitor field from 2014 to 2018. *Bioorg. Med. Chem. Lett.* **2019**, *29*, 761–777. (c) Mancini, F.; De Simone, A.; Andrisano, V. Beta-secretase as a target for Alzheimer's disease drug discovery: an overview of in vitro methods for characterization of inhibitors. *Anal. Bioanal. Chem.* **2011**, *400*, 1979–1996.

(38) (a) Fernández-Bachiller, M. I.; Pérez, C.; Monjas, L.; Rademann, J.; Rodríguez-Franco, M. I. New tacrine–4-oxo-4*H*-chromene hybrids as multifunctional agents for the treatment of

Alzheimer's disease, with cholinergic, antioxidant, and β-amyloid-reducing properties. *J. Med. Chem.* **2012**, *55*, 1303–1317. (b) Fu, H.; Li, W.; Luo, J.; Lee, N. T. K.; Li, M.; Tsim, K. W. K.; Pang, Y.; Youdim, M. B. H.; Han, Y. Promising anti-Alzheimer's dimer bis(7)-tacrine reduces β-amyloid generation by directly inhibiting BACE-1 activity. *Biochem. Biophys. Res. Commun.* **2008**, *366*, 631–636.

(39) (a) Espargaró, A.; Medina, A.; Di Pietro, O.; Muñoz-Torrero, D.; Sabate, R. Ultra rapid in vivo screening for anti-Alzheimer anti-amyloid drugs. *Sci. Rep.* **2016**, *6*, 23349. (b) Pouplana, S.; Espargaró, A.; Galdeano, C.; Viayna, E.; Sola, I.; Ventura, S.; Muñoz-Torrero, D.; Sabate, R. Thioflavin-S staining of bacterial inclusion bodies for the fast, simple, and inexpensive screening of amyloid aggregation inhibitors. *Curr. Med. Chem.* **2014**, *21*, 1152-1159.

(40) Di, L.; Kerns, E. H.; Fan, K.; McConnell, O. J.; Carter, G. T. High throughput artificial membrane permeability assay for blood–brain barrier. *Eur. J. Med. Chem.* **2003**, *38*, 223–232.

(41) Sola, I.; Aso, E.; Frattini, D.; López-González, I.; Espargaró, A.; Sabaté, R.; Di Pietro, O.; Luque, F. J.; Clos, M. V.; Ferrer, I.; Muñoz-Torrero, D. Novel levetiracetam derivatives that are effective against the Alzheimer-like phenotype in mice: synthesis, in vitro, ex vivo, and in vivo efficacy studies. *J. Med. Chem.* **2015**, *58*, 6018–6032.

(42) Borchelt, D. R.; Ratovitski, T.; van Lare, J.; Lee, M. K.; Gonzales, V.; Jenkins, N. A.; Copeland, N. G.; Price, D. L.; Sisodia, S. S. Accelerated amyloid deposition in the brains of transgenic mice coexpressing mutant presenilin 1 and amyloid precursor proteins. *Neuron* **1997**, *19*, 939–945.

(43) Vogel, C.; Marcotte, E. M. Insights into the regulation of protein abundance from proteomic and transcriptomic analyses. *Nat. Rev. Genet.* **2012**, *13*, 227–232.

(44) Cheignon, C.; Tomas, M.; Bonnefont-Rousselot, D.; Faller, P.; Hureau, C.; Collin, F. Oxidative stress and the amyloid beta peptide in Alzheimer's disease. *Redox Biol.* **2018**, *14*, 450–464.

(45) (a) Patocka, J.; Jun, D.; Kuca, K. Possible role of hydroxylated metabolites of tacrine in drug toxicity and therapy of Alzheimer's disease. *Curr. Drug Metab.* **2008**, *9*, 332−335. (b) Spaldin, V.; Madden, S.; Pool, W.; Woolf, T.; Park, B. The effect of enzyme inhibition on the metabolism and activation of tacrine by human liver microsomes. *Br. J. Clin. Pharmacol.* **1994**, *38*, 15–22. (c) Madden, S.; Woolf, T. F.; Pool, W. F.; Park, B. K. An investigation into the formation of stable, protein-reactive and cytotoxic metabolites from tacrine in vitro. *Biochem. Pharmacol.* **1993**, *46*, 13–20.

(46) Nepovimova, E.; Korabecny, J.; Dolezal, R.; Babkova, K.; Ondrejicek, A.; Jun, D.; Sepsova, V.; Horova, A.; Hrabinova, M.; Soukup, O.; Bukum, N.; Jost, P.; Muckova, L.; Kassa, J.; Malinak, D.; Andrs, M.; Kuca, K. Tacrine–trolox hybrids: A novel class of centrally active, nonhepatotoxic multi-target-directed ligands exerting anticholinesterase and antioxidant activities with low in vivo toxicity. *J. Med. Chem.* **2015**, *58*, 8985–9003.

(47) (a) Kamal-Eldin, A.; Appelqvist, L.-Å. The chemistry and antioxidant properties of tocopherols and tocotrienols. *Lipids* **1996**, *31*, 671–701. (b) Christen, S.; Woodall, A. A.; Shigenaga, M. K.; Southwell-Keely, P. T.; Duncan, M. W.; Ames, B. N. ɣ-Tocopherol traps mutagenic electrophiles such as NOx and complements α-tocopherol: Physiological implications. *Proc. Natl. Acad. Sci. U. S. A.* **1997**, *94*, 3217–3222.

(48) (a) Siegel, D.; Bolton, E. M.; Burr, J. A.; Liebler, D. C.; Ross, D. The reduction of α-tocopherolquinone by human NAD(P)H:quinone oxidoreductase: The role of α-tocopherolhydroquinone as a cellular antioxidant. *Mol Pharmacol* **1997**, *52*, 300–305. (b) Kohar, I.; Baca, M.; Suarna, C.; Stocker, R.; Southwell-Keely, P. T. Is α-tocopherol a reservoir for α-tocopheryl hydroquinone? *Free Radic. Biol. Med.* **1995**, *19*, 197–207. (c) Takaaki, H.; Akio, K.; Masao, N.; Mamoru, T.; Hharuhisa, S. Reduction of α-tocopherolquinone to α-tocopherolhydroquinone in rat hepatocytes. *Biochem. Pharmacol.* **1992**, *44*, 489–493.

(49) Yenes, S.; Commandeur, J. N. M.; Vermeulen, N. P. E.; Messeguer, A. In vitro biotransformation of 3,4-dihydro-6-hydroxy-2,2-dimethyl-7-methoxy-1(*2H*)-benzopyran (CR-6), a potent lipid peroxidation inhibitor and nitric oxide scavenger, in rat liver microsomes. *Chem. Res. Toxicol.* **2004**, *17*, 904–913.

(50) Słoczyńska, K.; Gunia-Krzyżak, A.; Koczurkiewicz, P.; Wójcik-Pszczoła, K.; Żelaszczyk, D.; Popiół, J.; Pękala, E. Metabolic stability and its role in the discovery of new chemical entities. *Acta Pharm.* **2019**, *69*, 345–361.

(51) Cornish-Bowden, A. A simple graphical method for determining the inhibition constants of mixed, uncompetitive and non-competitive inhibitors, *Biochem. J.* **1974**, *137*, 143e144.

(52) Silverman, R.B. The Organic Chemistry of Enzyme-Catalyzed Reactions, 1st ed.; Academic Press: San Diego, 2000.

(53) (a) Taylor, P.; Lwebuga-Mukasa, J.; Lappi, S.; Rademacher, J. Propidium – a fluorescent probe for a peripheral anionic site on acetylcholinesterase, *Mol. Pharmacol.* **1974**, *10*, 703–

708. (b) Taylor, P.; Lappi, S. Interaction of fluorescence probes with acetylcholinesterase, the site and specificity of propidium binding, *Biochemistry* **1975**, *14*, 1989–1997.

(54) Nunes-Tavares, N.; Nery da Matta, A.; Batista e Silva, C.M.; Araújo, G.M.N.; Louro, S.R.W.; Hassón-Voloch, A. Inhibition of acetylcholinesterase from *Electrophorus electricus* (L.) by tricyclic antidepressants, *Int. J. Biochem. Cell Biol.* **2002**, *34*, 1071–1079.

(55) Bourne, Y.; Kolb, H. C.; Radić, Z.; Sharpless, K. B.; Taylor, P.; Marchot, P. Freeze-frame inhibitor captures acetylcholinesterase in a unique conformation. *Proc. Natl. Acad. Sci. U.S.A.* **2004***, 101*, 1449–1454.

(56) Dighe, S. N.; Deora, G. S.; De la Mora, E.; Nachon, F.; Chan, S.; Parat, M. O.; Brazzolotto, X.; Ross, B. P. Discovery and structure–activity relationships of a highly selective butyrylcholinesterase inhibitor by structure-based virtual screening. *J. Med. Chem.* **2016**, *59*, 7683–7689.

(57) Nachon, F.; Carletti, E.; Ronco, C.; Trovaslet, M.; Nicolet, Y.; Jean, L.; Renard, P. Y. Crystal structures of human cholinesterases in complex with huprine W and tacrine: elements of specificity for anti-Alzheimer's drugs targeting acetyl- and butyryl-cholinesterase. *Biochem J.* **2013**, *453*, 393–399.

(58) Camps, P.; El Achab, R.; Morral, J.; Muñoz-Torrero, D.; Badia, A.; Baños, J. E.; Vivas, N. M.; Barril, X.; Orozco, M.; Luque, F. J. New tacrine-huperzine A hybrids (huprines): highly potent tight-binding acetylcholinesterase inhibitors of interest for the treatment of Alzheimer's disease. *J. Med. Chem.* **2000**, *43*, 4657–4666.

(59) Case, D. A.; Babin, V.; Berryman, J. T.; Betz, R. M.; Cai, Q.; Cerutti, D. S.; Cheatham, III, T. E.; Darden, T. A.; Duke, R. E.; Gohlke, H.; Goetz, A. W.; Gusarov, S.; Homeyer, N.; Janowski, P.; Kaus, J.; Kolossváry, I.; Kovalenko, A.; Lee, T. S.; LeGrand, S.; Luchko, T.; Luo, R.; Madej, B.; Merz, K. M.; Paesani, F.; Roe, D. R.; Roitberg, A.; Sagui, C.; Salomon-Ferrer, R.; Seabra, G.; Simmerling, C. L.; Smith, W.; Swails, J.; Walker, R. C.; Wang, J.; Wolf, R. M.; Wu, X.; Kollman, P. A. AMBER 14, 2014.

(60) Wang, J.; Wolf, R. M.; Caldwell, J. W.; Kollman, P. A.; Case, D. A. Development and testing of a general Amber force field. *J. Comput. Chem.* **2004**, *25*, 1157–1174.

(61) Frisch, M. J.; Trucks, G. W.; Schlegel, H. B.; Scuseria, G. E.; Robb, M. A.; Cheeseman, J. R.; Scalmani, G.; Barone, V.; Mennucci, B.; Petersson, G. A.; Nakatsuji, H.; Caricato, M.; Li, X.; Hratchian, H. P.; Izmaylov, A. F.; Bloino, J.; Zheng, G.; Sonnenberg, J. L.; Hada, M.; Ehara, M.; Toyota, K.; Fukuda, R.; Hasegawa, J.; Ishida, M.; Nakajima, T.; Honda, Y.; Kitao, O.; Nakai, H.; Vreven, T.; Montgomery, J. A. Jr.; Peralta, J. E.; Ogliaro, F.; Bearpark, M.; Heyd, J. J.; Brothers, E.; Kudin, K. N.; Staroverov, V. N.; Kobayashi, R.; Normand, J.; Raghavachari, K.; Rendell, A.; Burant, J. C.; Iyengar, S. S.; Tomasi, J.; Cossi, M.; Rega, N.; Millam, J. M.; Klene, M.; Knox, J. E.; Cross, J. B.; Bakken, V.; Adamo, C.; Jaramillo, J.; Gomperts, R.; Stratmann, R. E.; Yazyev, O.; Austin, A. J.; Cammi, R.; Pomelli, C.; Ochterski, J. W.; Martin, R. L.; Morokuma, K.; Zakrzewski, V. G.; Voth, G. A.; Salvador, P.; Dannenberg, J. J.; Dapprich, S.; Daniels, A. D.; Farkas, Ö.; Foresman, J. B.; Ortiz, J. V.; Cioslowski, J.; Fox, D. J. Gaussian, Inc.; Wallingford CT, Gaussian 09, 2009.

(62) Wang, J.; Cieplak, P.; Kollman, P. A. How well does a restrained electrostatic potential (RESP) model perform in calculating conformational energies of organic and biological molecules? *J. Comput. Chem.* **2000**, *21*, 1049–1074.

(63) (a) Søndergaard, C. R.; Olsson, M. H. M.; Rostkowski, M.; Jensen, J. H. Improved treatment of ligands and coupling effects in empirical calculation and rationalization of pKa values. *J. Chem. Theory Comput*. **2011**, *7*, 2284–2295. (b) Olsson, M. H. M.; Søndergaard, C. R.; Rostkowski, M.; Jensen, J. H. PROPKA3: consistent treatment of internal and surface residues in empirical pKa predictions. *J. Chem. Theory Comput*. **2011**, *7*, 525–537.

(64) Jorgensen, W. L.; Chandrasekhar, J.; Madura, J. D.; Impey, R. W.; Klein, M. L. Comparison of simple potential functions for simulating liquid water. *J. Chem. Phys*. **1983**, *79*, 926–935.

(65) Harel, M.; Schalk, I.; Ehret-Sabatier, L.; Bouet, F.; Goeldner, M.; Hirth, C.; Axelsen, P. H.; Silman, I.; Sussman, J. L. Quaternary ligand binding to aromatic residues in the active-site gorge of acetylcholinesterase. *Proc. Natl. Acad. Sci. U.S.A.* **1993**, *90*, 9031–9035.

(66) Ryckaert, J.-P.; Ciccotti, G.; Berendsen, H. J. C. Numerical integration of the cartesian equations of motion of a system with constraints: molecular dynamics of n-alkanes. *J. Comput. Phys.* **1977**, *23*, 327–341.

(67) Darden, T.; York, D.; Pedersen, L. Particle mesh Ewald: an N·log(*N*) method for Ewald sums in large systems. *J. Chem. Phys*. **1993**, *98*, 10089–10092.

(68) Berendsen, H. J. C.; Postma, J. P. M.; van Gunsteren, W. F.; DiNola, A.; Haak, J. R. Molecular dynamics with coupling to an external bath. *J. Chem. Phys*. **1984**, *81*, 3684–3690.

(69) Molyneux P. The use of the stable free radical diphenylpicrylhydrazyl (DPPH) for estimating antioxidant activity. *Songklanakarin J. Sci. Technol.* **2004**, *26*, 211–219.

(70) Tarozzi, A.; Bartolini, M.; Piazzi, L.; Valgimigli, L.; Amorati, R.; Bolondi, C.; Djemil, A.; Mancini, F.; Andrisano, V.; Rampa, A. From the dual function lead AP2238 to AP2469, a multi-target-directed ligand for the treatment of Alzheimer's disease. *Pharmacol. Res. Perspect.* **2014**, *2*, e00023.

(71) Clark, J. D.; Gebhart, G. F.; Gonder, J. C.; Keeling, M. E.; Kohn, D. F. The 1996 guide for the care and use of laboratory animals. *ILAR J.* **1997**, *38*, 41–48.

Table of Content (TOC) Graphic